ANALYSIS OF REVERSE OSMOSIS MEMBRANE PERFORMANCE DURING DESALINATION OF SIMULATED BRACKISH SURFACE WATERS

By

DAWOOD EISA SACHIT

Bachelor of Science in Civil Engineering
Al-Mustansiria University
Baghdad, Iraq
1994

Master of Science in Civil Engineering
Al-Mustansiria University
Baghdad, Iraq
2000

Submitted to the Faculty of the
Graduate College of the
Oklahoma State University
in partial fulfillment of
the requirements for
the Degree of
DOCTOR OF PHILOSOPHY
December, 2013

ANALYSIS OF REVERSE OSMOSIS MEMBRANE PERFORMANCE DURING DESALINATION OF SIMULATED BRACKISH SURFACE WATERS

Dissertation Approved:

Dr. John N Veenstra

Dissertation Adviser

Dr. Gregory G Wilber

Dr. Dee Ann Sanders

Dr. AJ Johannes

ACKNOWLEDGEMENTS

Credit goes to the Iraqi Ministry of Higher Education and Scientific Research for providing me with a full scholarship to pursue and complete my Ph.D. in the Civil and Environmental Engineering.

I would like to express my sincere appreciation to my adviser, Dr. John N Veenstra, for his advice, support, guidance, and encouragement throughout the developing of this research.

Also, special thanks are due to the other Ph.D. committee members, Gregory G Wilber, Dee Ann Sanders, and AJ Johannes for their advice and help.

I wish to thank Dr. Nicholas F. Materer and Dr. Allen Apblett, from the Chemistry Department of Oklahoma State University, for their help.

Credit is due to the faculty, particularly Dr. Tyler Ley for helping with the SEM, and staff, especially David Porter for helping to build the experimental system, in the Civil and Environmental Engineering Department of Oklahoma State University for their help.

Credit is due to Dr. Mark Fishbein from the Department of Botany, Oklahoma State University for his help in identifying the genius and species of the plants.

Additionally, I would like to thank Gary D. Thacker, building manager at the Advanced Technology Research Center (ATRC) of Oklahoma State University, for his help in setting the system and accessing other labs for the required stuff.

Credit is due to Kevin Drees, Engineering Librarian, Oklahoma State University, for his help.

I would like, also, to thank Mary Clinkenbeard for helping in the sentence structure of this dissertation.

Finally, I wish to thank all my family members for their best support and encouragement through all my endeavors.

Name: DAWOOD EISA SACHIT

Date of Degree: December, 2013

Title of Study: ANALYSIS OF REVERSE OSMOSIS MEMBRANE PERFORMANCE DURING DESALINATION OF SIMULATED BRACKISH SURFACE WATERS

Major Field: CIVIL AND ENVIRONMENTAL ENGINEERING

Abstract: In this study, three different brackish surface water qualities, which represented the water quality in the Iraqi marshes, were simulated and used as feed waters to run a flat sheet reverse osmosis (RO) membrane system. The performance of three different types of the RO membrane (Thin-Film Composite (SE), Cellulose Acetate (CE), and Polyamide (AD)), under these water qualities, was investigated. The effect of the high and low feed water temperature (37^{o}C and 11^{o}C) on the operation efficiency of the three RO membranes was also investigated. In addition, using the Microfiltration (MF) membrane to pretreat the feed water and its effect on the performance of the RO membrane was examined. The results revealed that the SE membrane produced the highest permeate flux, while the AD membrane produced the lowest permeate flux in all three feed waters. Also, the elemental analyses showed that the CE membrane had the least rejection percentage (from 91.1% to 99.2%), but the AD membrane had the highest rejection percentage (from 97.6% to 99.5%) for all the existing feed water ions. Moreover, using the MF membrane increased the permeate flux, particularly of the runs conducted with a high temperature, and slightly improved salt ions rejection ratios by the RO membranes. Additionally, all membranes at the temperature of 37^{o}C exhibited higher permeate fluxes than those of corresponding membranes at a lower temperature (11^{o}C). Furthermore, the main foulants from the simulated feed waters were diagnosed by using Scanning Electron Microscope (SEM) images and Energy-Dispersive X-ray Spectroscopy (EDXS) spectra. Finally, Fourier Transform Infrared Spectroscopy (FTIR) analysis was used to identify the functional groups of the organic matter deposited on the RO membrane surfaces. The SEM images and EDSX spectra suggested that the fouled material was mainly organic matter, and the major crystal deposited on the RO membrane was calcium carbonate ($CaCO_3$). The FTIR spectra of the fouled RO membranes suggested that the constituents of the fouled material included aliphatic and aromatic compounds.

TABLE OF CONTENTS

Chapter Page

LIST OF TABLES

Table Page

LIST OF FIGURES

Figure Page

Figure Page

CHAPTER I

INTRODUCTION

1.1. Background

Water is essential for life. Owing to the increase in population and the commercial and industrial applications worldwide, fresh water resources for drinking water and domestic uses continue to decline (Cotruvo et al., 2010). Most of the world's water is seawater, brackish water or groundwater. Approximately, 97.4% of the entire water mass available on earth is salty and 1.984% is located in the ice caps and glaciers, while 0.592% is located as groundwater and only 0.014% of the earth's water is readily available as fresh water (Delgado and Moreno, 2008). In addition, many dry or arid areas around the world do not have fresh water resources in the form of surface water such as rivers, lakes, etc. As a consequence, seawater and brackish water have become alternative resources for drinking water. Fresh water can be defined as the water that contains less than 1000 mg/L of the total dissolved solids (TDS) and waters containing 1000 mg/L to 10,000 mg/L of TDS are considered as brackish water while seawater contains 10,000 mg/L to 60,000 mg/L of TDS (Greenlee et al., 2009; Sandia, 2003; Mickley, 2001).

High concentration of TDS and other minerals that exist in brackish water and seawater need to be removed using advanced treatment. Desalination of seawater and brackish water is one of the technologies that have been introduced to remove salt and other minerals from saline and salty water to make it suitable for human consumption or industrial use. In 1983, the first major seawater desalination plant was built in Saudi Arabia (Escobar and Schafer, 2010). According to the NRC (2008) and GWI (2006), in 2006, the global desalination water production was approximately, 42 million m^3/day including seawater and brackish water for multiple purposes such as municipal, industrial, agricultural, power, military, and many other applications. By the end of 2007, there were over 14,000 desalination plants worldwide with total treatment capacity of about 53 million cubic meters of water per day (Cotruvo et al., 2010).

However, installation and operation of water desalinization facilities can negatively impact the environment. Some of the environmental impacts, which are needed to be crucially considered when a water desalination plant is planned, are: (1) impingement (trapping of fish or other larger organisms against the screens of the intake structures) and entrainment (pulling small aquatic organisms into the system) of marine organisms in coastal surface waters, (2) disposal of waste products and concentrate which contains most of the minerals and contaminants of the source water and the pretreatment processes, and (3) emission of air pollutants as a result of energy- intensive processes (Cotruvo et al., 2010; NRC, 2008).

1.2. Problem Statement

Iraq has plenty of water which is considered as brackish water that can be exploited for drinking water purposes (UNEP, 2007). Marshes (Mesopotamian Marshlands) which are located in southern of Iraq and were created by the Tigris and Euphrates rivers have a TDS ranging from 725 to 3308 mg/L and can be considered as a major source of surface brackish water (Al-Saad et al. 2010). Although the quantity of water in the marshes fluctuates, because it depends mainly on the water quantity in the Tigris and Euphrates rivers, it can also be used as a water source of drinking water

facilities for many cities in this region. The area of these marshes ranges from 5,791 to 7,722 sq.mile (15,000 to 20,000 sq.km) (Al-Saad et al. 2010). The quality of the water of the marshes compared to the available ground water in this region, which has high concentrations of elements (4,000 mg/L magnesium (Mg^{+2}), 2,000 mg/L calcium (Ca^{+2}), 10,000 mg/L sulfate (SO_4^{-2}), 1,750 mg/L chloride (Cl^-), 10,000 mg/L sodium (Na^+), and 64,613 mg/L TDS) as reported by Al-Dabbas and Manii (2007) makes it a potential good source for water treatment facilities.

Recently, taking advantage of the reverse osmosis process to help in drinking water production, several pilot desalination plants were implemented in the region of the Iraqi marshlands (UNEP, 2007), and more water desalination facilities are expected to be implemented and operated within the next decades. The expansion of the new technology of reverse osmosis membrane process in this area requires studies that can assess and minimize the problems this technology encounters. Some of these problems include membrane fouling, which limits both operation productivity and life-time of the membrane, and the environmental impacts of the concentrate.

In this study, the potential impacts of the variation of the feed water, which is similar or close to the water quality of the brackish surface water in the Iraqi marshes, on the fouling and the productivity of three different RO membrane types were investigated.

1.3. Objectives

The main objectives of this study are:

1. To investigate the performance of three different RO membrane types (Thin-Film Composite, SE, Cellulose Acetate, CE, and Polyamide, AD) in terms of permeate flux productivity and salt rejection percentage, using three different simulated feed water qualities which represent three brackish surface water analyses in the Iraqi marshes. These water analyses, which were situated in the upstream of the Euphrates River (location 1), the upstream of the Tigris River (location 5), and the downstream of the marsh area (location 6), represent nearly all the area of the marshes.

Also, the concentrations of the constituents of the water quality varied from high to low levels. For instance, the concentration of the TDS and TOC at location 6 (high levels) and location 5 (low levels) were 2411 mg/L and 4.71 mg/L, and 1144 mg/L and 1.2 mg/L, respectively. In addition, the concentration of the TDS and TOC at location 1 (moderate levels) were 1686 mg/L and 1.74 mg/L, respectively.

2. To examine the effect of the high and low feed water temperature (37^{o}C and 11^{o}C) on the operation efficiency of the three RO membrane types and the total time to achieve the required water recovery.
3. To study the effect of pretreating, with a Microfiltration (MF) membrane, the simulated feed water of the high TDS and TOC concentrations on permeate flux productivity and salt rejection percentage of the used RO membranes.
4. To diagnose the main foulants from the simulated feed water in the three locations on the three RO membranes.
5. To examine the effect of the feed water temperature and the pretreatment by the MF membrane on the morphology of the fouled materials deposited on the RO membrane surfaces.
6. To identify the functional groups of the organic matter deposited on the RO membrane surfaces.

CHAPTER II

DESALINATION TECHNOLOGIES

2.1. Types of Desalination Technologies

Typically, there are two general types of desalination technologies: thermal evaporation (distillation) and membrane separation technology (Li et al., 2008). Worldwide, thermal evaporation technologies account for nearly 43% while membrane separation processes account for 56% of the total desalination (NRC, 2008; GWI, 2006). In the United States, the membrane system is the predominant technology of water desalination, approximately 96%, while thermal technology accounts for 3% (NRC, 2008; GWI, 2006). In terms of region, about 48% of the desalinated water is produced in the Middle East, 19% in the Americas, 14% in Europe, 14% in the Asia-Pacific region, and 6% in Africa. In terms of seawater as a source water for desalination processes, the Middle East represents more than 61% of the global desalinated water production, Southern Europe represents 11%, and 7% is located in North Africa.

However, brackish water is the main source of water desalination processes in North America which accounts for 36% of the global brackish water desalination capacity. In the Middle East, brackish water represents 21% while 13% takes place in Southern Europe (Escobar and Schafer, 2010; IDA and GWI, 2008).

2.1.1. Distillation/Thermal Technologies

In distillation processes, a source water is heated by a thermal energy source and then vaporized. The condensed vapor has very low total dissolved solids (TDS), typically less than 25 mg/L TDS (Cooley et al., 2006; USBR, 2003) or in the range 1- 50 mg/L (Cotruvo et al., 2010), whereas a concentrated brine is produced as residual. Distillation/thermal systems include multi-stage flash distillation (MSF), multiple-effect distillation (MED), and vapor compression distillation (VCD).

In the MSF process, seawater is first heated and then rapidly boiled and evaporated in chambers by successive flashing to lower pressures as shown in Figure 2.1. After that, the generated vapor is condensed on the feed seawater tubes surfaces that are located in the upper portion of each chamber. The MSF process can recover 25% - 50% of the flow into freshwater (Cotruvo et al., 2010; Delgado and Moreno, 2008). MSF is the dominant process of thermal distillation technology, and it represents 93% of the worldwide thermal process production (Delgado and Moreno, 2008).

In the MED process, steam is introduced inside horizontal or vertical tubes in several consecutive cells or stages. As top tubes in each cell are sprayed with seawater (Figure 2.2) steam condenses into distilled water inside the tubes. Pressure and temperature are sequentially reduced along with the stages and more heat is added to each cell to improve system performance (Cotruvo et al., 2010; Delgado and Moreno, 2008; Ribeiro, 1996). Although, MED plants are initially designed to be small in size, an 800,000 m^3/day MED plant is planned to be built in a Middle Eastern country (NRC, 2008).

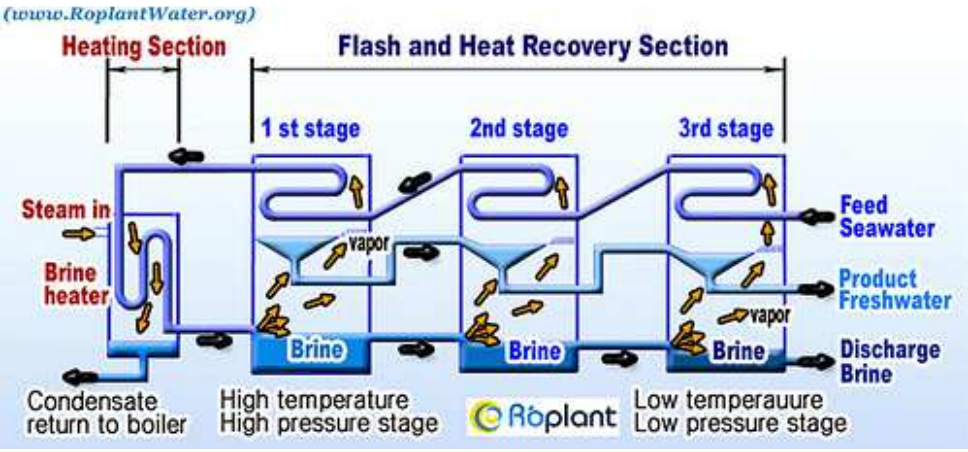

Figure 2.1. Multi-stage flash distillation (MSF) (ROplant's photostream, 2009a).

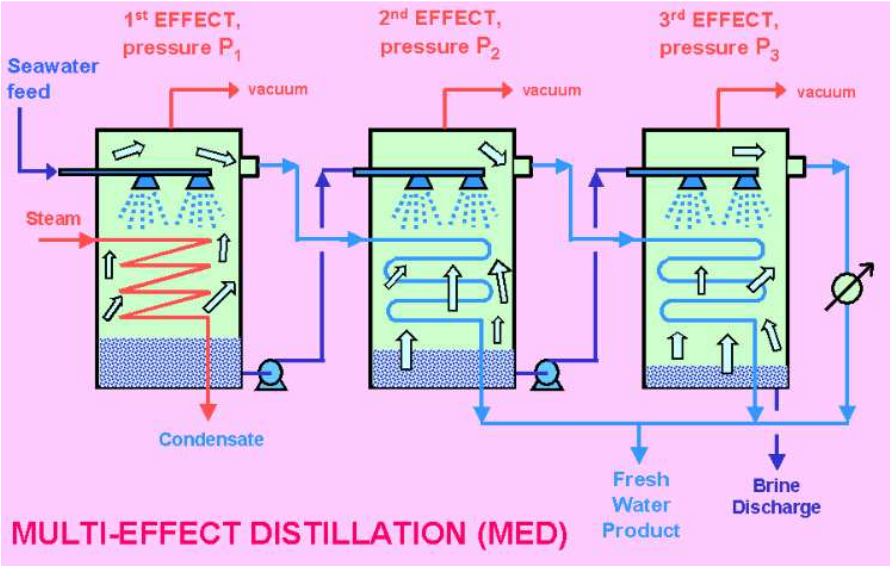

Figure 2.2. Multi-effect distillation (MED) (Cheah, 2000).

While MSF and MED systems use external sources of heat, the VCD system uses its own steam as the principle energy requirement; however, an initial supply of vapor is needed to start the system. After the initial vapor is provided, it is compressed to generate the heat necessary for the boiling process on the other side of the tubes, causing the evaporation of seawater (Cotruvo et al., 2010; Delgado and Moreno, 2008; Ribeiro, 1996). Figure 2.3 displays the principle of vapor compression distillation processes.

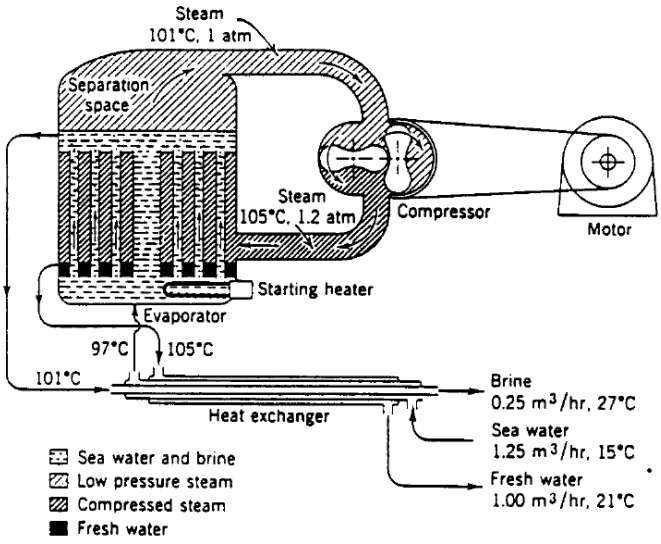

Figure 2.3. Principle of vapor compression distillation (VCD) (Ribeiro, 1996; Spiegler and El-Sayed, 1994).

2.1.2. Membrane Technologies

In membrane technology, a filtration process through a membrane is used to separate a solvent (dissolved solids) from a solution (source water) (Delgado and Moreno, 2008). Membrane technologies can desalinate both seawater and brackish water to produce water with salt content less than 500 mg/L of TDS (Cooley et al., 2006; USBR, 2003). Several types of membranes are used in the water desalination processes: microfiltration (MF), ultrafiltration (UF), nanofiltration (NF), reverse osmosis (RO) and electrodialysis (ED). Table 2.1 summarizes the performance characteristics of the five types of membranes.

MF membranes have the largest pore size 1 to 10 µm, and typically operate at low pressures to reject large particles and various microorganisms such as colloids and bacteria. In contrast, UF membranes have pore sizes of 0.01 to 0.1 µm which is smaller than MF pore size. UF membranes remove large organic molecules such as protein and viruses. NF membranes are relatively new, with the first applications reported during the second half of the 1980s (Erikson, 1988; Conlon and Clellan, 1989; Li et al., 2008).

Table 2.1

Comparison of membrane process performance characteristics (Cotruvo et al., 2010; Oveolia, 2010; TecCommentary, 1997).

Parameters	Membrane Process				
	MF	UF	NF	RO	ED
Nominal Pore Size (µm) (Approximate)	0.1 - 1	0.01 - 0.1	0.001 - 0.01	0.0001 - 0.001	
Gradient	Pressure				Electrical Potential
Transport of the Main Species	Water				Ions
Removal of the Smallest Species	very small suspended particles, some colloids most bacteria	large organics molecules > 1000 MW, viruses, bacteria, colloids	small organic molecules > 300 MW, divalent ions	all dissolved species including ions, organics > 100 MW	
Operating Pressure psi (kPa)	2.9 to 29 (20 to 200)	14.5 to 72.5 (100 to 500)	72.5 to 290 (500 to 2,000)	290 to 1160 (2,000 to 8,000)	14.5 to 43.5 (100 to 300)
Typical Flux gal/day/ft^2 (l/h/m^2)	58.8 to 588 100 to 1,000	29.4 to 118 50 to 200	11.8 to 29.4 20 to 50	5.88 to 29.4 10 to 50	
Maximum Temperature ^{O}F (^{O}C)	80 (27)	80 (27)	80 (27)	100 (38)	
Recovery Rate (%)	100	75	85	50 - 85	
Water Treatment Applications	clarification	clarification	water softening, color, natural organic matter, micro-pollutant removal	desalination of seawater and brackish water	desalination of brackish water, ion removal (NO_3)

NF membranes have pore size of 0.001 to 0.01 µm and are applied in water softening, food processing, color removal, natural organic removal, and pharmaceutical applications. RO membranes have pore sizes of 0.0001 to 0.001µm and they are considered effectively non-porous

membrane. They can exclude all dissolved species such as salt ions and organics. RO membranes typically operate at high pressures which can exceed 1000 psi (6,895 kPa) (Kucera, 2010). RO membrane technology is applied for drinking water production from seawater and brackish water, water softening, boiler feed water production, food processing, dairy products, water reclamation of wastewater, and many other applications (Malaeb and Ayoub, 2011; Kucera, 2010; Cotruvo et al., 2010; Oveolia, 2010). The ED process, which was introduced to the market in the early 1960s, is used to desalt brackish water by using an electrical potential to selectively transport ions through membranes to electrodes of opposite charge (Escobar and Schafer, 2010). In general, microfiltration and ultrafiltration membranes with larger pore sizes are used as pretreatment units for RO membranes, the more restrictive membranes, to reduce fouling and extend running time of the membrane (Cotruvo et al., 2010).

2.2. Energy Consumption and Desalination Costs

Desalination processes need significant amounts of energy (electricity and heat or steam). Energy consumption varies with the type of desalination system, the operating temperature, and the type and concentration of the constituents of source water (Cotruvo et al., 2010). Thermal desalination processes need more energy than reverse osmosis membrane processes as shown in Table 2.2. Because multi-stages flash (MSF) plants have operating temperatures of 248^{o}F (120^{o}C), they consume about 107-141 Btu/lb (250-330 kJ/kg) of thermal energy and 3-5 kWh of electrical energy per 1 m^3 of water production, while multiple-effect distillation (MED) plants demand 62-167 Btu/lb (145-390 kJ/kg) of thermal energy and 1.5-2.5 kWh of electrical energy per 1 m^3 of water production to have operating temperatures that can reach 158^{o}F (70^{o}C). However, RO plants require 2.5-7 kWh of electrical energy per 1 m^3 of water production for operating temperatures below 113^{o}F (45^{o}C) (Escobar and Schafer, 2010). Table 2.2 displays energy data of RO, MSF, and MED systems.

Table 2.2

Energy data of RO, MSF, and MED systems (Escobar and Schafer, 2010; NRC, 2008).

	RO Systems	**MSF systems**	**MED systems**
Operating temperature	Below 45^{o}C	Below 120^{o}C	Below 70^{o}C
Main energy source	Electrical energy	Steam (heat)	Steam (heat)
Thermal Energy demand per 1 m^3 of water production	None	107-141 Btu/Ib (250-330 kJ/kg)	62-167 Btu/Ib (145-390 kJ/kg)
Electrical energy demand per 1 m^3 of water production	2.5-7 kWh	3-5 kWh	1.5-2.5 kWh
Typical water recovery	35-50 %	35-45 %	35-45 %

Cotruvo et al. (2010) reported that thermal desalination plants can consume about 50 million kWh/year to produce 26,500 m^3/day of distilled water. In other words, thermal desalination systems consume around 5 kWh to produce one cubic meter of water. In California, the average energy use for water desalination processes was 3.4 kWh/m^3 in 2001(Escobar and Schafer, 2010; Cooley et al., 2006). Energy consumption from desalination can account for 14 % of the total energy demands on Canary Islands and 1.4 % of national electricity generation in Spain (Escobar and Schafer, 2010; Dolnicar and Schafer, 2006). In the Middle East, over 50% of the fuel used as an energy source for electricity and water desalination is natural gas, which is either locally produced or imported. The second main sources of the generating fuels are the petroleum products and crude oil, which account for 40% of the total fuel sources. In Kuwait, annually, 462 million GJ of energy is consumed (10% of the national fuel use) by the cogeneration plants that produce desalinated water and electricity (Escobar and Schafer, 2010; UNEP, 1999). Another source of fuel is coal-fired energy, which is used in Israel (Ouki, 2010).

In terms of cost, water production costs worldwide differ from country to country depending on the source water quality, plant size, the cost and availability of fuel, and the type of desalination technology. The capital costs of MED and MSF processes can be estimated as 1.5

and 2 times the capital costs of the RO systems, respectively. Moreover, based on a desalination system of 100,000 m^3/day and electricity use of 4.5, 4.0, and 1.25 kWh/m^3 for RO, MSF, and MED, respectively, the cost of one cubic meter of desalinated water by the RO system is \$0.61 compared to \$0.72/m^3 for MED and \$0.89/m^3 for MSF (NRC, 2008; GWI, 2006). In addition, Escobar and Schafer (2010) reported that water production capital cost of RO plants is \$0.46/m^3, while the capital costs for MSF and MED plants are \$0.60/m^3 and \$0.50/m^3, respectively, as shown in Figure 2.4.

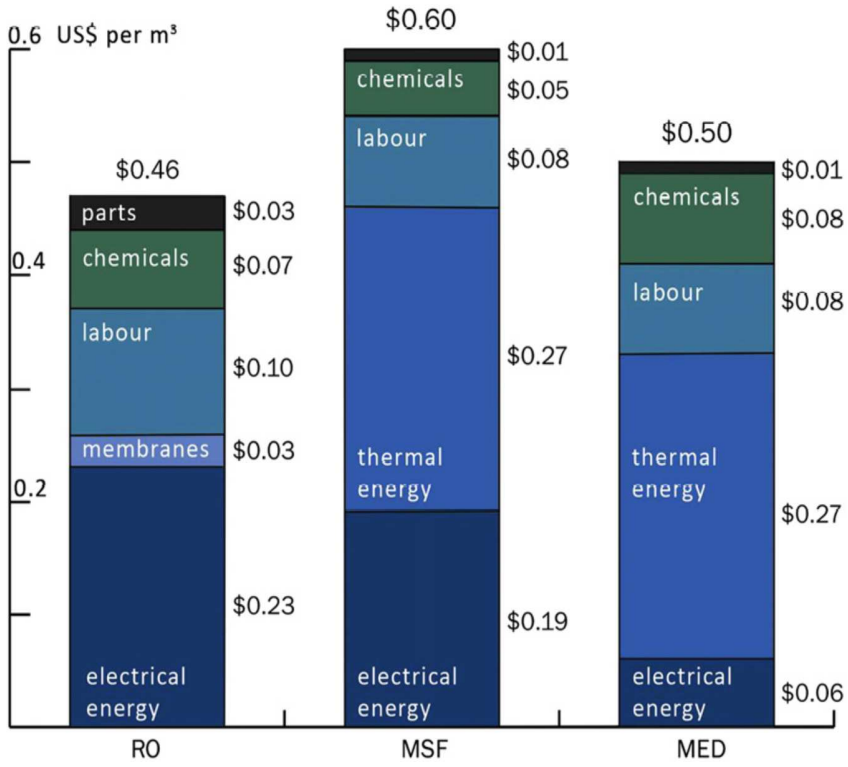

Figure 2.4. Capital costs of one cubic meter of desalinated water of RO, MSF, and MED systems (Escobar and Schafer, 2010; GWI, 2007).

However, energy consumption and capital costs associated with brackish water reverse osmosis desalination plant account for about 11% and 50% of the total costs water production, respectively. Production of one cubic meter of desalinated water by brackish water reverse osmosis system can range from \$0.41 to \$0.73. On the other hand, energy consumption and capital costs associated with seawater reverse osmosis desalination plant account for 36% and

37% of the total costs water production, respectively, and production of one cubic meter of desalinated water by seawater reverse osmosis system can range from $0.73 to $2.03 (WRF, 2010; NRC 2008).

CHAPTER III

REVERSE OSMOSIS MEMBRANE SYSTEM

3.1. Membrane Separation Process

Reverse osmosis process is the most common method used in desalination technology. Approximately, 50% of the desalination plants around the world are RO desalination plants (Greenlee et al., 2009; Li et al., 2008). The increase of RO technology against thermal desalination technology is a result of the membrane technology developments that has led to many advantages in reducing the required energy and water production cost as well as temperature of the operation (Abbas, 2005; Wade, 2001).

To understand the RO process, it is important, first, to understand the natural phenomena of osmosis. Osmosis or Forward Osmosis (FO) occurs when water flows through a semipermeable barrier (permeable to the solvent, but not the solute) from the side with lower solute concentration to the higher solute concentration side. A simple diagram of the osmosis and reverse osmosis phenomena are illustrated in Figure 3.1.

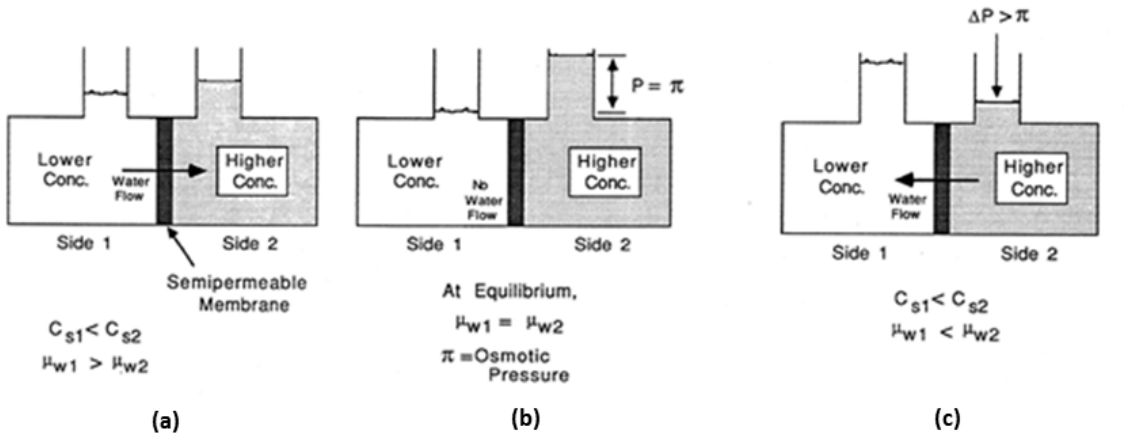

Figure 3.1. Schematic of osmosis and reverse osmosis phenomena (Williams, 2003).

Sub-Figure 3.1 (a) displays two solutions of different concentrations, C_{S1}, low solute concentration of solution 1 and C_{S2}, high solute concentration of solution 2. The water chemical potentials (water pressure) in solution 1 and solution 2 are μ_{W1} and μ_{W2}, respectively. To equalize the solute concentrations on the two sides of the membrane as shown in sub-Figure 3.1 (b), water molecules move through the membrane into the higher solute concentration side creating a physical process known as osmosis (Kucera, 2010; Hessami et al., 2009; Williams, 2003).

Forward Osmosis has been used for many applications such as industrial wastewaters treatment, landfill leachate concentration, and liquid foods treatment in the food industry (Cath et al., 2006). According to Cotruvo et al., (2010), "In forward osmosis, ammonia and carbon dioxide are added to fresh water on the opposite side of the membrane from the saline water to increase the ionic ammonium carbonate concentration so that water from the salt solution naturally migrates through the membrane to the ammonium carbonate "draw" solution without external pressure." Finally, Ammonia, NH_3, and carbon dioxide, CO_2, are evaporated by heating the diluted draw solution, leaving behind freshwater (Cotruvo et al., 2010; Patel-Predd, P. 2006). In the RO process, on the contrary, a pressure greater than the osmotic pressure is applied on the side of higher solute concentration to first stop and then reverse the flow of water as shown in sub-Figure 3.1 (c) (Williams, 2003).

3.2. RO Membrane Configuration

RO membranes are found in a variety of module configurations. Commercially, the two major configurations are the hollow fiber and spiral wound (Malaeb and Ayoub, 2011; Kucera, 2010; Li et al., 2008; TechCommentary, 1997). Today, the most common membrane module configuration for RO is the spiral wound membrane module. In this module, several leaves (RO membrane sheets plus permeate water carriers) and feed channel spacers are wrapped around a perforated tube and then installed in a vessel (Lee et al. 2011; Kucera, 2010; Paul and Abanmy, 1990). An RO membrane sheet is comprised of either cellulose acetate membrane, which is made from a combination of cellulose diacetate and triacetate, or a thin-film composite polyamide membrane, which is manufactured by combining three structurally different layers (Kucera, 2010; HCTAB, 2005; TechCommentary, 1997). Figure 3.2 illustrates the configuration of the thin-film composite polyamide membrane. The first layer is typically made of a thin-film of cross-linked aromatic polyamide materials with a thickness of approximately 0.2 micron. The function of this layer is to reject dissolved and suspended solids in the feed water on one side and allow water to permeate. The second and the third layers are supporting layers which are polysulfone layer with a thickness of 50 micron and a non-woven polyester fabric layer with a thickness of 150 micron (Kucera, 2010; HCTAB, 2005; TechCommentary, 1997).

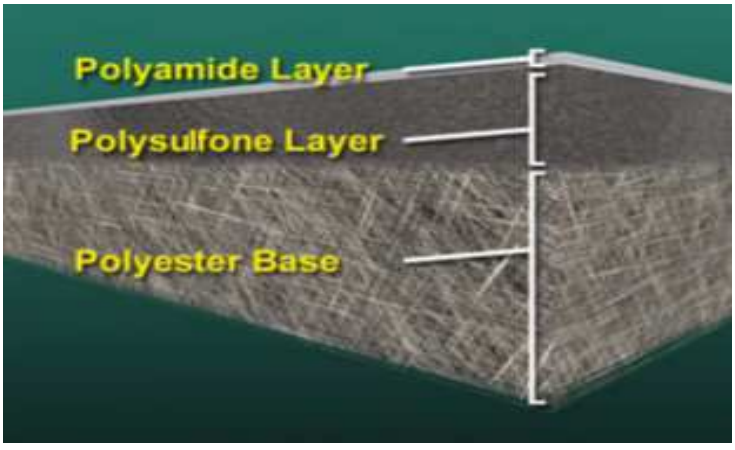

Figure 3.2. Configuration of the composite polyamide RO membrane (HCTAB, 2005).

In general, water flux and salt rejection of thin-film composite polyamide membranes are higher than those of cellulose acetate membranes (Saehan, 2006; HCTAB, 2005). Cellulose acetate membrane has a smooth hydrophilic (has affinity for water) surface that makes this type of membrane less susceptible to fouling than the polyamide membrane which has a rough hydrophobic (has no affinity for water) surface (Kucera, 2010; HCTAB, 2005; USBR, 2003b). The chemical structures of cellulose acetate membrane and polyamide membrane materials are shown in figure 3.3.

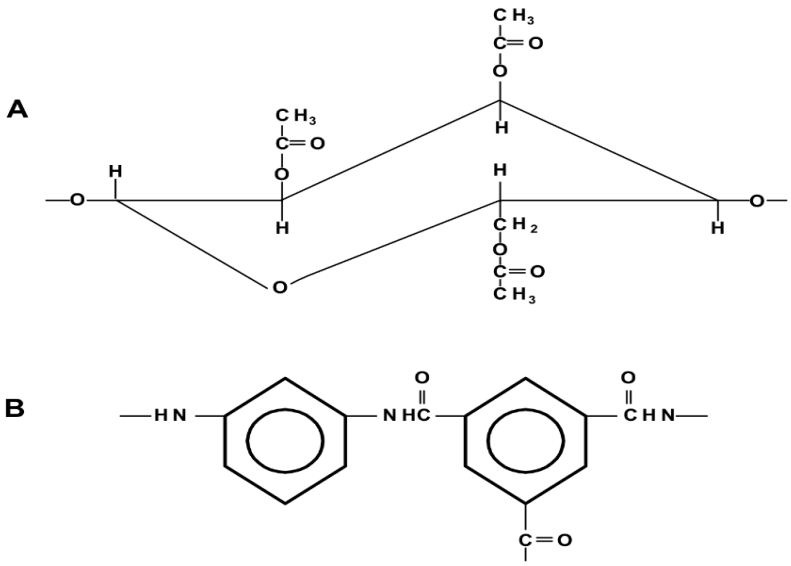

Figure 3.3. Chemical structures of cellulose acetate (A) and polyamide (B) membrane material (HCTAB, 2005).

The feed channel spacer is a netting material with a thickness of approximately 0.028 inch (0.71 mm) placed between the flat sheets of the RO membrane to provide a space or channel for feed-water or concentrate stream (Eriksson, 1998). Permeate water carrier, which is a fabric material, is the channel for permeate to flow between two sheets of the membrane in a spiral path and ending at the central perforated tube of the vessel (Paul and Abanmy, 1990). Figure 3.4 displays the configuration of a membrane element for the spiral wound module.

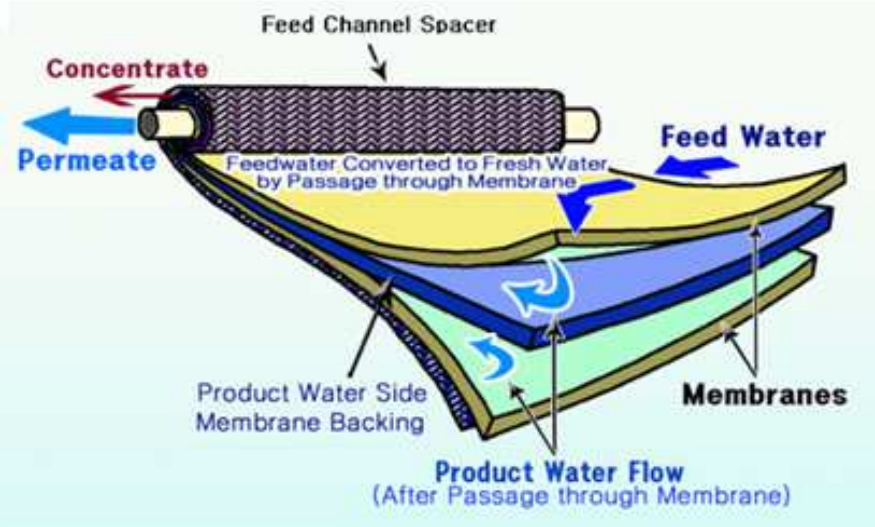

Figure 3.4. Configuration of a membrane element for the spiral wound RO module (ROplant's photostream, 2009b).

3.3.Theory of RO System

To understand the operation of an RO system, many parameters such as flux, recovery, rejection, concentration polarization, fouling, silt density index (SDI), solute-diffusion and other variables need to be defined and mathematically understood. Many mathematical models of reverse osmosis system were developed in the last two decades and most of the models have the same basic equations. In the mathematical models done by Avlonitis et al., (1993), Geraldes et al., (2005), and Hoek et al. (2008), flat feed channels of the spiral wound modules with width of W, length of L and height of h were assumed as shown in Figure 3.5. The reason behind this assumption is because of the small thickness of the feed channel compared to the radius of the vessel.

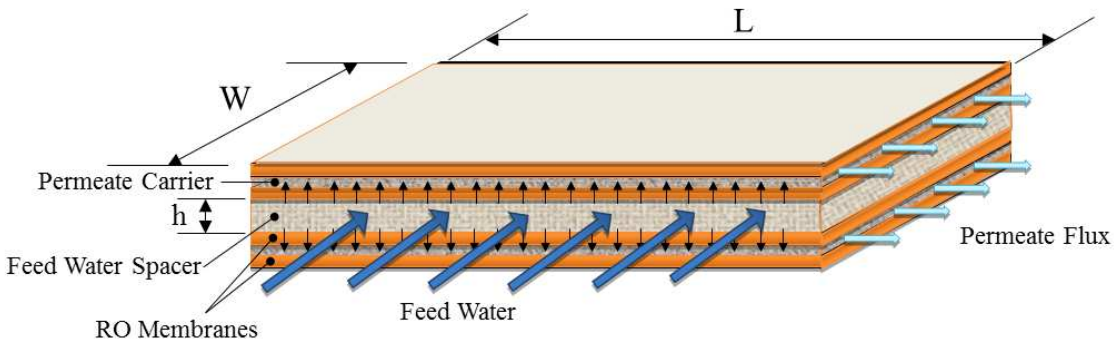

Figure 3.5. Schematic of the rectangular channels of spiral wound module.

Flux can be defined as the volumetric flow rate of a fluid (in this case water) through a given area (RO membrane area) per a time. Water flux through an RO membrane is proportional to the net pressure driving force applied to the water. As a result of the osmotic pressure between the two sides of the membrane, the net driving force for the product (water) across the membrane is the difference between the feed pressure and the osmotic pressure (Kucera, 2010; Song et al., 2002).

$$\text{Net Driving Force} = (\Delta P - \Delta \pi^{\circ}) \qquad (3\text{-}1)$$

Where, $\Delta\pi^{\circ}$ is the difference in osmotic pressure, psi (kPa) and ΔP is the difference in the driving pressure, psi (kPa).

Osmotic pressure, π°, in dilute solutions varies with the concentration and temperature of the solution in the same variation as the ideal gas. For highly concentrated solutions, the osmotic pressure coefficient, $\emptyset_c$, should be considered as in the following equation (Weber, 1972):

$$\pi^{\circ} = \emptyset_c \frac{n}{V_m} RT \qquad (3\text{-}2)$$

Where, $\emptyset_c$= osmotic pressure coefficient, n = number of moles of solute, V_m = molar volume of water (18 cm^3/mole at 25°C), R = universal gas constant (0.083145 bar/mole.K) and T = absolute temperature (T°C+273).

Solvent permeate flux, F_w^o, can be calculated by using the following equation developed by Geraldes et al., (2005) in their model:

$$F_w^o = W_p[P - \pi_m + \pi_p] \qquad (3\text{-}3)$$

Where P is the driving pressure, psi (kPa) in the feed channel and π_m and π_p are the osmotic pressures at the surface of the membrane in the feed channel and the permeate channel, respectively. W_p is the water permeability coefficient or water flux through the membrane, $m.sec^{-1}.atm$, which is a characteristic of the membrane and the solution. Water permeability coefficient through the membrane, W_p, is often provided by the membrane manufacturers (Kucera, 2010; Hessami et al., 2009) or it can be calculated according to the following equation if the effective diffusion coefficient of water through the membrane, $D_{l,w}^o$, is reported by the manufacturer (Geise et al., 2011; Weber, 1972):

$$W_p = \frac{D_{l,w}^o C_w V_m}{RT\delta_m} \qquad (3\text{-}4)$$

In the last equation, C_w is the concentration of the water in the membrane (obtained from the manufacturer) and, δ_m is thickness of the membrane, m.

Equation (3-4) coupled with equation (3-3) indicates the obvious correlation between the thickness of the membrane and the solvent permeate flux, F_w^o. In other words, by increasing membrane thickness, solvent permeate flux will decrease (Weber, 1972).

Solute flux through the membrane, F_i^o, exists as a result of the high difference in the solute concentration across the membrane and can be estimated by the following equation (Geise et al., 2011; Kucera, 2010; Hoek et al. 2008; Geraldes et al., 2005; Avlonitis et al., 1993):

$$F_i^o = K_p(C_F - C_p) \qquad (3\text{-}5)$$

Where C_F and C_p are the solute concentrations at the membrane surfaces in the feed side and the permeate side, respectively. K_p is the solute permeability coefficient of the membrane, m.sec^{-1}, (salt diffusivity through the membrane) and can be calculated according to the following equation (Geise et al., 2011; Weber, 1972):

$$\mathrm{K_p} = \frac{\mathrm{D_{l,i}^{o} K_d}}{\delta_m} \qquad (3\text{-}6)$$

$D_{l,i}^{o}$ in equation (3-6) is the average diffusion coefficient of solute within the membrane and K_d is the solute partition coefficient between the solution and membrane phases. In other words, $\mathrm{K_d}$ is the ratio between the solute concentration in the membrane face in contact with the feed solution, $\mathrm{C_F^m}$, to the solute concentration in the feed solution, $\mathrm{C_F}$ (Geise et al., 2011).

$$\mathrm{K_d} = \frac{\mathrm{C_F^m}}{\mathrm{C_F}} \qquad (3\text{-}7)$$

The solute-permeability coefficient of the membrane, K_p, is determined by the manufacturer for each particular membrane type. According to Weber, (1972) and Lonsdale et al., (1965), "the distribution coefficient, $\mathrm{K_d}$, is usually constant in the range of interest for cellulose acetate membranes." Solute permeability through a membrane is affected by many parameters. Increase of feed water temperature, for example, can increase the salt permeability through the membrane. Also, brackish water membranes have higher salt passage rates than seawater membranes. Moreover, monovalent ions pass more readily than divalent ions (Bartels et al., 2005).

The difference of solute concentration between the feed side, $\mathrm{C_F}$, and permeate side, $\mathrm{C_p}$, to the concentration of the solute in the feed channel, $\mathrm{C_F}$, can be defined as the *solute rejection* by the reverse osmosis membrane, R_i°, and can be estimated by using the following equation (Weber, 1972; Hoek et al. 2008);

$$R_i^{\circ} = \frac{C_F - C_p}{C_F} \qquad (3\text{-}8)$$

Membrane fouling can be indicated by calculating the *concentration polarization factor*, CP, which can be defined as the ratio of solute or salt concentration at the membrane surface in the feed side, C_{FL}, (laminar boundary layer) to the solute concentration in the feed channel, C_{FT}, (turbulent region). Concentration polarization factor can be found in the turbulent flow of the feed channel as follow (Weber, 1972; Brian, 1966):

$$CP = \frac{C_{FL}}{C_{FT}} \qquad (3\text{-}9)$$

In addition, *silt density index* (SDI) is the most widely used parameter to measure the potential of feed water suspended solids to cause membrane fouling. SDI is calculated according to the following equation (Kucera, 2010; Nakamura et al., 2009; Paul and Abanmy, 1990):

$$SDI = \frac{(1-\frac{t_1}{t_2})}{T} \qquad (3\text{-}10)$$

Where, t_1 is time required to fill the initial 500 ml of influent water, t_2 is the time required to fill 500 ml after the time (T) and T is the total run time which is normally 15 minutes.

Water *recovery* is referred to as the volume percentage of influent water recovered as permeate. In general, the recovery rate ranges from 50% to 85% and the typical designed rate is 75%. Recovery rate can be calculated using the following equation (Kucera, 2010):

$$\%\ \text{Recovery} = \frac{\text{permeate flow } (\frac{m}{s})}{\text{feed flow } (\frac{m}{s})} \times 100 \qquad (3\text{-}11)$$

3.4. Review of Previous Studies

Today, reverse osmosis membranes are the leading technology that is used to desalinate seawater and brackish water which are high in total dissolved solids (TDS). These two sources of water have different reverse osmosis parameters including foulants, salinity, waste brine (concentrate) disposal options and location of the plant (Greenlee et al., 2009). Much desalination research has been conducted using reverse osmosis membranes, making this technology a more competitive option among water supply alternatives. These studies included assessing and minimizing environmental impacts of concentrate, membrane fouling studies and control techniques including improvements of water pretreatment for membrane desalination, improving membrane configuration to achieve high-permeability of water and high-rejection of salts, and studies concerning reducing the costs of desalination (Malaeb and Ayoub, 2011; Greenlee et al., 2009; National Research Council, 2008).

Membrane fouling is the reduction in water (flux) transport across a unit area of membrane which is caused by feed water particles deposition on the membrane surface or in its pores in a way that degrades the membrane's performance. Fouling may occur as a result of microbial growth, scaling, or accumulating of dissolved organic materials, particulate and colloidal matters (Malaeb & Ayoub, 2011; Kucera, 2010; Tran et al., 2007; Speth et al., 2000). Since RO membranes are considered non-porous membrane, surface fouling of RO membrane can be considered the main fouling mechanism which occurs in the membrane (Greenlee et al., 2009; Amiri and Samiei, 2007). In general, seawater reverse osmosis membranes are fouled by organic matters, particulate materials, and biological growth. Colloidal particles such as clays and flocs, and suspended particles, such as aluminum and iron silicates, form a cake-layer on the membrane surface, while dissolved inorganic materials such as calcium carbonate cause fouling by interacting with the surface of the membrane (Greenlee et al., 2009; Reverter et al., 2001; Magara et al., 2000; Amjad et al., 1996). However, brackish water reverse osmosis membranes

are fouled by inorganic materials, such as calcium sulfate and calcium carbonate, and the most important fouling factor of the dissolved inorganic materials is concentration polarization (Greenlee et al., 2009). Another kind of fouling that occurs by accumulating or attaching microorganisms to the membrane surface, leading to the formation of biofilms, is a biological fouling or biofouling which causes a premature decrease of flux and pressure across the membrane (Greenlee et al., 2009; Morenski, 1992).

RO membrane fouling has been extensively studied in order to gain a better understanding of the fouling layer formation and morphology. The most common tools used in fouling layer investigation and providing morphological images are Scanning Electron Microscope (SEM), which is directly used to observe the fouling morphology, and the Atomic Force Microscope (AFM), which is used to measure the roughness of the membrane surface and the change of fouling layers. To obtain more precise information about the fouling layer such as the chemical composition, SEM is coupled with energy dispersive X-ray spectroscope (EDS) (Malaeb and Ayoub, 2011). Other spectroscopic tools, which have been used in RO membrane fouling studies, are confocal laser scanning microscopy (CLSM), inductively coupled plasma - atomic emission spectrometry (ICP-AES), infrared (IR) spectroscopy, and Fourier transform infrared spectroscopy (FTIR) (Karime et al., 2008; Tran et al., 2007; Chu and Li, 2005).

As mentioned earlier, brackish water RO plants consume lower energy than seawater RO plants resulting in lower price of water production. Thus, despite the small production capacity of brackish water RO plants, their number around the world is about two fold of seawater RO plants (Greenlee et al., 2009; Wangnick, 2002). Differences in typical operating parameters between brackish water RO system and seawater RO system which were reported by Greenlee et al., (2009) are shown in Table 3.1.

Table 3.1

Comparison of typical parameter values for seawater RO system and brackish water RO system (Greenlee et al., 2009).

Parameter	**Seawater RO system**	**Brackish water system**
RO permeate flux ($L/m^2/h$)	12 – 15 (open water intake) 15 – 17 (beach well)	12 – 45 (ground water)
Hydrostatic pressure (psi) (kPa)	800 – 1,160 5,500 – 8,000	87 – 435 600 – 3,000
Membrane replacement	20% per year Every 2 – 5 years	5% per year Every 5 – 7 years
Recovery (%)	35 – 45	75 – 90
pH	5.5 – 7	5.5 – 7
Salt rejection (%)	99.4 – 99.7	95 – 99

The main focus in the following literature is on brackish water RO membrane studies. However, some research on seawater RO membrane fouling is included. Cohen and Probstein (1986) developed a theoretical model of membrane fouling using colloidal material for a laminar flow. They used cellulose acetate membranes fouled by colloidal ferric hydroxide as an experimental part of the study to verify their model's results. They observed that in laminar flow the foulant growth rate was weak and became stronger once the flow turned turbulent. In addition, they found that, below 5×10^{-4}cm/s threshold trans-membrane velocity, no flux decline or fouling was observed. Sheikholeslami (1999) reported that in industrial water systems, several types of fouling (for instance inorganic and biological fouling) simultaneously occurred, for example crystallization fouling of calcium salts may promote biological fouling. Sheikholeslami and Tan (1999) used a flat sheet RO membrane and simulated silica solutions to investigate the relative effects of different concentrations of Ca^{+2}, Mg^{+2}, and SiO_2 on precipitation characteristics of silica. They concluded that dissolved silica concentration was significantly decreased by increase Mg^{+2}/Ca^{+2} ratio and, consequently, influenced silica polymerization rate. In addition,

they found that the concentration of dissolved silica in solution rapidly decreased by increase degree of super-saturation of magnesium and calcium ions. Moreover, the initial rapidly declined at the lowest initial silica concentration and higher Mg^{+2}/Ca^{+2} ratio after a period of operation.

Boerlage et al. (2000) investigated the application of the MFI-UF test (modified fouling index coupled with ultrafiltration membranes) as a tool to predict RO fouling potential. They found that this tool is reliable for measuring particulate fouling potential of RO feed water and can be used as an indication of the efficiency of various pretreatment processes for different particle size removals. Abbas and Al-Bastaki (2001) investigated the changes in water permeability coefficient and salt rejection of RO membranes after they had been used for more than 500 days to desalinate low salinity brackish water (2540 to 2870 mg/L). The results showed that water permeability coefficient dropped by 25% while salt permeability coefficient increased by about 85% resulting in salt rejection decline by 1.9%. They reported that variation of feed temperature with the seasons is one of the factors that influenced the performance of RO membranes.

Vrijenhoek et al. (2001) used a lab-scale RO membrane unit and Atomic Force Microscope (AFM) images to investigate the effects of membrane surface morphology on colloidal fouling rate of RO and NF membranes. Their results showed that flux decline was highly correlated with membrane surface roughness rather than smooth membranes because particles accumulate in the valleys of rough membranes and, consequently, valley clogging and membrane fouling. Using a flat sheet RO unit and scanning electron microscope (SEM) images, Sahachaiyunta et al. (2002) investigated the effect of presence of minute amounts of several inorganic cations on silica fouling of RO membrane. They concluded that iron was the most important inorganic cations which influenced silica fouling on the membrane surface compared to manganese, nickel and barium. Hoek et al. (2002) tested the change of the channel height (feed spacer) and shear rate (velocity gradient through a laminar hydrodynamic boundary layer) on

colloidal fouling of RO and NF membranes. Different channel heights noticeably influenced flux decline and the greater channel height produced thicker cake-enhanced osmotic pressure causing greater loss of flux. However, salt-rejecting membranes and cake enhanced osmotic pressure can lead to flux decline as a result of a combination of hindered back-diffusion of salt ions and enhanced salt concentration polarization (Hoek and Elimelech, 2003). Lee et al. (2005) investigated colloidal and natural organic matter (NOM) fouling mechanisms in RO and NF membranes. The results clarified that cake-enhanced osmotic pressure is the predominant mechanism of colloidal fouling of RO membranes and NOM-calcium complexion fouling of NF membranes. Bartels et al. (2005) reported that the composition and concentration of salt in feed water and membrane charge and chemistry can affect fouling and salt passage through RO membranes. The nature of foulants can vary not only in the feed water applied to the membrane but also in the type of the membrane process applied such as low versus high-pressure technologies; therefore, improvement of understanding of the membrane separation process, the composition of foulants, foulant effect on membrane permeability, and contaminant rejection are the key tools to improve membrane materials and the characteristics of membrane surfaces in order for fouling reduction (AWWA Membrane Technology Research Committee, 2005).

Chu and Li (2005) used Confocal Laser Scanning Microscopy (CLSM) and Scanning Electron Microscopy (SEM) images to study the distribution of the cake-layer thickness on the membrane. They reported that the fouling material was not uniformly distributed on the membrane surface. The membrane fibers were partially covered by an irremovable static sludge cake and partially by a thin sludge film that could wash away by aeration turbulence. Other studies investigated the effect of pretreatment of the feed water before its introduction to the RO membrane. Koyuncu et al. (2006) examined the effect of using several advanced pretreatment operations including conventional treatment by coagulation through filtration on membrane fouling. Their results suggested a reduction in membrane fouling, when biologically-enhanced

granular activated carbon filtration is used as an advanced pretreatment of a NF membrane. Kumar et al. (2006) used lab-scale equipment with a flat sheet membrane to evaluate the effect of pretreatment on seawater RO membrane fouling using different filtration size ranges. The results revealed that particulates matter greater than 1µm were the predominant matter of RO fouling. RO membrane fouling was significantly reduced after using a 0.1µm microfiltration membrane. Another study, Rover and Huisman, (2007), revealed that several used RO membranes showed large particles up to 1 mm in size on the surface of the membrane and some particles were sharp and irregular in shape with the potential to deeply penetrate the surface. In terms of mineral precipitate morphology, Koyuncu and Wiesner (2007) reported that calcium carbonate ($CaCO_3$) and calcium sulfate ($CaSO_4$) are the common precipitated salts on the membranes. Furthermore, their study showed that variation of organic matter concentration can change the crystal morphology of calcium carbonate and, hence, increases its precipitation on reverse osmosis membrane.

Further, Kim and Hoek (2007) investigated the hydrophilicity and hydrophobicity of the organic matter and their correlation to the RO membrane fouling and flux decline. They concluded that hydrophilic macromolecules can form a polarization layer as a result of foulant-membrane and foulant-foulant interfacial forces resulting in minimal flux decline, while hydrophobic macromolecules can lead to severe flux decline as a result of forming cake layers on the membrane surface. Norberg et al. (2007) used high organic brackish surface water (TOC ~ 21 mg/L) and 20 types of RO membranes to characterize and evaluate fouling resistant of low-pressure RO membrane [67-150 psi (462-1034 Kpa)]. They found that minimizing fouling was different from one membrane to another depending on membrane surface charge, hydrophobicity, and roughness. Hence, selecting commercial fouling resistant membranes depends on both foulants' characteristics and membrane surface properties. Tran et al. (2007) investigated the fouling of RO membrane after it had been used in a brackish water treatment desalination plant

for one year. The RO membrane was used to treat water which had total dissolved solids of 900 mg/L, a total organic carbon of 12 mg/L, and a turbidity of 0.5 NTU. Advanced analytical and microscopic techniques such as Inductively Coupled Plasma Atomic Emission Spectrometry (ICP-AES), Fourier Transform Infrared Spectroscopy (FTIR), and Optical and Electron Microscopic methods were used in the autopsy analysis of the top surface and the cross-section of the fouled RO membrane. The results showed that the fouling layer on the RO membrane surface had a varied thickness which ranged from less than 1µm to about 10 µm. The fouling layer with a thickness of less than 1µm, mainly consisted of particulate matter, which was mostly aluminum silicates. The fouling layer with a thickness of about 3 µm contained mostly extracellular polymeric substances from organisms and aluminum silicate. The fouling layer which had a thickness of about 10 µm consisted of two distinct regions. The first region with a thickness of (5-7) µm solely consisted of aluminum silicate crystals. The second region contained two distinct zones: an inner amorphous layer and an outer crystalline layer. In addition, the results showed that high concentration in the deposits including aluminum, calcium, chloride, and phosphorous were found on fouled RO membrane.

An autopsy has been done by Karime et al., (2008) on an RO membrane after it had been used to desalinate brackish water with salinity of 6000 mg/L in Zarzis, Tunisia. Autopsy results, using SEM, atomic force microscopy (AFM), FTIR, and infrared analysis and diffraction by X-ray as well as TOC measurement, revealed that 56% SiO_2, 16% clay, 13% organic matter, 6% $CaSiO_3$, 3% Fe_3O_4, 3% $AlPO_4$, and 3% $CaSO_4$ were the predominant compounds in the fouling layer. Another study conducted by Yang et al. (2008) investigated the composition of the fouling material on two-stage RO membranes in a brackish water treatment desalination plant located in Taiwan. Membrane autopsy, element analysis, dry weight identification, microbiological quantification, scanning electron microscopy- energy dispersive X-ray spectroscopy (SEM-EDX), ICP, and FTIR were used to characterize and identify the foulants on the RO membrane. Yang et

al. (2008) found that 85-93% of the total foulants were organic matter in the first stage, while 92-95% were inorganic matter in the second stage. In addition, the results displayed that about 85% of the inorganic fouling in the second stage was calcium. However, the major inorganic foulants in the first stage were aluminum (Al^{+3}), strontium (Sr^{+2}), silicon (Si), and barium (Ba^{+2}).

Jin et al. (2009) conducted a study to investigate the effects of change of feed water temperature on brackish water RO membrane performance. The results elucidated that increasing feed water temperature resulted in increasing solute diffusivity and decreasing solvent viscosity accompanied by increase in both water and salt permeability coefficients. In addition, mass transfer coefficient increased and concentration polarization factor decreased as feed water temperature increased. Further investigation of the influence of feed water temperature on organic (humic acid) fouling for the same membranes was conducted. Jin et al. (2009) reported that fouling by humic acid improved salt rejection as a result of its initial deposit causing increase in the negative charges density at the membrane-solution interface resulting in sealing the defects of the molecules in the polyamide thin film membrane. Furthermore, increasing feed water temperature reduced humic acid rejection. In a different study, Jawor and Hoek (2009) investigated the effects of feed water temperature on flux, rejection, and inorganic fouling by gypsum scale formation for brackish water RO membrane. The results showed that salt rejection and concentration polarization decreased by increase feed water temperature. This attributed to the diffusion of salt through the membrane. As temperature of the feed water increased, diffusion of salt through the membrane quickly increased and reduced concentration polarization. In addition, flux decline was observed to be fast as a result of quick gypsum crystallization occurrence. Also, a significant different flux decline with the variation of temperature was observed. Alspach et al. (2011) conducted a study on a two-stage RO brackish surface water treatment plant in Rifle, Colorado to investigate the fouling of RO membrane and its correlation to the level of pretreatment and the operating processes of RO in terms of recovery, cleaning

frequency, and other factors. The study included monitoring the trend of water permeation coefficient, salt permeation coefficient, and the differential pressure during four test runs of the RO system. In addition, feed pressure, permeate flux and salt density index (SDI) were also monitored. RO membranes were cleaned after each run by using low and high pH clean. The results indicated that water permeability coefficient dropped by about 40% in the first three runs while it was more gradual in run 4. Moreover, the salt permeability coefficient, unlike what was expected, slightly dropped indicating that scaling was not the source of fouling. Autopsy results revealed that colloidal particulate matters were the major foulants of RO membranes.

Many other studies worldwide related to brackish water as a source of water desalination plants have been done such as brackish water RO desalination plant in the Gaza Strip by Frenkel and Gourgi (1995), brackish groundwater treatment by reverse osmosis in Jordan by Afonso, et al. (2004), and desalination of brackish groundwater in Zahedan city in Iran by Lashkaripour and Zivdar (2005).

The previous studies displayed the problems that can face seawater and brackish water RO systems which mainly focused on membrane fouling and the dominant constituents in the fouling layer depending on the type of source water. Also, many factors that can affect or reduce membrane fouling layer such as feed temperature, height of feed channel, feed pressure, type of pretreatment and filtration size, and the type of RO membrane itself were investigated. Other studies investigated the effect of the change of the organic matter concentration on RO fouling.

CHAPTER IV

MATERIAL AND METHODS

4.1. Feed Water

Several studies (Al-Saad et al. 2010; Hamdan et al. 2010; UNEP, 2007; Richardson and Hussain, 2006) conducted water quality investigations in different locations of the Iraqi marshes and some of the selected sites are shown in Figure 4.1. In addition, Table 4.1 displays some of the water quality parameters of 19 sites (denoted in Figure 4.1) located in these marshes, which were reported by Al-Saad et al. (2010), Hamdan et al. (2010), United Nation Environment Program, UNEP, (2007), and Richardson and Hussain (2006). The minimum and maximum values of major parameters included in this table are 7.36 - 9.52 pH, 3.6 - 52 NTU turbidity, 84 - 366 mg $CaCO_3$/L alkalinity, 420 – 1,480 mg $CaCO_3$/L total hardness, 98 – 1,278 mg/L sulfate (SO_4^{-2}), 30 – 1,595 mg/L chloride (Cl^-), 148 – 920.2 mg/L sodium (Na^+), and 1.2 – 13.9 mg/L total organic carbon (TOC).

From Table 4.1, it can be seen that some of the important constituents of the water quality are missing. TOC, for example, is available only at the first six locations (1, 2, 3, 4, 5, and 6) which were reported by UNEP (2007), and the last three locations (17, 18, and 19), which were reported by Richardson and Hussain (2006). Moreover, sodium is available at two locations (13 and 14) which were reported by Al-Saad et al. (2010), and two other locations (15 and 16) which were reported by Hamdan et al. (2010). After studying the available data in Table 4.1 and their distribution over the Iraqi marshes, three water analyses were selected as feed water to run a lab-scale RO membrane system in this study. The locations of these water analyses, which are 1 (Al-Jeweber), 5 (Al-Hadam), and 6 (Al-Masahab), are circled in Figure 4.1. One of the reasons behind selecting these water analyses is that their locations represent nearly all the area of the marshes because they were located in three different provinces in the south of Iraq (Thi-Qar, Maysan, and Al Basrah). Moreover, the concentration of the constituents of water quality of these sites varied from high levels to low levels. For instance, the concentrations of TDS, SO_4^{-2}, Cl^-, Ca^{+2}, and Mg^{+2} at location 6 were 2,750, 692, 1,100, 118, and 85 mg/L, respectively, which are considered as high levels of concentration. However, the concentrations of TDS, SO_4^{-2}, Cl^-, Ca^{+2}, and Mg^{+2} at location 5 were 1,270, 310, 440, 49.9, and 17.2 mg/L, respectively, which are considered as low levels of concentration. At location 1, the concentrations of TDS, SO_4^{+2}, Cl^-, Ca^{+2}, and Mg^{+2} were 2,380, 670, 710, 79.4, and 51.7 mg/L, respectively, which can be considered as moderate levels of concentration compared to the other two locations (5 and 6) (UNEP, 2007).

Salinity and TOC were also considered in selecting the locations of the water quality samples. Location 5 had low salinity (700 mg/L) and low TOC (1.2 mg/L), while location 6 had high salinity (2,000 mg/L) and high TOC (4.71 mg/L). In addition, these three sites were chosen in different places that have different sources of water. Location 1 is located where the source of the water for the marshes is the Euphrates River, while location 5 is located where the Tigris

River is the source water. However, location 6 is located further to the south near Shatt al-Arab where the Tigris and Euphrates Rivers are joined.

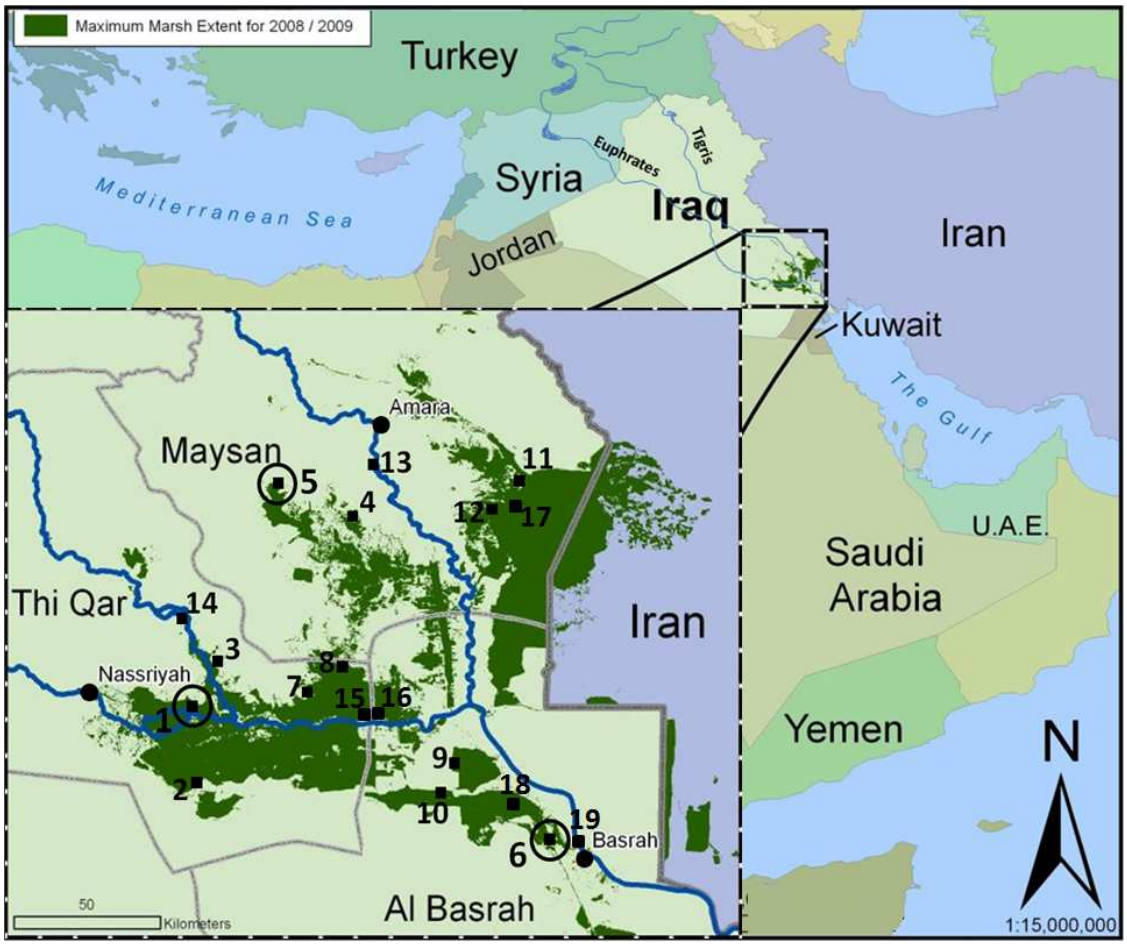

Figure 4.1. Map of the Iraqi marshes and the locations (■) of the water quality tests: (1) Al-Jeweber; (2) Al-Kirmashiya; (3) Badir Al-Rumaidh; (4) Al-Sewelmat; (5) Al-Hadam; (6) Al-Masahab; (7) Baghdadia 1; (8) Baghdadia 2; (9) Al-Barga; (10) Al-Nagara; (11) Um-Al-Neiage; (12) Um-Al-Warid; (13) Tigris River in Maisan; (14) Euphrates River in Thi-Qar; (15) Abu Al-Narssy; (16) Abu Chwelan; (17) Al- Hawizeh; (18) Al-Hammar; (19) Downstream Shatt Al-Arab (adopted from UNEP (2007) and Holmes (2010)).

Table 4.1

Water quality analysis of the marshes in southern Iraq (Al-Saad et al. 2010; Hamdan et al. 2010; UNEP, 2007; Richardson and Hussain, 2006).

Location / Parameter				pH	Electrical Conductivity mS/cm	Salinity, mg/L	Total Dissolved Solids (TDS), mg/L	Turbidity, NTU	Total Suspended solids (TSS), mg/L	Alkalinity, mg $CaCO_3$/L	Total Hardness, mg $CaCO_3$/L	Sulfates (SO_4^{-2}), mg/L	Chloride (Cl), mg/L	Biochemical Oxygen Demand (BOD_5) mg/L	Sodium (Na^+), mg/L	Total Organic Carbon (TOC) mg/L	Calcium (Ca^{+2}), mg/L	Magnesium (Mg^{+2}), mg/L	Nitrate (NO_3^-) (mg/L)	Potassium (K^+) mg/L	Zinc (Zn^{+2}) (mg/L)	Phosphate (PO_4^{-3}) (mg/L)
1	Al-Jeweber	2006	Max.	8.32	3.57	1800	2380	9.3	45	142	1000	670	710	6.3	–	1.74	79.4	51.7	0.22	–	0.017	0.02
			Avg.	8.23	2.55	1200	1686	9.3	20	122	840	314	520	6.1	–	1.74	79.4	51.7	0.033	–	0.017	0.0013
2	Al-Kirmashiya	2006	Max.	7.66	4.9	2500	2748	3.6	41	210	1460	586	920	3	–	2.05	91.1	30	0.023	–	0.011	0.018
			Avg.	7.46	3.47	1700	1632	3.6	17	128	822	362	750	1.95	–	2.05	91.1	30	0.012	–	0.011	0.0017
3	Badir Al-Rumaidh	2006	Max.	9.52	1.74	700	1213	7	14	94	610	300	320	4.6	–	3.92	37.6	45.9	0.005	–	–	0.01
			Avg.	8.6	1.47	500	1090	7	12	94	490	250	300	3.5	–	3.92	37.6	45.9	0.004	–	–	0.0017
4	Al-Sewelmat	2006	Max.	8.77	1.95	800	2100	21.1	53	128	560	250	390	8.2	–	1.57	53.2	19	0.204	–	0.007	0.0147
			Avg.	8.6	1.2	400	822	21.1	35	124	460	102	300	6.5	–	1.57	53.2	19	0.193	–	0.007	0.0007
5	Al-Hadam	2006	Max.	8.53	1.7	700	1270	51	149	152	630	310	440	6	–	1.2	49.9	17.2	0.21	–	0.009	0.0334
			Avg.	8.2	1.29	400	1144	51	135	148	500	90	280	5	–	1.2	49.9	17.2	0.18	–	0.009	0.0031
6	Al-Masahab	2006	Max.	7.93	5.5	2000	2750	52	92	134	1040	692	1100	3	–	4.71	118	85	0.042	–	0.015	0.0162
			Avg.	7.8	3.4	1700	2411	32.8	34	118	890	680	960	2.5	–	4.71	118	85	0.042	–	0.015	0.0012
7	Baghdadia 1	2005	Max.	8.8	4.94	2600	3308	11.98	35	317	1480	1278	1595	36	–	–	248	238	0.016	–	–	0.0024
			Avg.	7.8	3.18	1690	2042	5.01	16	197	791	648	747	9.2	–	–	133	112	0.016	–	–	0.0024
8	Baghdadia 2	2005	Max.	8.76	4.94	2600	3040	11.98	34	292	1336	1109	886	20.8	–	–	192	208	0.021	–	–	0.0021
			Avg.	7.7	2.8	1460	1729	5.71	16	219	689	617	575	2.28	–	–	117	96	0.021	–	–	0.0021

Table 4.1 (continued)

9	Al-Barga	2005	Max.	8.7	3.97	2000	2758	25.11	36	280	1140	973	1098	13.14	–	–	184	165	0.006	–	–	0.0022
			Avg.	7.8	3.17	1630	2040	12.09	18.2	209	696	612	738	3.75	–	–	129	90	0.006	–	–	0.0022
10	Al-Nagara	2005	Max.	8.17	3.85	1900	2708	26.82	51	280	1120	893	1028	12.6	–	–	176	204	0.006	–	–	0.0023
			Avg.	7.7	1.6	1600	2029	14.96	28	225	711	562	655	4.64	–	–	118	101	0.006	–	–	0.0023
11	Um-Al-Neiage	2005	Max.	7.92	2.04	900	1606	9.76	28	366	920	464	431	7.2	–	–	128	160	0.048	–	–	0.008
			Avg.	7.5	1.35	540	900	4.57	11	255	484	305	304	3.55	–	–	87	62	0.048	–	–	0.008
12	Um-Al-Warid	2005	Max.	8.64	1.93	800	1474	86	71	292	900	450	673	10	–	–	200	155	0.059	–	–	0.0086
			Avg.	7.8	1.29	530	891	39	38.58	227	481	285	320	5.07	–	–	93	60	0.059	–	–	0.0086
13	Tigris in Maisan	1999	–	8	2.3	–	1566	–	–	149	620	487	373	–	266	–	137	65	–	4.5	–	0.16
		2003	–	7.85	1.4	–	–	–	–	195	–	384	234	–	148	–	88	96	–	–	–	–
14	Euphrates in Thi-Qar	2001	–	7.9	5.3	–	3841	–	–	191	1261	1073	1162	–	780	–	204	180	–	15.0	–	0.09
		2003	–	7.75	3.4	–	–	–	–	122	–	960	660	–	437	–	200	124	–	–	–	–
15	Abu Al-Narssy	2006	April	7.8	2.2	–	–	–	4.4	–	–	560	581.3	–	398.2	–	68.1	37.5	0.0003	5.2	–	0.00005
			Aug.	7.4	3.5	–	–	–	5.8	–	–	779.7	784.7	–	920.2	–	200	141.4	0.0006	14.9	–	0.00018
16	Abu Chwelan	2006	April	7.5	2.8	–	–	–	12	–	–	515.6	374.2	–	618.4	–	155.7	71.3	0.0006	10.2	–	0.00011
			Aug.	7.4	3.2	–	–	–	1.8	–	–	594.5	746.9	–	892.2	–	367.7	146.2	0.0012	15.1	–	0.00023
17	Al- Hawizeh	2003	June	7.64	1.74	870	1130	–	–	–	–	–	–	–	–	4.68	–	–	2.055	–	–	0.408
18	Al-Hammar	2003	June	7.95	1.91	960	1240	–	–	–	–	–	–	–	–	13.9	–	–	7.316	–	–	2.013
19	Downstream Shatt Al-Arab	2003	June	7.51	4.1	2130	3020	–	–	–	–	–	–	–	–	4.95	–	–	3.76	–	–	0.45

The most common vegetation in the Iraqi marshes are common reed (*phragmites australis*), reed mace (*typha angustifolia*), giant reed (*arundo donax*), and papyrus (*cyperus papyrus*) (ArabHunter.com 2012; Hamdan et al. 2010). In order to create TOC and add it to the simulated water at the same TOC concentration, as seen in the Iraqi marshes, reed mace (*typha angustifolia*) and giant reed (*arundo donax*), which were available in Oklahoma, were used. The genius and species of the plants were identified by Dr. Mark Fishbein (Personal Communication, 2013). Two mixed bunches of these plants were submerged into distilled water. One bunch was already wet (submerged in the water) denoted as S1, and the other one was dried denoted as S2. The plants were left in the distilled water for more than 9 months, and the pH of the two solutions was frequently measured. After significant breakdown of the plants, the solutions of S1 and S2 were decanted and their COD was measured by using the Hach Chemical Oxygen Demand (COD) high range method (method 8000) (Hach Company, Loveland, CO). The main purpose of measuring COD was to know the approximate level of TOC concentration in each solution. In addition, the Hach Total Organic Carbon (TOC) low range direct method (method 10129) (Hach Company, Ames, IA) was used to test the TOC level of the two solutions. A DR5000 spectrophotometer (Hach Company, Loveland, CO) was used in both COD and TOC test methods. The results of TOC concentration of solution S1 were confirmed by Accurate Environmental laboratory (Accurate Environmental, Stillwater, OK). To keep the TOC concentration constant for both samples, the solution was screened through sieve number 40 (0.422 mm) to remove all the remaining plant material and the remaining solution was stored in dark containers at room temperature.

The two samples (S1 and S2) were further analyzed to determine the concentration of ions which need to be considered during the making of the feed water batches. Ion chromatography analysis (DX-120, Ion Chromatograph, Dionex, Hayward, CA) was used to determine the concentrations of the anions (SO_4^{-2}, Cl^-, and PO_4^{-3}) of each sample. In addition,

Inductively Coupled Plasma (ICP) spectrometer (Spectro Ciros at the Soil, Water and Forage Analytical Laboratory, Oklahoma State University) was used to find the concentrations of the cations (Ca^{+2}, Mg^{+2}, Na^{+}, Fe^{+2}, K^{+}, and Zn^{+2}) of S1 and S2. Based on the available ions in Table 4.1, an electrical balance was used to determine the missing concentrations of sodium for the three selected sites.

The following inorganic salts were used to prepare the salt stock solutions. Zinc sulfate ($ZnSO_4.7H_2O$, certified A.C.S.), calcium nitrate ($Ca(NO_3)_2.4H_2O$, certified A.C.S.), magnesium chloride ($MgCl_2.6H_2O$, certified A.C.S.), sodium bicarbonate ($NaHCO_3$, certified A.C.S.), sodium sulfate anhydrous (Na_2SO_4, certified A.C.S.), and sodium chloride (NaCl, certified A.C.S.) were purchased from Fisher Scientific Company (Fisher Chemical, Fair Lawn, New Jersey). Calcium chloride dihydrate ($CaCl_2.2H_2O$, A.C.S. grade) was purchased from Hach Company (Ames, Iowa). After calculating the required weight of each chemical compound to make up the selected water quality, the salt was dissolved in 48 liters of distilled water using two glass bottles (25 liter each), and a calculated volume of prepared TOC solution was added to approach the TOC concentration of the selected water quality. A magnetic stirrer (Thermolyne Magnetic Cimarec 3 Stirrer, Lab Extreme, Inc., Kent City, MI) was used to stir the mixture at a moderate speed for 24 hours to make sure of the solution homogeneity. To ensure that the concentrations of the prepared solution constituents were close or similar to the selected site water quality, water analysis of each prepared batch was frequently done. In addition to the ions (cations and anions) and the TOC concentration, the water analysis included electrical conductivity, which was measured by a conductivity meter (Accumet 30, Fisher Scientific, Pittsburgh, PA), alkalinity of the stock, which was determined by using acid-base titrations method (Jenkins et al., 1980a), and hardness (Jenkins et al., 1980b). Moreover, because of the water temperature of the marshes ranges from 11°C to 37°C during the year (UNEP, 2007), the selected feed water temperatures in this study were 11°C and 37°C.

4.2. Lab-Scale Filtration System

A commercial bench-scale cross-flow filtration unit, a stainless steel SEPA CF Membrane Element Cell (purchased from Sterlitech Corporation, Kent, WA) was used to conduct all fouling experiments in this study. The SEPA CF Membrane Cell is designed to handle a maximum pressure of 1000 psi (6,895 kPa) and to accommodate a 7.5 inch × 5.5 inch (19.1 cm × 14 cm) flat sheet membrane. A 2 mil (0.051 mm) Sepa CF shim which has dimensions of 5.74 inch × 3.74 inch (14.6 cm × 9.5 cm) was installed in the bottom of the cavity of the cell body bottom to prevent the membrane from distorting or wrinkling. Then, a 17 mil (0.432 mm) Sepa CF feed spacer (feed channel) which has the same dimensions of the shim was placed on top of the shim. After that, the membrane was placed over the feed spacer. Hence, the effective area of the RO membrane was 21.5 $inch^2$ (138.7 cm^2). In addition, a permeate carrier that has similar dimensions to the feed spacer and the shim was used as a product channel. The SEPA CF membrane element cell, membrane cell, shim, feed spacer, precut RO membrane, and permeate carrier are shown in Figure 4.2.

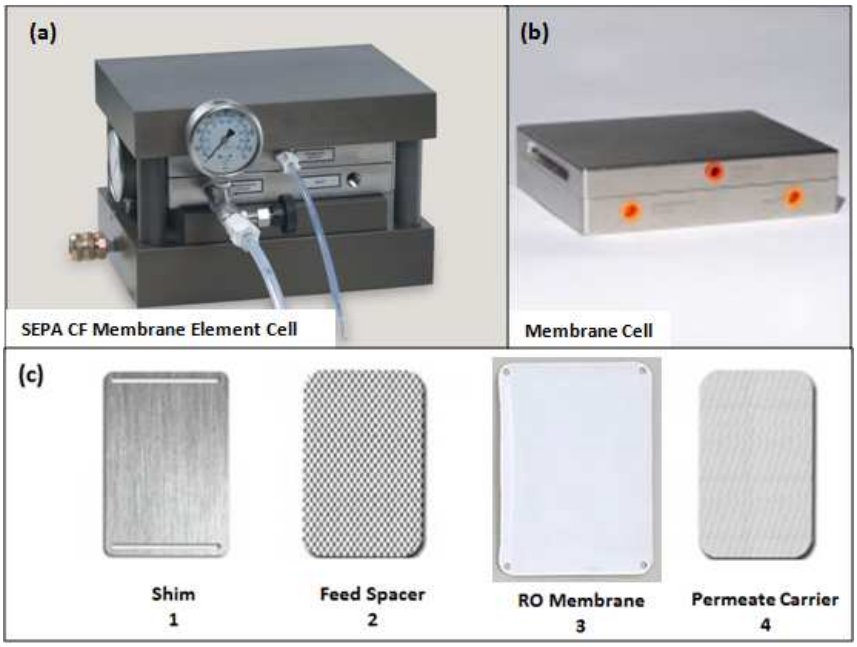

Figure 4.2. (a) SEPA CF membrane element cell (b) membrane cell (c) Parts of filtration system inside membrane cell (from bottom to the top) (Sterlitech Corporation, 2010).

In addition to the SEPA CF Membrane Element Cell, the experimental system contained the following parts: (1) low pressure feed pump which consisted of two MasterFlex drives (Cole-Parmer Instrument Co. Chicago, IL), five MasterFlex standard pump heads for L/S 16 tubing, and three MasterFlex standard pump heads for L/S 14 tubing, all combined together; (2) 15 gallon (56.78 L) heavy duty polyethylene feed tank (13.75 inch x 27.5 inch (35 cm x 70 cm), U.S. Plastic Corp., Lima, OH); (3) heated immersion circulator (PolyScience, Global Scientific Supply, Wilmington, NC); (4) 1 µm micron spun polypropylene filter cartridge (Pentek, Pentair Water, Milwaukee, WI) to prevent membrane damage from large particles; (5) 15 gallon (56.78 L) heavy duty polyethylene break tank (13.75 inch x 27.5 inch (35 cm x 70 cm), U.S. Plastic Corp., Lima, OH); (6) 1.8 gpm (6.83 Lpm) high pressure pump (M-03S Hydracell CC Pump, Wanner Engineering, Inc. Minneapolis, MN) connected to a 4 cubic inch pulsation dampener (Blacoh Fluid Control Co., Riverside, CA) to produce steady fluid flow and protect the pump from cavitation; (7) high pressure relief valve (SS - R3A series, Swagelok, Camarillo, CA) to make sure that the system pressure is not exceeding 1000 psi (6,895 kPa); (8) variable speed drive for use with variable speed 1.5 Hp motor (Commander SK, Emerson Industrial Automation); (9) Sepa CF hydraulic hand pump (SPX Power Team, Rockford, IL) to raise and constantly maintain the hydraulic pressure inside the cell holder; (10) two high pressure needle valves (SS-1RS6, Swagelok, Camarillo, CA) to control the flow of the feed water; (11) two pressure gauges (SS PG1500, Swagelok, Camarillo, CA and 2 In LM 0-100 psi, WIKA Instrument Corporation, Lawrenceville, GA) to monitor high feed water pressure and low feed water pressure, respectively; (12) site read panel mount flow meter (F-550, Blue-White Industries Ltd., Huntington Beach, CA), in-line water flow meter (H213A-020, Hedland Division of Racine Federated Inc., Racine, WI), and Glass Tube Flowmeter (3/4-SLG-01 King Instrument Company, Garden Grove, CA) used to measure the flow of the concentrate, high pressure feed water, and low pressure feed water, respectively; and (13) 12 gallon (45.43 L) plastic tank (Centrex Plastics, LLC, Findlay, OH) to collect the permeate. In addition, two 16 gallon (60.57 L) plastic tanks

(Duraflex 70qt Muck Tub, Miller Manufacturing Co. Inc., Glencoe, MN) were used as ice containers for low temperature runs. Moreover, a 250 ml graduated Pyrex cylinder (number 3023, USA) and an 1000 ml graduated Pyrex cylinder (number 1000, Germany) with a ±5% accuracy, were used to volumetrically measure the flow rate of the permeate. The experimental design used in this study followed the experiment system done by Sahachaiyuta et al. (2002). The concentrate of the RO system was recycled to the feed tank leading to a higher TDS concentration in the feed water. This process represented the successive stages of the brackish water RO plants, where the feed water to a second stage is the concentrate from the first stage as opposed to most seawater RO plants where the feed water to the second stage is the permeate from the first stage (Greenlee et al., 2009). A schematic diagram of the experimental system is presented in Figure 4.3, and the primary assembled parts are shown in Figure 4.4.

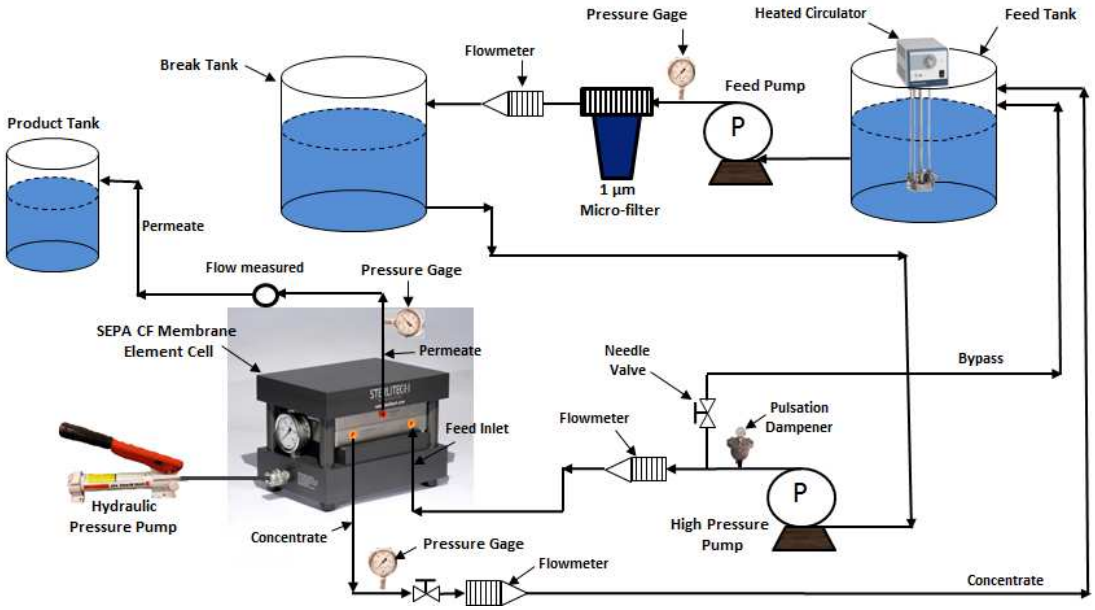

Figure 4.3. Schematic diagram of the experimental RO system.

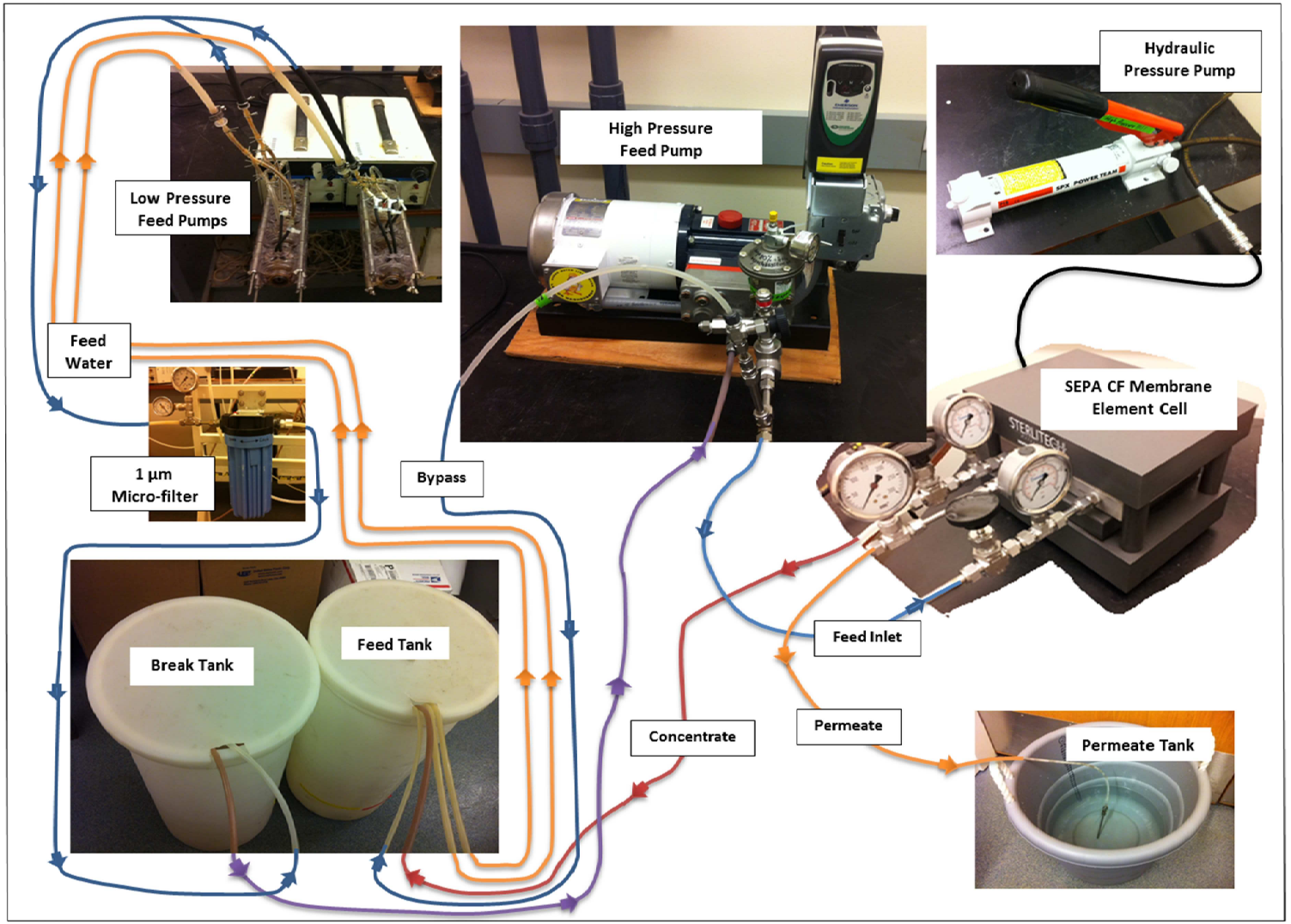

Figure 4.4. Schematic and Photographic diagram of the experimental RO system.

Three different types of RO membranes were tested in this study, and are listed in Table 4.2. These types were selected from eight different available types of membranes (purchased from Sterlitech Corporation, Kent, WA). The selection of the membranes was based on the material that they were manufactured from (polyamide, cellulose acetate, and thin-film composite polyamide). These materials represent the vast majority of materials used to make RO membranes (Kucera, 2010). In terms of comparison among these three types of membrane, cellulose acetate membrane has a smooth surface that makes this type of membrane less susceptible to fouling than the other types (Kucera, 2010; HCTAB, 2005). However, thin-film composite polyamide membranes are easier to foul, but easier to clean than the polyamide membranes (Sheikholeslami and Zhou, 2000). In addition, cellulose acetate membranes can tolerate free chlorine (up to 1 ppm continuously), while polyamide membranes are susceptible to oxidation by free chlorine. However, thin-film composite polyamide membranes can tolerate free chlorine less than 0.02 ppm (Kucera, 2010). Typical water fluxes produced by polyamide membranes are lower than those produced by cellulose acetate and thin-film composite polyamide membranes, but have the least salt passage, as shown in Table 4.2. In terms of temperature, thin-film composite polyamide membranes can be operated at temperatures up to 45^{o}C, while cellulose acetate membranes can tolerate temperatures up to 35^{o}C (Kucera, 2010). However, the cellulose acetate membrane used in this study can tolerate temperature up to 135 °C (275 °F) (Sterlitech Corporation, 2010).

Table 4.2

Flat sheet RO membranes specifications of the system (Sterlitech Corporation, 2010).

Designation	**Manufacturer**	**Polymer**	**Rejection Percentage (%)**	**Typical Flux, gal/day/ft^2 (L/day/m^2)**	**Typical Pressure, psi (kPa)**
AD	GE Osmonics	Polyamide	99.5	15 (612)	800 (5,516)
CE	GE Osmonics	Cellulose Acetate	97	23.5 (958)	420 (2,896)
SE	GE Osmonics	Thin Film Composite Polyamide	98.9	22 (897)	425 (2,930)

4.3. Experimental Procedures

Prior to each experiment, the system was run for 24 hours, using deionized water with the selected RO membrane, at the pressure of 250 psi (1,724 kPa), feed water flow of 0.55 gpm (2.08 Lpm), and at the selected temperature (11°C or 37°C) for the run. The purpose of running deionized water through the system is to avoid any change in the physical properties of the membrane, consequently avoiding permeate decline by membrane compaction during an experiment run (Jawor and Hoek, 2009), and also, to ensure that the system is properly working. Then, the deionized water was replaced with 12.68 gallon (48 L) of prepared feed water for each run. The temperature of feed water was adjusted and maintained at the selected value using a heated immersion circulator for a high temperature (37°C) and lab ice held in the outer containers for a low temperature (11°C), as shown in Figure 4.5.

Figure 4.5. Ice containers used for low temperature runs.

The feed water was pumped at a constant flow rate of 0.6 gpm (2.27 Lpm) from feed tank through a 1 µm filter cartridge to the break tank using low pressure pumps. Then, feed water was pumped at the same flow rate through the RO membrane filtration cell. The system pressure was

kept in the range of 380 psi - 400 psi (2,620 kPa – 2,757 kPa) by using the two high pressure needle valves. Each run continued until 70% to 80% water recovery of the total volume (48 L) was achieved. Permeate flow was measured continuously during the run time. In addition, conductivity and pH of both permeate and concentrate were measured for each run. Moreover, three corresponding samples (at the beginning, middle, and end of each run) were taken from the concentrate and permeate to measure the concentration of the ions.

A total of 24 runs, as shown in Figure 4.6, were implemented by repeating the same experimental procedures which were mentioned above. Three different feed waters, three different RO membranes, and two temperature values were used as the primary variables to run the experiments. Using prepared feed water for location 6, shown in Figure 4.1, 12 runs were conducted under different conditions. Runs 1 through 6 were carried out without using the MF membrane as a pretreatment. Runs 1, 3, and 5 were implemented by using the SE, CE, and AD - RO membranes, respectively, under the water temperature of 37^{o}C. Runs 2, 4, and 6 were also implemented by using the SE, CE, and AD - RO membranes, respectively, but under the water temperature of 11^{o}C. To investigate the effect of the pretreatment on fouling, feed waters of runs 7 through 12 were filtered through a 0.1 micron MF membrane (HFK-618, Koch membrane) before using the RO membrane. Feed water was pumped through the MF membrane at the same conditions as the RO membrane run with the exception of the feed pressure which was kept at 150 psi (1,034 kPa).

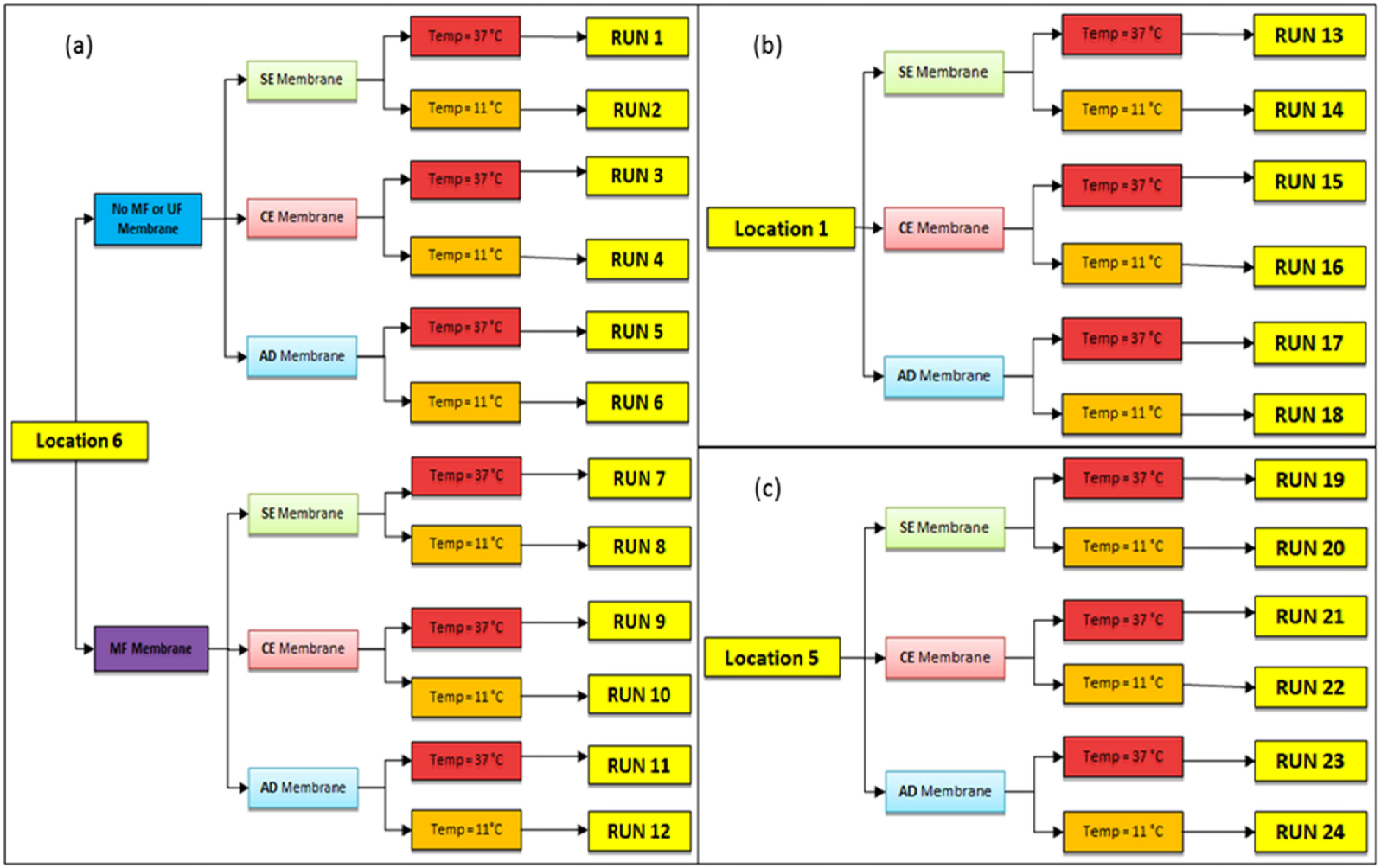

Figure 4.6. Diagram of all the implemented runs for the experimental RO system (a) location 6; (b) location 1; (c) location 5.

Using prepared water of location 1 as feed water, runs 13 through 18 were conducted under the same conditions of runs 1 through 6. Likewise, prepared water of location 5 was used as feed water of runs 19 through 24. Operation time of all runs was determined by achieving 70 to 80 % water recoveries. After achieving the required water recovery for each experiment, the fouled membrane was gently removed from the cell. Fourier Transform Infrared Spectroscopy (FTIR) (Nexus, Thermo Electron Corporation; Madison, WI) spectrum (500 – 4000 cm^{-1}) on the unused and fouled membrane was taken to identify the organic matter present on the membrane surface. In addition, Zeiss NEON High Resolution Scanning Electron Microscope (SEM), equipped with Energy-Dispersive X-ray Spectroscopy (EDXS) and Secondary Ion Beam (FIB) (Samuel Roberts Noble Electron Microscopy Laboratory, University of Oklahoma), was used to directly observe the fouled materials deposited on the surface of the RO membrane. Samples from the unused membranes and different fouled membranes were cautiously cut to preserve the original biomass composition of the material. Then, the samples were sputter-coated with iridium (Ir) to prevent charge up of the material surface which can cause high brightness and result in weak contrast in the image.

CHAPTER V

RESULTS AND DISCUSSION

5.1. Feed Water

During the breakdown time of the plants which were used to produce TOC for the feed water, the pH of S1 and S2 was repeatedly measured. Figure 5.1 shows the trend of the pH of both samples during this time.

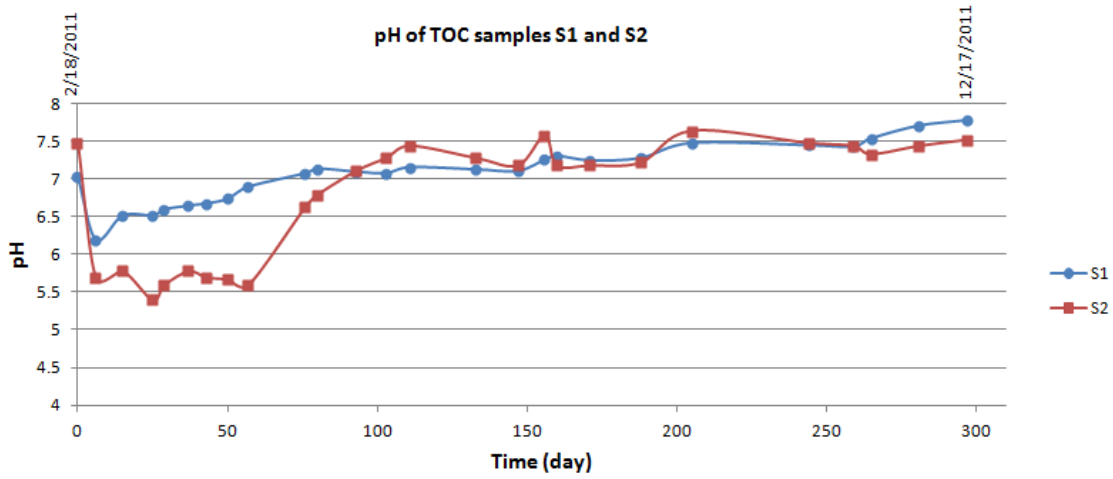

Figure 5.1. Trends of pH of TOC samples (S1 and S2) for the period from 2/18/2011 to 12/17/2011.

COD test results revealed that S1 and S2 had 352 and 155 mg/L, respectively. Using the low range Hach TOC test, TOC results were 54 and 14 mg/L for sample S1 and S2, respectively. As expected, the TOC of S1 was much higher than that of S2, because the color of S1 (18 NTU turbidity) was clearly darker than S2 (10 NTU turbidity), as shown in Figure 5.2. In addition, Accurate Environmental Laboratory results [APHA, AWWA, and WER (2005)] for TOC concentration of solution S1 was 59.6 mg/L which was very close to Hach TOC result.

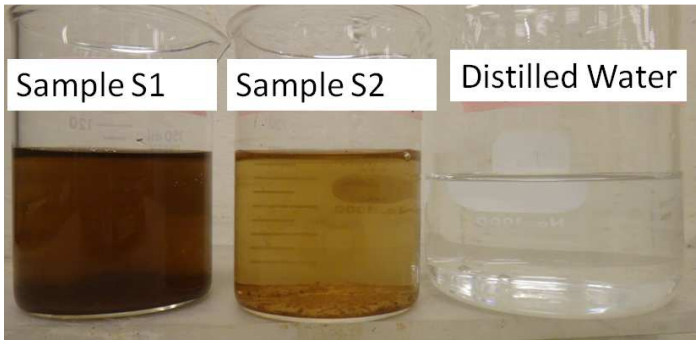

Figure 5.2. Color comparison between TOC of S1, S2, and distilled water.

Data analysis of S1 revealed that the following ion concentrations existed in this sample: 110.3 mg/L Ca^{+2}, 65.5 mg/L Mg^{+2}, 119.1 mg/L Na^{+}, 5.9 mg/L SO_4^{-2}, 119.8 Cl^{-}, 6.3 mg/L PO_4^{-3}, 1.5 mg/L Fe^{+2}, 31.3 mg/L K^{+}, and 0.2 mg/L Zn^{+2}. However, S2 had the following concentrations: 96.2 mg/L Ca^{+2}, 29.1 mg/L Mg^{+2}, 53.9 mg/L Na^{+}, 7.7 mg/L SO_4^{-2}, 52.2 mg/L Cl^{-}, 1.9 mg/L PO_4^{-3}, 1.6 mg/L Fe^{+2}, 11.2 mg/L K^{+}, and 0.01 mg/L Zn^{+2}.

Next, the missing concentration of sodium, Na^{+}, for the three selected sites were calculated, as stated before, by using the electrical balance, and the results were 324.8, 170.2, and 680 mg/L in locations 1, 5, and 6, respectively. The results revealed that the calculated concentrations of Na^{+} were reasonable compared to the available values of Na^{+} in nearby locations. For instance, the calculated value of Na^{+} of 170.2 mg/L in location 5 was within the range of the measured value of Na^{+} (148 mg/L to 266 mg/L) reported by Al-Saad et al. (2010) in location 13. Locations 5 and 13 were at the same province (Maysan). In addition, the calculated

value of Na^+ (680 mg/L) in location 6 was within the range of the measured value of Na^+ (618.4 mg/L to 892.2 mg/L) reported by Hamdan et al. (2010) in location 16. Locations 6 and 16 were at the same province (Al Basrah) (see Figure 4.1). Test results of the water quality parameters of the prepared/simulated feed waters used in this study, as well as the measured parameters of water analysis of the three locations of the Iraqi marshes, are listed in Table 5.1.

Table 5.1

Water quality analysis of measured and prepared feed waters of locations 1, 5, and 6.

Parameter	**Location # 1 (Medium TDS & TOC)**		**Location # 5 (Low TDS & TOC)**		**Location # 6 (High TDS & TOC)**	
	Measured	Prepared	Measured	Prepared	Measured	Prepared
pH	8.23	7.4 - 8.2	8.2	8.2 – 8.31	7.8	7.02 - 8
Electrical Conductivity (mS/cm)	2.55	2.4- 2.7	1.29	1.1 - 1.4	3.4	3.4 – 3.7
Total Hardness as $CaCO_3$ (mg/L)	840	390 - 438	500	192 - 202	890	579 - 645
Total Organic Carbon (TOC) (mg/L)	1.74	1.4 – 2.3	1.2	1.2 – 1.4	4.71	4.6 – 4.8
Calcium (Ca^{+2}) (mg/L)	79.4	77.4 – 8	49.9	42.1 – 47	118	98.4 – 115.8
Magnesium (Mg^{+2}) (mg/L)	51.7	47 – 53.5	17.2	17.2 – 19.4	85	81.4 – 88.2
Sodium (Na^+) (mg/L)	324.76*	320 – 356	170.2*	178.1 – 189	680*	682 - 714
Total Alkalinity as HCO_3^- (mg/L)	74.42	73 – 94.2	90.28	95.4 – 111.2	71.98	72 - 82.4
Sulfate (SO_4^{-2}) (mg/L)	314	312 – 320	90	88.8 – 91.4	680	681 – 687.4
Chloride (Cl^-)(mg/L)	520	509 – 522	280	257 – 284.4	960	954 – 968.5
Nitrate (NO_3^-) (mg/L)	0.033	0.1 – 0.2	0.21	0.1 – 0.3	0.044	0.1 – 0.4
Phosphate (PO_4^{-3}) (mg/L)	0.0013	0.03 – 0.2	0.0008	0.01 – 0.05	0.001	0.03 – 0.21
Iron (Fe^{+2}) (mg/L)	< 0.01	0.0– 0.05	< 0.01	0.01 – 0.03	< 0.01	0.01 – 0.13
Potassium (K^+) (mg/L)	--	0.2 – 0.4	--	0.2 – 0.34	--	0.4 – 0.8
Zinc (Zn^{+2}) (mg/L)	0.017	0.01–0.03	0.009	0.01 – 0.03	0.015	0.01 – 0.05
TDS (mg/L)	1686	1338 - 1428	1144	679 - 742	2411	2569 - 2657

* These values were estimated.

5.2. RO System Runs

5.2.1. Membranes Performance

As previously mentioned, three different RO membrane types (SE, CE, and AD) were utilized in this study with three different water qualities. Table 5.2 summarizes the experimental data and results which include run number, location of the prepared/simulated feed water, type of the RO membrane used in each run, simulated temperature, permeate flux range of each run, total permeate flux drop, and total time of each run. A performance comparison in terms of permeate flux and permeate conductivity among the used membranes is illustrated in Figures 5.3 and 5.4, respectively. In general, the results explained that a gradual decrease in permeate flux over time was observed for all runs. In addition, the SE-RO membrane generally produced the highest permeate flux whereas AD-RO membrane produced the least permeate conductivity.

Sub-Figures 5.3 (a) and (b) illustrate that, in location 6 (runs 1 through 6) where the highest TDS (2569 - 2657 mg/L) and highest TOC (4.55 – 4.8 mg/L) existed, the initial permeate fluxes ranged from 0.36 to 0.66 Lpm/m^2, and the final permeate fluxes ended at the range of 0.254 to 0.334 Lpm/m^2 to achieve the required water recovery percentage (70%). In sub-Figure 5.3 (a), at the temperature of 37^{o}C, the permeate flux of SE membrane (run 1) was considerably higher than that of CE (run 3) and AD (run 5) membranes, and the difference of permeate production among these membranes started to shrink after 25 hours. After that, the general propensity of the flux decline was similar for all membranes. However, although the difference in flux decline between CE and AD membranes within the first 10 hours was not noticeable, it was clear in the next 50 hours. After 75 hours, the production rate of all membrane was about the same. Total permeate flux drop of SE, CE, and AD membranes at high temperatures were 50%, 34.7%, and 30.5%, at 75.4 hr, 80.8 hr, and 85.6 hr, respectively.

At the low temperature (11^{o}C), the tendency of the permeate flux decline for both SE (run 2) and CE (run 4) membranes was identical, and the permeate flux of SE membrane (run 6) for

the majority of run-time was slightly higher than that of CE membrane, as shown in sub-Figure 5.3 (b). However, the permeate flux of the AD membrane (run 4) was considerably lower than that of SE and CE membranes. Total permeate flux drop of AD membrane at the temperature of 11^{o}C was 26.2% compared to 57.9% and 42.8% for the SE and CE membranes, respectively. The total time of the runs of SE, CE, and AD membranes at low temperature to achieve 70% of water recovery was 96.1 hr, 103.5 hr, and 95.9 hr, respectively.

Table 5.2

Summary of permeate fluxes and total time of RO membrane experiments.

RUN's Number	Location	Type of RO membrane	Temperature (°C)	Permeate flux range (Lpm/m^2)	Total permeate flux drop (%)	Total time (hrs)
1	6	SE	37	0.656 - 0.327	50	75.4
2	6	SE	11	0.604 - 0.254	57.9	96.1
3	6	CE	37	0.481 - 0.314	34.7	80.8
4	6	CE	11	0.584 - 0.334	42.8	103.5
5	6	AD	37	0.467 - 0.325	30.5	85.6
6	6	AD	11	0.36 - 0.266	26.2	95.9
7*	6	SE	37	0.872 - 0.381	56.3	63
8*	6	SE	11	0.74 - 0.389	47.4	86.9
9*	6	CE	37	0.716 - 0.365	49.1	76.5
10*	6	CE	11	0.561 - 0.309	44.9	92.1
11*	6	AD	37	0.671 - 0.323	51.8	81.1
12*	6	AD	11	0.31 - 0.238	3.5	119.9
13	1	SE	37	0.991 - 0.514	48.2	62.2
14	1	SE	11	0.643 - 0.397	38.2	88.3
15	1	CE	37	0.632 - 0.399	36.9	77.4
16	1	CE	11	0.50 - 0.344	31.2	94.4
17	1	AD	37	0.691 - 0.449	35.1	73.7
18	1	AD	11	0.583 - 0.307	47.4	96.5
19	5	SE	37	0.949 - 0.38	60	68.9
20	5	SE	11	0.919 - 0.323	64.8	74
21	5	CE	37	0.655 - 0.439	33.1	74.9
22	5	CE	11	0.643 - 0.424	34.1	82.7
23	5	AD	37	0.572 - 0.423	26.1	71.6
24	5	AD	11	0.439 - 0.296	32.5	107.7

* Run conducted with MF membrane as a pretreatment unit of the feed water.

In location 1 (runs 13 through 18), where TDS was between 1338 and 1428 mg/L and TOC was between 1.4 and 2.3 mg/L, the range of the initial permeate fluxes was 0.50 to 0.991 Lpm/m^2, and the final permeate fluxes ended in the range of 0.307 to 0.514 Lpm/m^2 to achieve the required water recovery percentage (75%), as shown in sub-Figures 5.3 (c) and (d). Similar to the runs of location 6, the permeate flux of SE membrane (run 13) at the temperature of 37^{o}C was higher than that of CE (run 15) and AD (run 17) membranes, as shown in sub-Figure 5.3 (c). The initial permeate flux of SE membrane started at a high rate (0.991 Lpm/m^2), but rapidly dropped to about 0.63 Lpm/m^2 after 25 hrs. After that, the permeate flux of the three membrane types continued to drop at a constant rate. Total permeate flux drops of the SE, CE, and AD membranes at the high temperature were 48.2%, 36.9%, and 35.1%, at 62.2 hr, 77.4 hr, and 73.7 hr, respectively. In addition, at a low temperature (11^{o}C), the membranes used in location 1 performed identically to those of location 6 except that the permeate flux of AD membrane (run 6) in location 6 was clearly lower than those of SE (run 2) and CE (run 4), as illustrated in sub-Figure 5.3 (b). The total permeate decline of SE, CE, and AD membranes at a low temperature to achieve 75% water recovery were 38.2%, 31.2%, and 47.4 % at 88.3 hr, 94.4 hr, and 96.5 hr, respectively. Overall, the results indicated that all permeate fluxes produced by the three types of membranes in location 1 were higher than those in location 6.

In location 5 (runs 19 through 24), where the lowest TDS (679 - 742 mg/L) and lowest TOC (1.2 – 1.4 mg/L) existed, the initial permeate fluxes ranged from 0.439 to 0.949 Lpm/m^2, and the final permeate fluxes were between 0.296 to 0.439 Lpm/m^2 to achieve the required water recovery percentage (80%). Similar to the previous runs in locations 6 and 1, the permeate flux of the SE membrane was distinctly high for the first 25 hr of the total time of the run, as shown in sub-Figures 5.3 (e) and (f). However, at a high temperature (37^{o}C), the permeate flux of the SE membrane (run 19) started to drop and became lower than that of the AD membrane (run 23) after 28 hr. Moreover, as opposed to the other runs, run 23 (AD membrane at high temperature)

produced a permeate flux higher than that of run 21 (CE membrane) during the whole run time except for the very beginning and end of the run. Consequently, the total time of run 23 (71.6 hr) was lower than that of run 21 (74.9 hr) to achieve 80% water recovery, as shown in sub-Figure 5.3 (e). The total permeate flux drop of SE, CE, and AD membranes at high temperature was 60%, 33.1%, and 26.1%, respectively.

At low temperature (11^{o}C), the difference among the permeate fluxes of the three RO membranes (runs 20, 22, and 24) was very obvious, as illustrated in sub-Figure 5.3 (f). The initial permeate flux of SE, CE, and AD membranes were 0.919, 0.643, and 0.439 Lpm/m^2, respectively. The flux of the SE membrane continuously dropped at a high constant rate, and reached a total permeate flux drop of 64.8% when the desired water recovery of 80% was achieved. However, the flux drops of the CE (34.1%) and AD (32.5%) membranes were distinctly lower than that of the SE membrane; therefore, the final rate of permeate flux of the SE membrane was lower than that of the CE membrane, but about the same of that of the AD membrane.

The observed permeate flux decline in all runs is likely due to the scale formation from the feed water on the RO membrane surface, which reduces the available filtration area. High TOC forms complexes that enhance RO membrane fouling when some metals are present, such as Ca^{+2} (Antony et al., 2011; Tran et al., 2007; Koyuncu & Wiesner, 2007). The high permeate fluxes observed in the runs of locations 1 and 5, compared to those of location 6, are apparently due to a lesser scale formation on the membrane surface from the feed water with lower TOC and TDS concentrations. The difference in the TOC and TDS concentration between locations 1 and 5 is smaller than those between 1 and 6 and between 5 and 6. Also, as mentioned earlier, the results illustrated that generally the SE membrane produced the highest permeate flux, while the AD membrane produced the lowest permeate flux in all three feed waters of locations 6, 1, and 5.

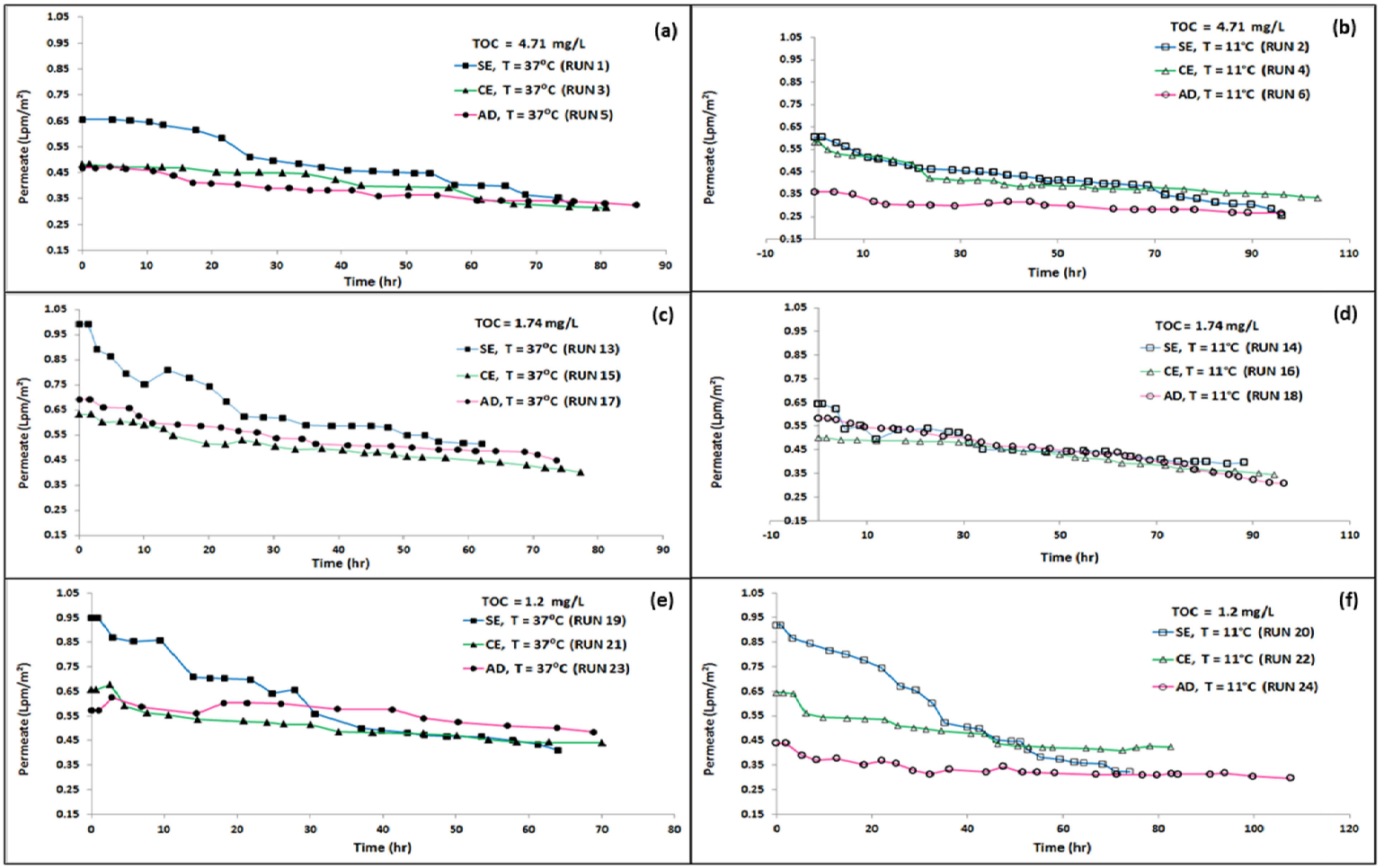

Figure 5.3. Evolution of the drop in permeate flux of the SE, CE, and AD membranes: (a) and (b) for location 6 (runs 1 through 6); (c) and (d) for location 1 (runs 13 through 18); (e) and (f) for location 5 (runs 19 through 24) at 37°C and 11°C. All experiments were conducted at a feed flow rate of 0.6 gpm (2.27 Lpm) and a range of feed pressure of 380 psi - 400 psi (2,620 kPa – 2,757 kPa). Solid lines were used with symbols for clarity.

Moreover, all membranes at the temperature of 37^{o}C exhibited higher permeate fluxes than those of corresponding membranes at lower temperature (11^{o}C) (see appendix E). The temperature of the feed water can affect the morphology of the cake layer deposited on the RO membrane surface, and consequently, quantitatively and qualitatively affects the permeate flux produced by the RO membrane (Jin et al., 2009). The high permeate fluxes of the three membrane types at high temperature can be attributed to the decrease in the feed water viscosity and the polymeric membrane swelling, thus allowing for the higher diffusion of water rate through the membrane (Jawor and Hoek, 2009).

To investigate the salt rejection of the membranes, salt concentration (conductivity) in permeate and feed water samples of each run was periodically measured, and the changes in the permeate conductivity of the runs for the three locations at the temperatures of 37^{o}C and 11^{o}C are shown in Figure 5.4. The results demonstrated that the AD membrane displayed the highest salt rejection, whereas the CE membrane had the least salt rejection. It is noted that the permeate conductivity of the CE membrane in all runs was considerably higher than that of the SE and AD membranes. In addition, the increase of the permeate conductivity of all runs of the SE and CE membranes was approximately constant in the first 36 to 45 hours of the run time. After that, the permeate conductivity of the CE and SE membranes had a rapid increase, particularly in runs 1 through 18 in locations 6 and 1, as shown in sub-Figures 5.4 (a-d) indicating higher salt passage through the membrane. It is also noted that the level of the permeate conductivity for each membrane in location 6 (runs 1 through 6), shown in sub-Figures 5.4 (a) and (b) was much higher than that of the corresponding membrane in location 5 (runs 19 through 24), shown in sub-Figures 5.4 (e) and (f). Additionally, the permeate conductivity of the membranes under high temperature (37^{o}C) was higher than that of the corresponding membranes under low temperature (11^{o}C). Moreover, the results demonstrated that the AD membrane maintained a relatively constant level of salt rejection until the end of each run.

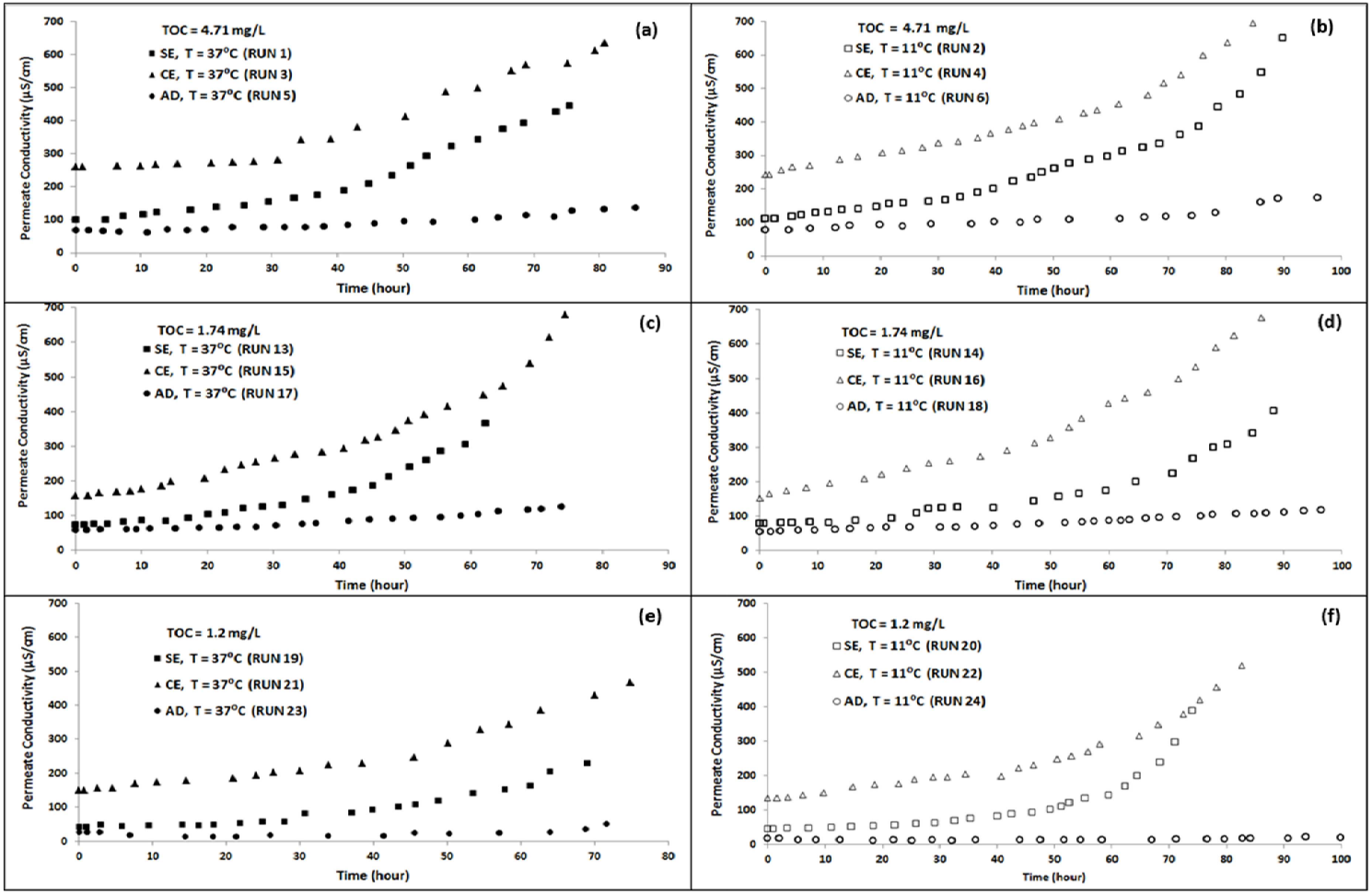

Figure 5.4. Evolution of the increase permeate conductivity of the SE, CE, and AD membranes: (a) and (b) for location 6 (runs 1 through 6); (c) and (d) for location 1 (runs 13 through 18); (e) and (f) for location 5 (runs 19 through 24) at 37°C and 11°C. All experiments were conducted at a feed flow rate of 0.6 gpm (2.27 Lpm) and a range of feed pressure of 380 psi - 400 psi (2,620 kPa – 2,757 kPa).

In general, it was observed that the permeate conductivity of all runs increased with the run time to achieve the desired water recovery. The noted increase in the permeate conductivity is likely attributable to the decrease in salt ions rejection by the RO membrane. This observation disagrees with the findings by Jawor and Hoek (2009) who reported that the TDS rejection by the RO membrane increases with the increase of the water recovery.

Furthermore, elemental analysis of permeate and feed water samples for each run was done, and the removal percentage of the major ions (Na^{+}, Ca^{+2}, Mg^{+2}, SO_4^{-2}, and Cl^{-}) are shown in Figures 5.5 and 5.6. Sub-Figures 5.5 (a) and (b) display the mineral salt ion rejection percentage by the three types of the membrane (SE, CE, and AD) for location 6 at 37^{o}C and 11^{o}C, respectively. Sub-Figures 5.6 (a) and (b) show the ion rejection ratio for location 5 at 37^{o}C and 11^{o}C, respectively. Overall, the results revealed that all three types of the tested RO membranes exhibited relatively high rejection for all ions. The SE membrane achieved more than 97.5%, 99.3%, 99.4%, 99.5%, and 97.9% removal of Na^{+}, Ca^{+2}, Mg^{+2}, SO_4^{-2}, and Cl^{-}, respectively. The CE membrane showed more than 95.6%, 98.4%, 99%, 99.2%, and 95.1% removal of Na^{+}, Ca^{+2}, Mg^{+2}, SO_4^{-2}, and Cl^{-}, respectively. However, the AD membrane exhibited more than 99%, 99.2%, 99.5%, 99.4%, and 99.4% removal of Na^{+}, Ca^{+2}, Mg^{+2}, SO_4^{-2}, and Cl^{-}, respectively. Overall, the results of the elemental analyses confirmed that the CE membrane had the least rejection level (from 91.1% to 99.2%), but the AD membrane had the highest rejection percentage (from 97.6% to 99.5%) for all the existing ions, as illustrated in Figures 5.5 and 5.6.

The effect of the feed water temperature on the salt rejection percentage varied among the types of the membranes and the rejected ions. As an example, the rejection ratio of Ca^{+2} by an AD membrane at high TOC feed water (location 6) slightly increased from 99.1% at high temperature, to 99.2% at low temperature, but was a little reduced from 99% and 98.4% to 98.9% and 97.7%, respectively, by the SE and CE membranes. Another example is the rejection percentage of Mg^{+2} by the CE membrane for location 5 which slightly reduced from 97% at high

temperature to 96.6% at low temperature, as shown in Figure 5.6. In general, it was found that, when the temperature was dropped from 37°C to 11°C, the rejection levels of the RO membranes for most of the ions increased throughout the fouling runs. To conclude, when the feed water temperature increases, more salt ions can pass through the RO membrane as a result of the increase in salt ions diffusivity through the expanded membrane materials which are attributed to high temperature (Jawor and Hoek, 2009). This phenomenon increases the permeate conductivity.

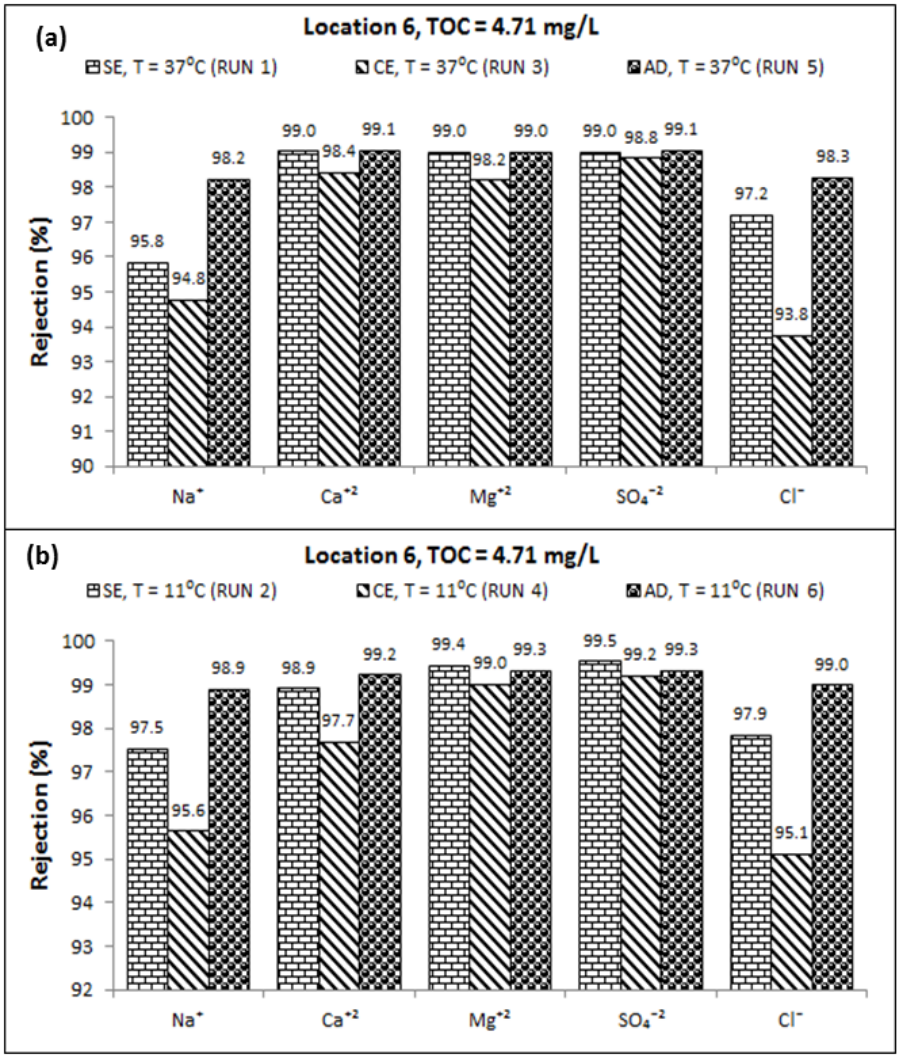

Figure 5.5. Salt ion rejection percentage of the SE, CE, and AD membranes for location 6 (TOC = 4.71 mg/L): (a) runs 1, 3, and 5 (at 37°C); (b) runs 2, 4, and 6 (at 11°C).

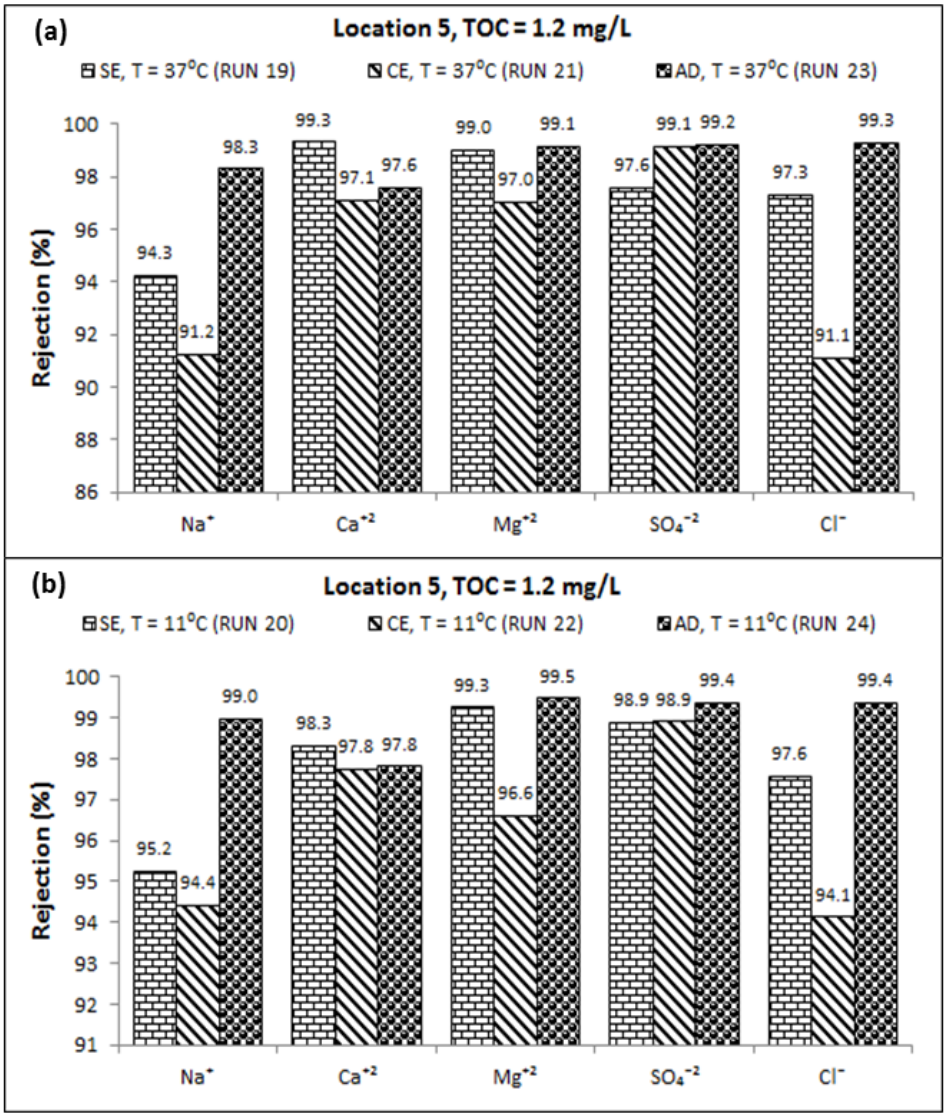

Figure 5.6. Salt ion rejection percentage of the SE, CE, and AD membranes for location 5 (TOC = 1.2 mg/L): (a) runs 19, 21, and 23 (at 37°C); (b) runs 20, 22, and 24 (at 11°C).

Additionally, the Reynolds number of the flow in the feed water channel (feed water spacer) at low and high temperatures was also calculated. The feed water channel, as stated earlier, has the height of 0.432 mm (17 mil). The flow of feed water through an RO membrane can be considered similar to that of the flow of water through a pipe (Kucera, 2010). The calculated Reynolds number at the temperatures of 11ºC and 37ºC was 155 and 282, respectively and the calculation steps are given in appendix A. Wiley et al., (2002) reported that "Practical

application of spiral-wound modules often requires flow rates which exceed subcritical Reynolds numbers, leading to transient flow conditions in the feed channel." They stated that the transient flow can occur at Reynolds numbers higher than 200, but it also can occur at a Reynolds number as low as 80 for the very small feed spacers. Examination of the fouled membrane surface operated at low temperature showed that the feed water flowed smoothly or in regular paths on the membrane surface indicating laminar flow (Re = 155). However, recirculating regions on the fouled membrane surface operated under high temperature were seen indicating more turbulence of the flow occurred (Re = 282). Moreover, the current study results indicated that, as stated earlier, the flux decline at the low Reynolds number (low temperature) was higher than that of the high Reynolds number (high temperature).

5.2.2. Effect of Pretreatment

To investigate the influence of the pretreatment of the feed water on the RO membrane performance, a 0.1 micron MF membrane was employed as pretreatment unit for the feed water at the same conditions used to operate the RO membrane system. The MF membrane was only employed as pretreatment unit for the feed water of location 6 in runs 7 through 12. However, as previously mentioned, the feed water of location 6 was used to conduct runs 1 through 6 without using the MF membrane as a pretreatment. Therefore, to show the effect of using the MF membrane on the permeate flux, the results of runs 7 through 12 were compared to those of the corresponding runs (1 through 6), as shown in Figures 5.7 and 5.8.

The results demonstrated that the initial permeate fluxes of the SE, CE, and AD membranes at high temperature (37^{o}C) were considerably improved. The initial flux of the SE membrane increased from 0.656 Lpm/m^2 (run 1) to 0.872 Lpm/m^2 (run 7), as illustrated in sub-Figure 5.7 (a). The permeate flux of run 7 was distinctly higher than the flux rate of run 1 for the first 12 hours of the run time. Over the time period from 12 hours to about 45 hours, the permeate flux of run 7 was slightly higher than that of run 1. Then, from the time of 45 hours to the end of

the runs, both permeate fluxes of run 1 and run 7 were about the same, as seen in sub-Figure 5.7 (a). However, when the feed water of the run was pretreated with the MF membrane, the CE membrane exhibited a longer improvement of initial flux (run 9), and consequently longer time (27 hours) to decline to the same flux rate of the un-pretreated feed water run (run 3), as shown in sub-Figure 5.7 (b). The initial permeate flux of the pretreated feed water with the MF membrane (run 9) was 0.716 Lpm/m^2 compared to 0.481 Lpm/m^2 (run 3). Over the time period from 27 hours to about 57 hours, the permeate fluxes of both run 3 and run 9 were about the same. After that, the permeate flux of run 3 rapidly declined while the flux of run 9 kept a smaller constant rate of decrease. Moreover, sub-Figure 5.7 (c) displayed that the initial permeate flux of the CE membrane was also improved and increased from 0.467 Lpm/m^2 (run 5) to 0.671 Lpm/m^2 (run 11). However, the gap between run 5 and run 11 started to shrink after about 12 hours.

At low temperature (11^{o}C), the effect of using an MF membrane to treat the feed water before running it through the RO membranes was clearly different from the impact of high temperature, and is presented in Figure 5.8. Using an MF membrane in advance of an SE membrane showed a distinct continuous difference in the permeate flux between run 2 and run 8 from the beginning to the end, as shown in sub-Figure 5.8 (a). However, the permeate fluxes produced by the CE and AD membranes did not exhibit a noticeable improvement when the feed water was pretreated by the MF membrane, as illustrated in sub-Figures 5.8 (b) and (c). The permeate flux rate of the CE membrane at a low temperature of the pretreated feed water (run 10) was lower than that of un-pretreated feed water (run 2) from the very beginning until about 22 hours of the run time, when the flux of run 2 rapidly declined in a short time. After that, the permeate flux of run 2 was lower than that of run 10 and both fluxes declined at the same rate to the end of both runs, as displayed in sub-Figure 5.8 (b).

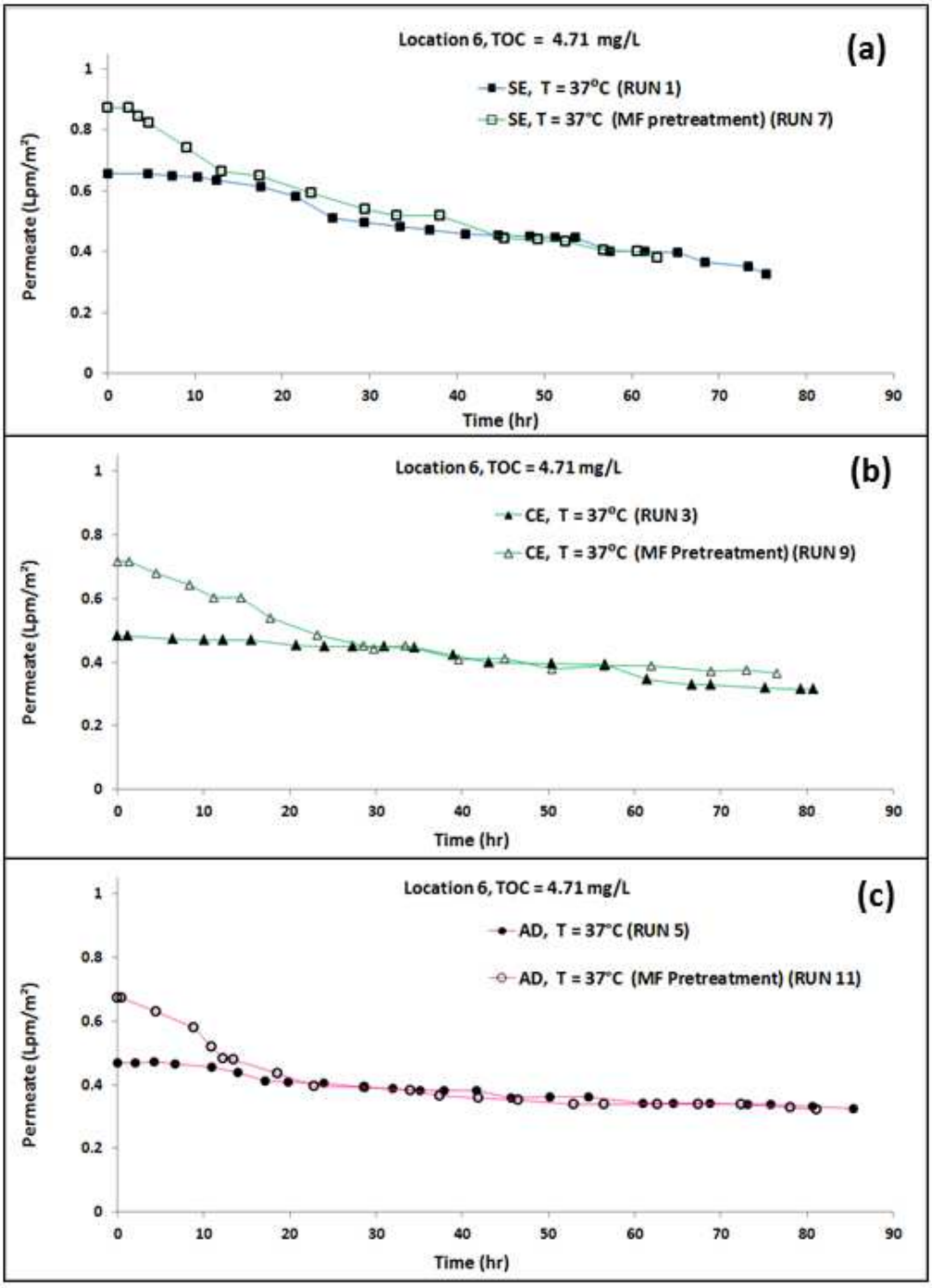

Figure 5.7. Flux decline of un-pretreated and pretreated feed water with the MF membrane for location 6 at 37°C: (a) SE membrane; (b) CE membrane; (c) AD membrane.

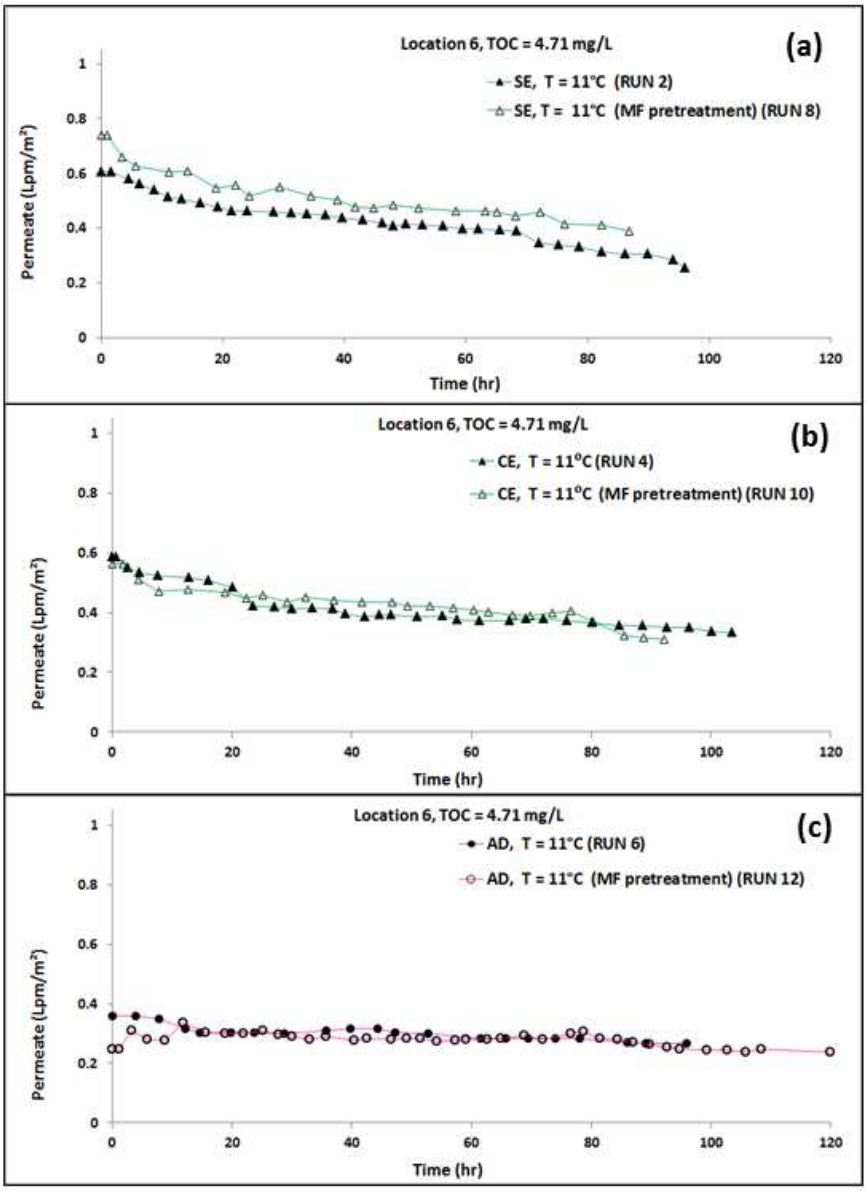

Figure 5.8. Flux decline of un-pretreated and pretreated feed water with the MF membrane for location 6 at 11°C: (a) SE membrane; (b) CE membrane; (c) AD membrane.

The trend of the permeate flux of the AD membrane in run 12, as shown in sub-Figure 5.8 (c), was not explainable because the initial permeate flux of the pretreated feed water run (run 12) started at a much lower rate (0.25 Lpm/m^2) than that of run 6 (0.36 Lpm/m^2); then, the permeate flux of run 12 increased and approached the permeate flux of run 6 after 11 hours. Both permeate fluxes of run 6 and run 12 were about the same for the next 20 hours of the run time.

Over the time period from 28 hours to 62 hours, the permeate flux of run 12 was lower than that of run 6. Then, from the time of 62 hours to the end of the runs, the permeate flux of run 12 became higher than that of run 6.

In general, employing the MF membrane as a pretreatment unit for the feed water to operate the RO system increased the permeate flux, particularly of the runs conducted with a high temperature. The observed permeate flux increase in all runs conducted with the MF membrane was probably due to the reduction of organic and particulate matter from the feed water on the RO membrane surface which increases the available filtration area (Greenlee et al., 2009). Also, it was noted that the permeate flux considerably improved only during the first 12 to 27 hours of the run time for most of the runs. This observation suggested that more fine materials, which were not captured by the MF membrane, deposited on the RO membrane surface and blocked the pores of the membrane, thus reducing the permeate flux. In addition, the MF membrane resulted in reducing the total time of most of the runs compared to those of the corresponding runs conducted without the MF membrane, as illustrated in Table 5.2. For instance, the total time of run 7, which was operated with the MF membrane, was 63 hours to achieve 70% of water recovery compared to 75.4 hours total time of run 1. Overall, the results demonstrated that the RO membrane fouling by the feed water of the brackish surface water was considerably reduced after using the 0.1 µm MF membrane. Therefore, it is recommended to use the MF membrane as a pretreatment unit in advance of the RO membrane system. Also, Alspach et al., (2011) reported that using large pore size membrane as a pretreatment process in the RO brackish surface water treatment plants provides a better particulate removal.

The effect of treating the feed water in location 6 with an MF membrane before running the RO membrane system on the conductivity of the permeate was also investigated, and the results of the runs with and without the MF membrane are compared in Figures 5.9 and 5.10 for the temperatures of 37ºC and 11ºC, respectively. The results revealed that the conductivity of the

permeate produced by the SE membrane at both temperatures had almost the same tendency. Both runs (1 and 7) had the same permeate conductivity from the beginning to about 38 hours of the run time, when the permeate conductivity of run 1 rapidly started to increase, while the permeate conductivity of run 7 kept a constant rate of increase, as shown in sub-Figure 5.9 (a). Likewise, the permeate conductivity of runs 2 and 8 for the first 35 hours were about the same level, as illustrated in sub-Figure 5.10 (a). After that, the difference of the permeate conductivity between run 2 and 8 increased as a result of the rapid increase in the conductivity level of run 2 compared to a lower increase in run 8.

However, at high temperature, the CE membrane showed a noticeable decrease in the permeate conductivity from the beginning to the end of the run, when an MF membrane was used to treat the feed water before pumping it to the RO membrane, as displayed in sub-Figures 5.9 (b). At low temperature, the effect of the pretreatment by the MF membrane on the permeate conductivity of the CE membrane started to be clear after about 33 hours of the run time, as presented in sub-Figure 5.10 (b). Also, the results showed that, at a high temperature, the AD membrane had a slight decrease in conductivity of the permeate at the very beginning time of run 11, as shown in sub-Figure 5.9 (c); however, the level of the permeate conductivity of runs 5 and 11was approximately the same over the total run time. On the contrary, at a low temperature, the pretreatment by the MF membrane considerably reduced the permeate conductivity of the AD membrane (run 12 compared to run 6) over the total run time, as illustrated in sub-Figure 5.10 (c).

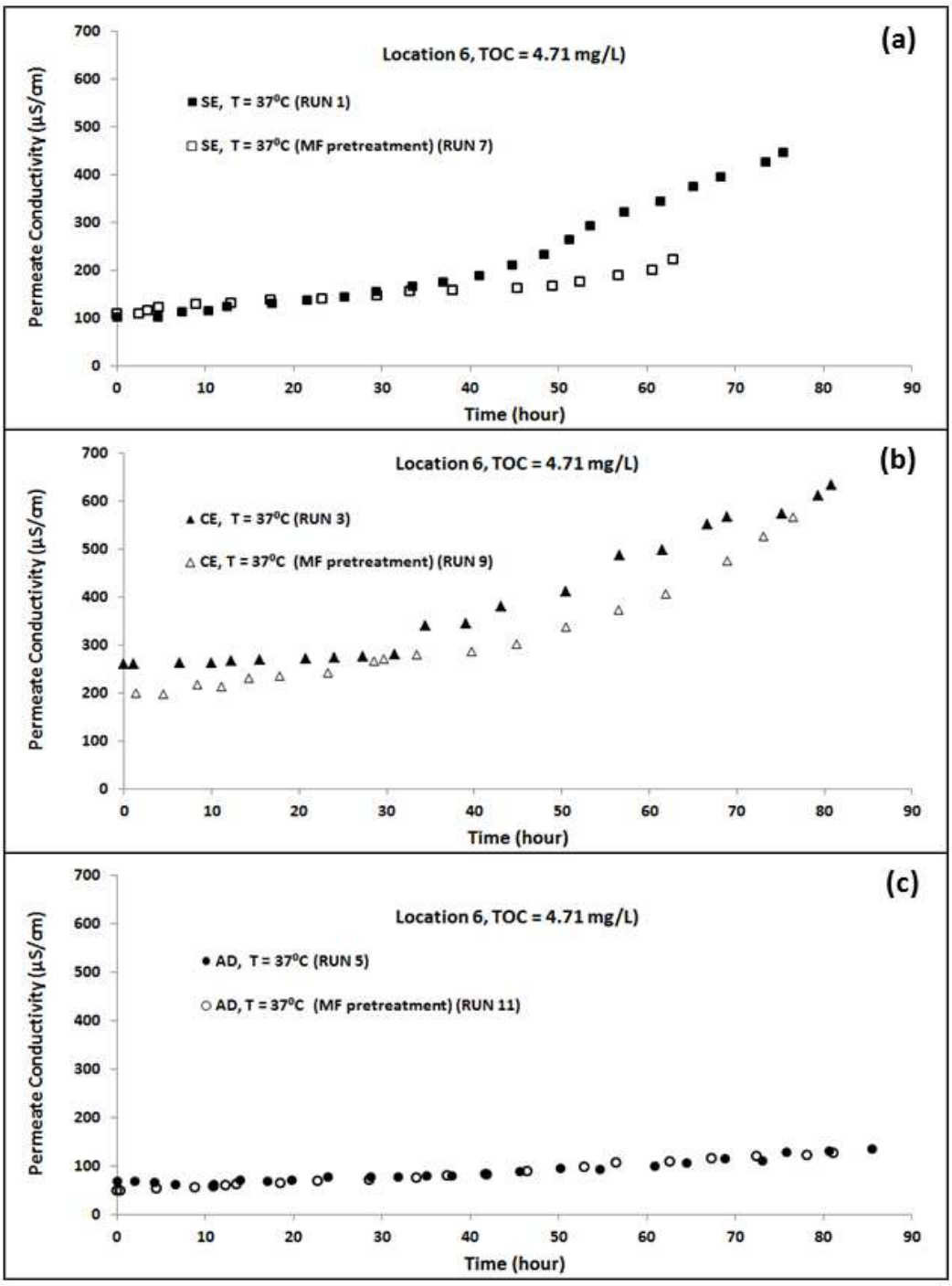

Figure 5.9. The effect of pretreating the feed water of location 6 by using the MF membrane on permeate conductivity of SE, CE, and AD membranes: (a) SE membrane; (b) CE membrane; (c) AD membrane. All runs were conducted at a temperature of 37°C, feed flow rate of 0.6 gpm (2.27 Lpm), and a range of feed pressure of 380 psi - 400 psi (2,620 kPa – 2,757 kPa).

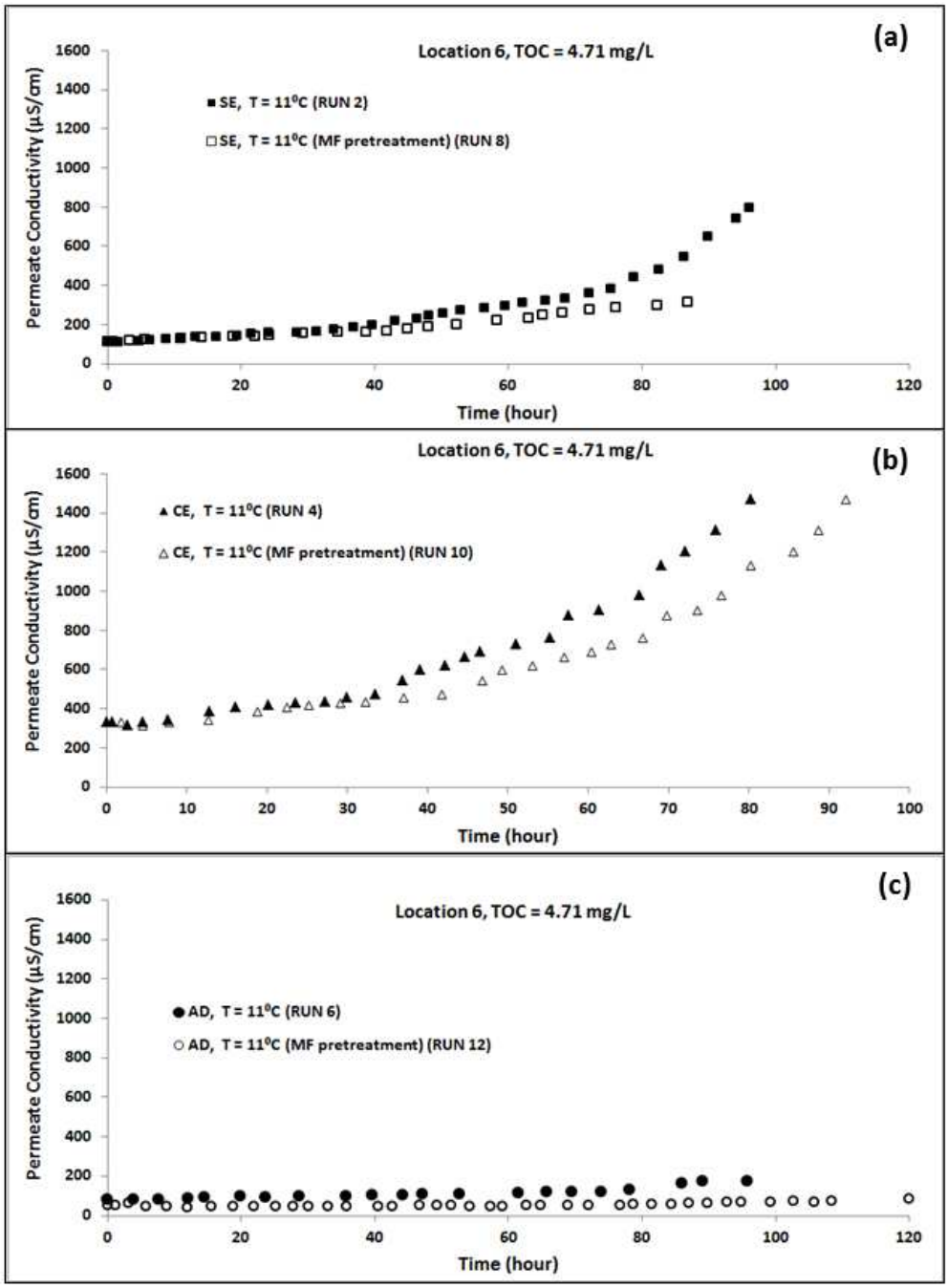

Figure 5.10. The effect of pretreating the feed water of location 6 by using MF membrane on permeate conductivity of SE, CE, and AD membranes: (a) SE membrane; (b) CE membrane; (c) AD membrane. All runs were conducted at a temperature of 11°C, feed flow rate of 0.6 gpm (2.27 Lpm), and a range of feed pressure of 380 psi - 400 psi (2,620 kPa – 2,757 kPa).

Furthermore, the effect of the pretreatment of the feed water by the MF membrane on salt ion rejection by an RO membrane was investigated. The removal percentage of the major ions (Na^{+}, Ca^{+2}, Mg^{+2}, SO_4^{-2}, and Cl^{-}) by the SE and CE membranes with and without an MF membrane was compared in Figure 5.11. At the temperature of 37^{o}C, the rejection percentages of all ions of run 7 by the SE membrane were slightly improved compared to run 1, except the Na^{+} ion which increased by 2.3%, as shown in sub-Figure 5.11 (a). In addition, at the temperature of 37^{o}C, the rejection percentages of all ions by the CE membrane of run 9 were slightly improved compared to run 3, as presented in sub-Figure 5.11 (b). At the temperature of 11^{o}C, the effect of the pretreatment by the MF on the salt ion rejection by the CE membrane (run 10 compared to run 4) was similar to that of the high temperature, as displayed in sub-Figure 5.11 (c) with the exception of the Ca^{+2} ion which increased by 1.8% and the Cl^{-} ion which reduced from 95.1% to 94.8%. In general, the results revealed that the MF membrane slightly improved salt ions rejection ratios by the RO membrane.

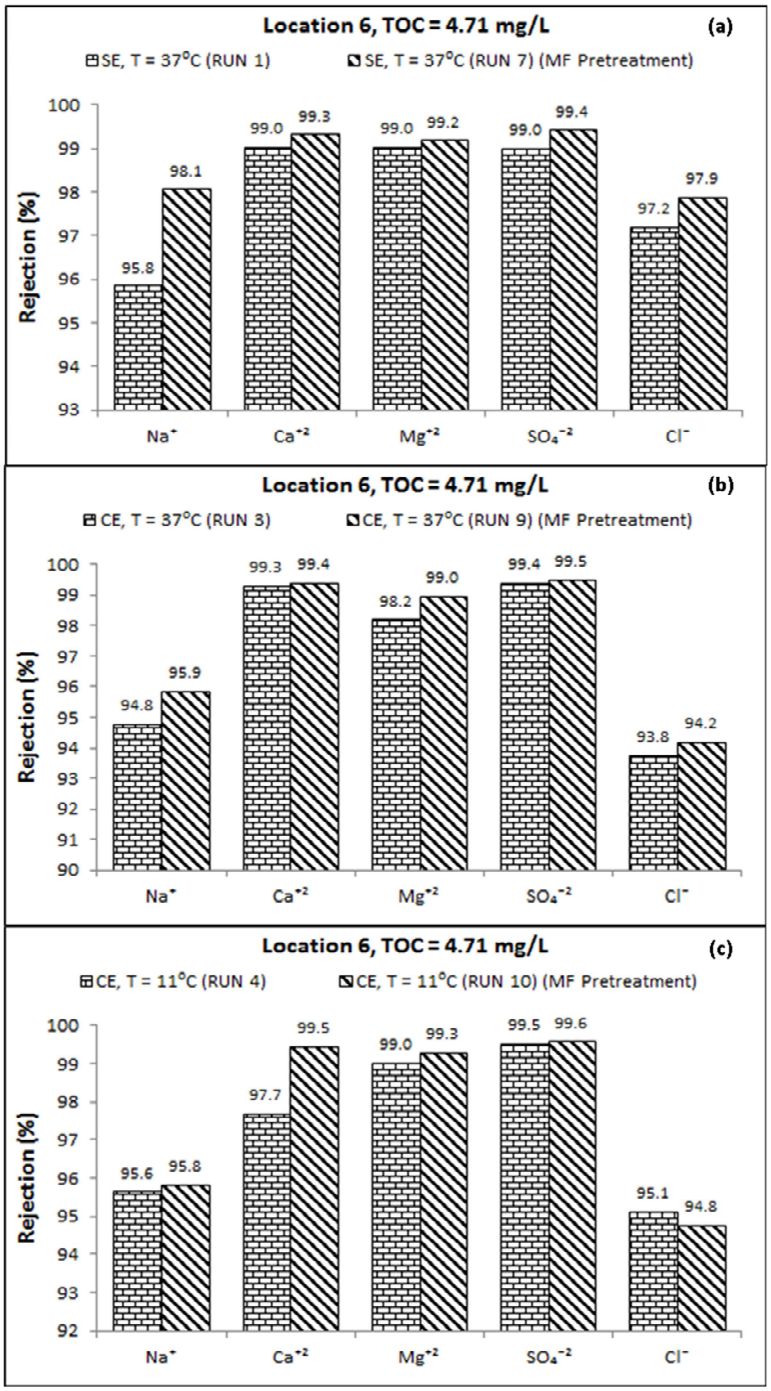

Figure 5.11. Effect of the MF pretreatment on salt ions rejection ratio of: (a) SE membrane at 37°C (run 1 versus run 7); (b) CE membrane at 37°C (run 3 versus run 9); (c) CE membrane at 11°C (run 4 versus run 10). All runs were conducted by using the feed water of location 6 at a feed flow rate of 0.6 gpm (2.27 Lpm) and a range of feed pressure of 380 psi - 400 psi (2,620 kPa – 2,757 kPa).

5.2.3. Fourier Transform Infrared Spectroscopy (FTIR) Analyses

Several FTIR spectra from unused and used RO membranes were done in this study. FTIR spectral interpretation of the absorption bands was provided by the software with the FTIR spectrometer, itself (see Appendix B). The spectra of the unused SE, CE, and AD membranes are shown in sub-Figures 5.12 (a), (b), and (c), respectively. The spectrum of the SE membrane (Thin Film Composite Polyamide) shows a main absorption in the vicinity of 3337 cm^{-1} which is due to the O-H stretches of the primary aliphatic alcohols and phenols. Also, it shows a peak in the vicinity of 2936 cm^{-1} which is attributed to the C-H stretching of the aliphatic hydrocarbons. Strong absorption between 1609 and 560 cm^{-1} is due to a variety of functional groups, such as aliphatic alcohols, phenols, and aliphatic hydrocarbons is observed in sub-Figure 5.12 (a).

The FTIR spectrum of the CE membrane shows a different trend in the absorption from the one observed in the SE membrane. A low peak in the vicinity of 2929 cm^{-1} which is attributed to C-H stretching of aliphatic hydrocarbons is presented in sub-Figure 5.12 (b). The band in the neighborhood of 1744 cm^{-1} is due to C=O stretching of aliphatic acetate esters. Also, a peak of 1369 cm^{-1} is noticed in sub-Figure 5.12 (b) which is attributed to the C-H stretching of aliphatic hydrocarbons. Moreover, two sharp absorption peaks at 1230 and 1045 cm^{-1} are due to C-O stretching of aliphatic acetate esters.

However, the FTIR spectrum of the AD membrane shows similar absorption peaks to those presented in the FTIR spectrum of the SE membrane. A range of absorption between 3600 and 3200 cm^{-1} is due to O-H stretches of the primary aliphatic alcohols as shown in sub-Figure 5.12 (c). In the vicinity of 2929 cm^{-1}, a peak is attributed to C-H stretching of the aliphatic hydrocarbons and O-H stretching of carboxylic acids. Also, the strong absorption between 1700 and 650 cm^{-1} is due to aliphatic C-H deformation of hydrocarbons and aliphatic O-H stretching of alcohols.

Furthermore, the FTIR spectral interpretation of the prepared TOC sample displayed in Figure B4 indicates that the main functional groups of the organic matter are aromatic hydrocarbons, aliphatic alcohols, aromatic ethers, and aliphatic hydrocarbons. In addition, FTIR spectra from fouled RO membranes are shown in Figures 5.13, 5.14, 5.15, and 5.16 for the runs 1 through 6 and runs 19 through 24. The FTIR spectral interpretation for the absorption peaks present in the spectra of the runs shows that the predominant functional groups are aromatic hydrocarbons (between 3100 and 3000 cm^{-1}, and between 840 and 800 cm^{-1}), aliphatic alcohols (between 3600 and 3200 cm^{-1}, and between 1150 and 1100 cm^{-1}), aromatic ethers (between 1300 and 1200 cm^{-1}), aliphatic hydrocarbons (between 2990 and 2850 cm^{-1}, and between 1460 and 1350 cm^{-1}), and inorganic carbonate (between 1550 and 1300 cm^{-1}, and between 880 and 700 cm^{-1}) and lower amounts of olefins (between 3100 and 3000 cm^{-1}).

Moreover, the FTIR spectra of the fouled SE membrane with and without using an MF membrane as a pretreatment unit for the feed water of run 7 and run 1, respectively, are shown in Figure 5.17. The results revealed that, in run 1, the main absorption functional group is the aromatic hydrocarbons which is located in the vicinity of 3050 cm^{-1}, 1500 cm^{-1}, and 820 cm^{-1}. However, the FTIR spectrum of run 7 shows a main absorption in the vicinity of 3367 cm^{-1} which is due to the O-H stretches of the aliphatic alcohols and amides and a lower absorption in the vicinity of 1638 cm^{-1} due to aliphatic C=O deformation (see Appendix B). The main absorption functional group seen in the FTIR spectra of run 7 is also the main absorption functional group seen in the FTIR spectra of the clean SE membrane, indicating lower (than run 1) fouled material deposited on the membrane surface of run 7.

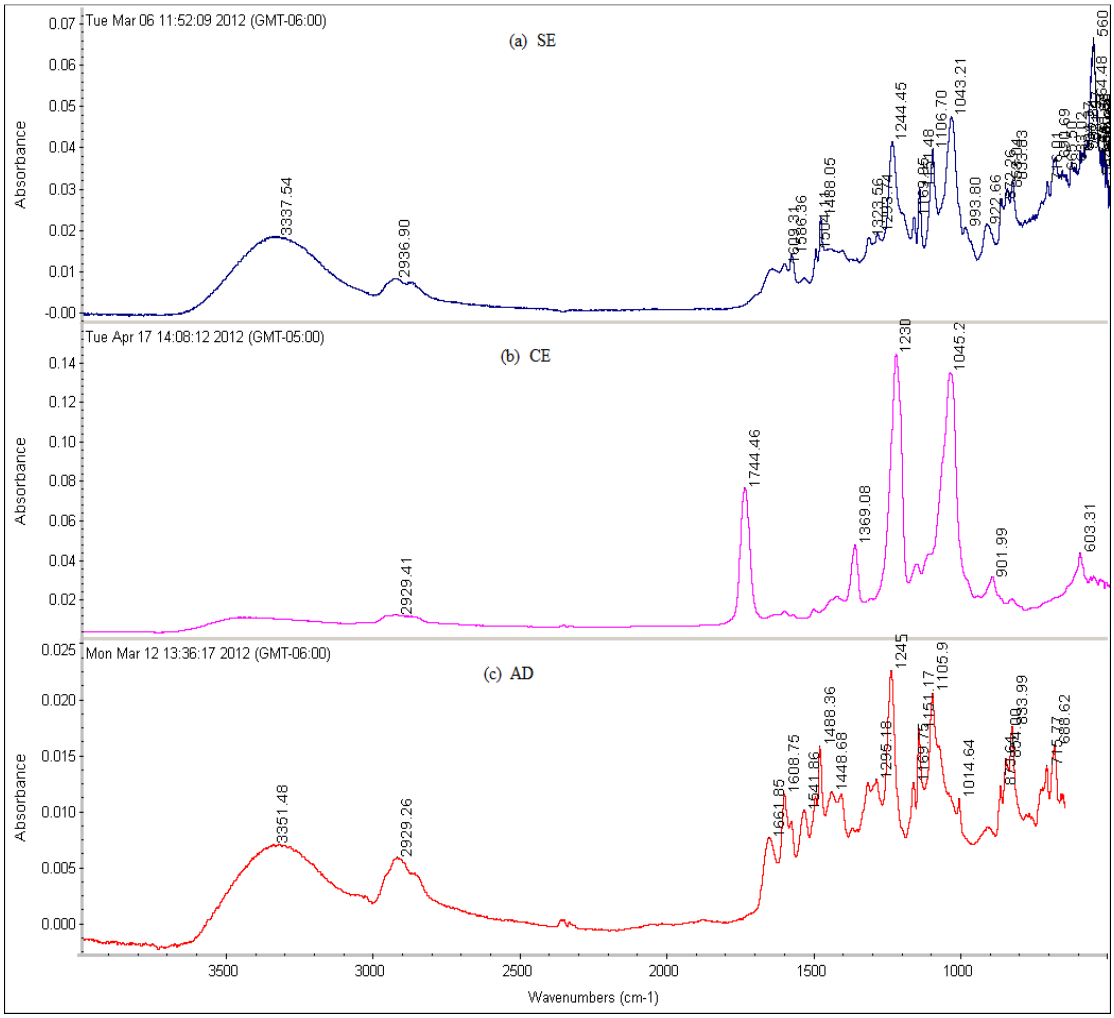

Figure 5.12. FTIR spectra for the unused RO membrane: (a) SE membrane; (b) CE membrane; (c) AD membrane.

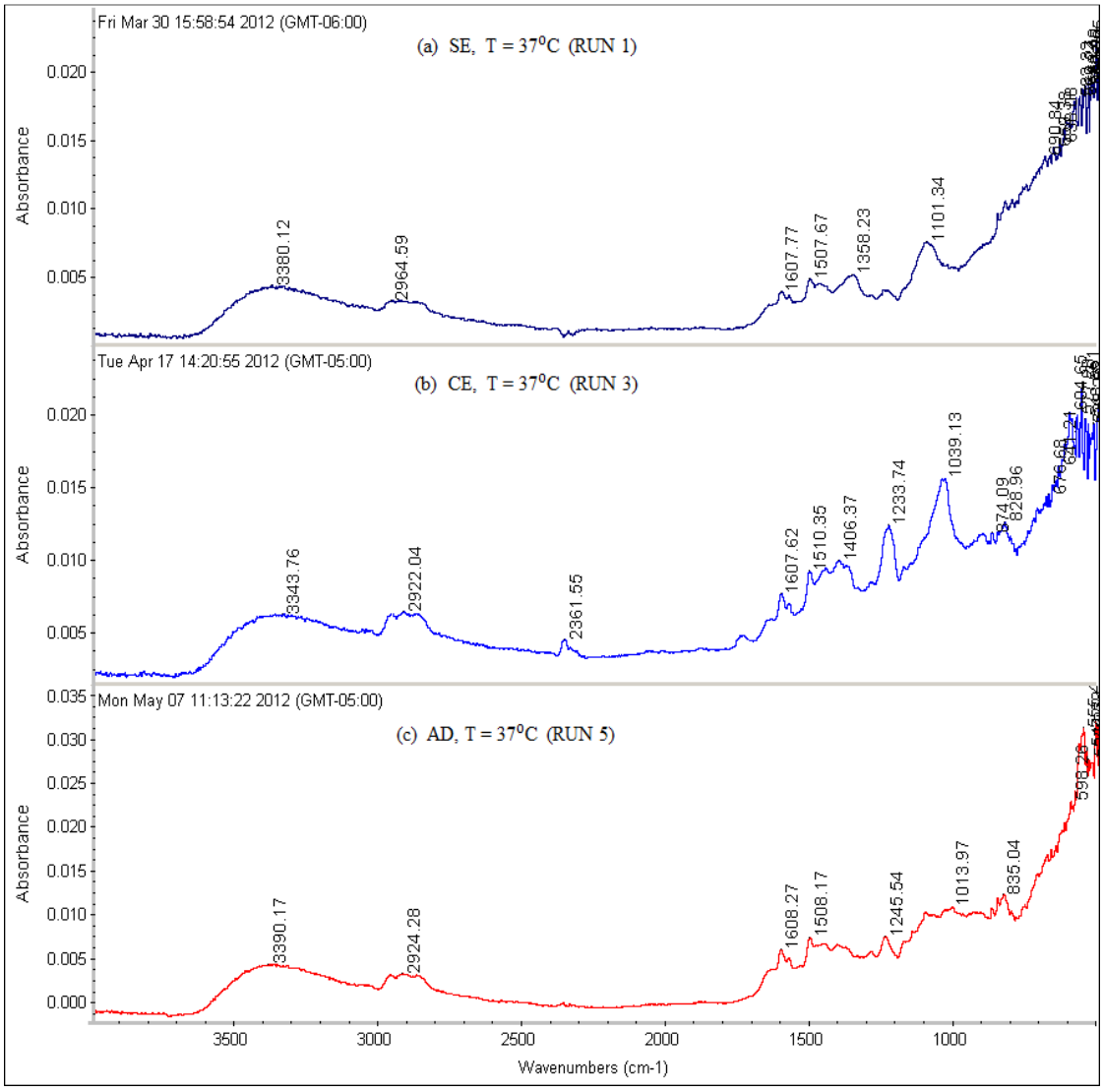

Figure 5.13. FTIR spectra for the RO membrane fouled by the feed water of location 6 at 37°C: (a) SE membrane (RUN 1); (b) CE membrane (RUN 3; (c) AD membrane (RUN 5).

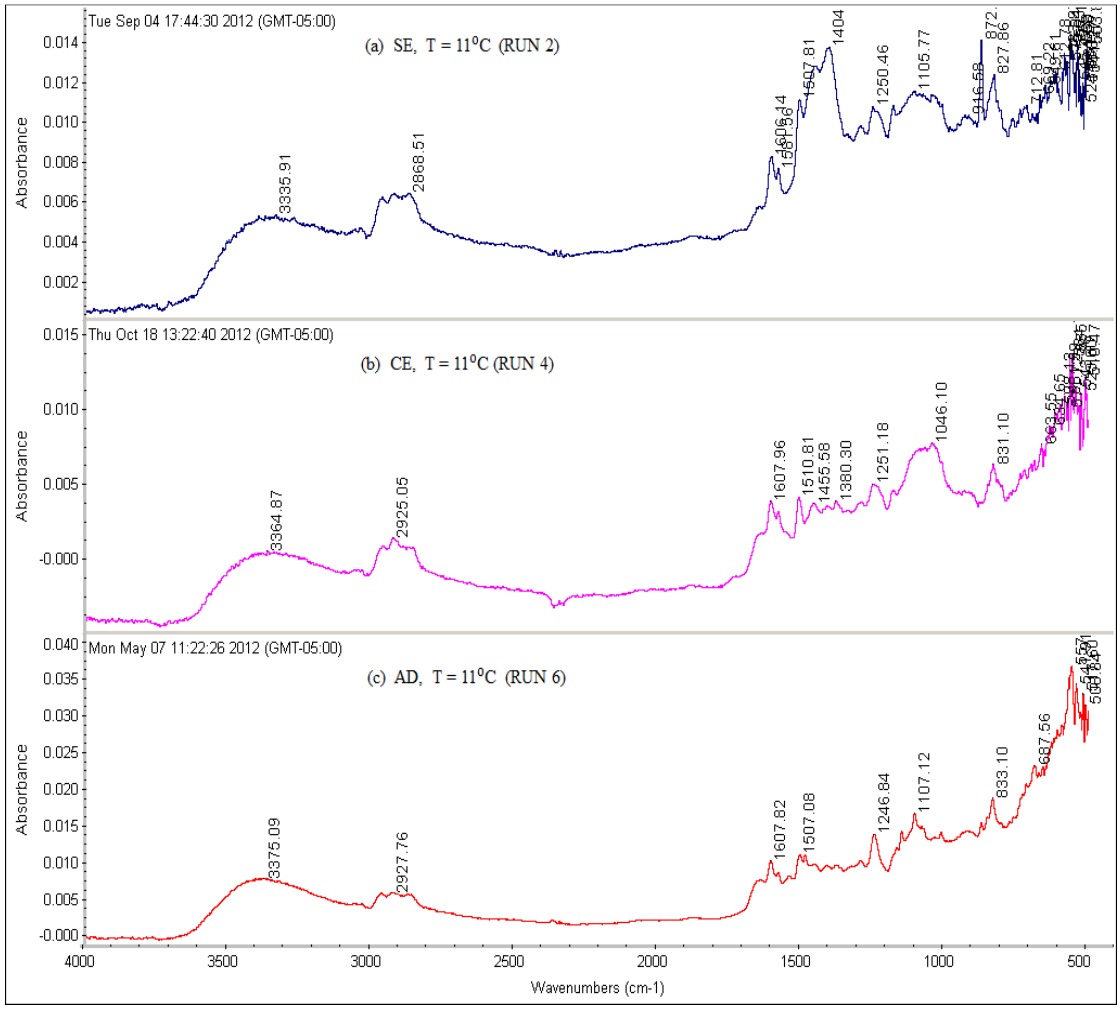

Figure 5.14. FTIR spectra for the RO membrane fouled by the feed water of location 6 at 11°C: (a) SE membrane (RUN 2); (b) CE membrane (RUN 4); (c) AD membrane (RUN 6).

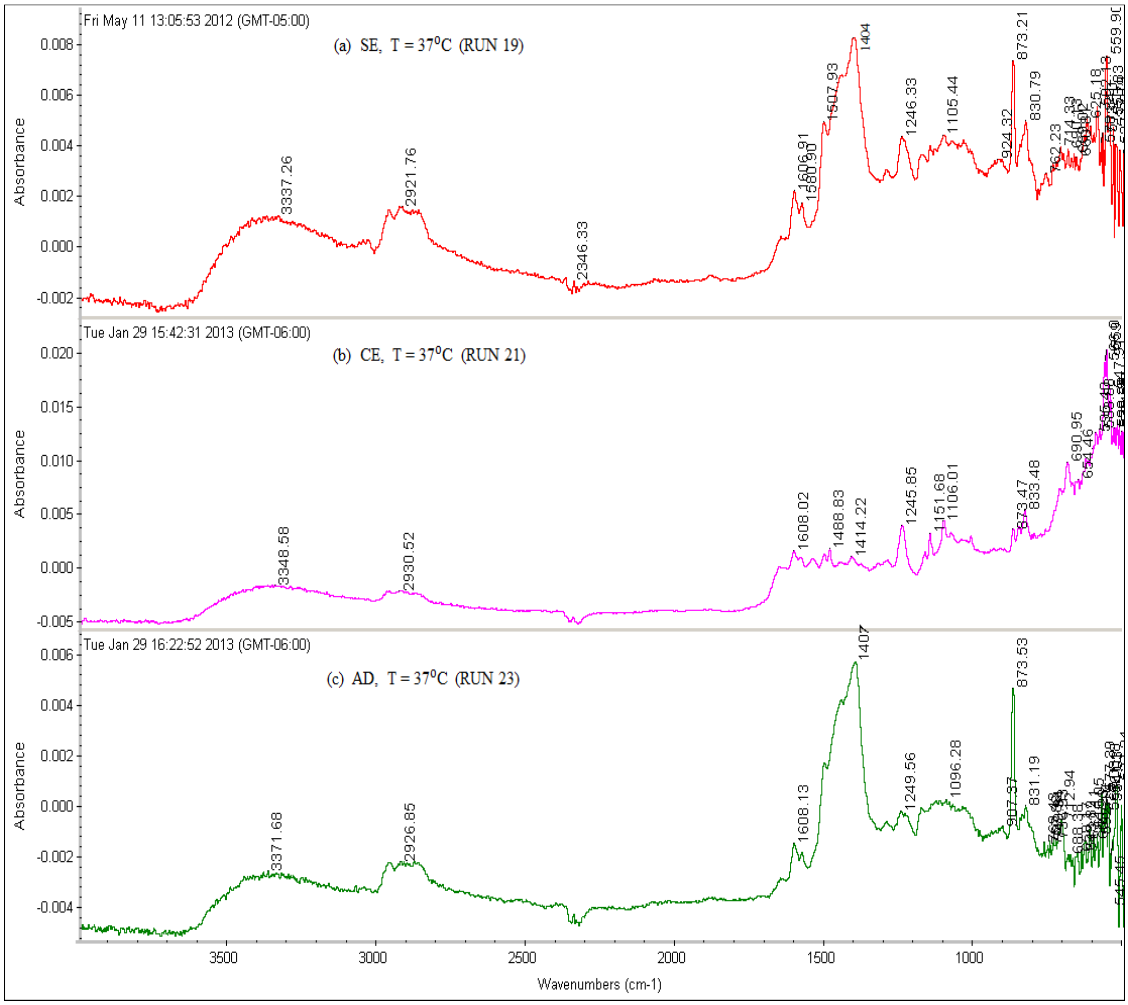

Figure 5.15. FTIR spectra for the RO membrane fouled by the feed water of location 5 at 37°C: (a) SE membrane (RUN 19); (b) CE membrane (RUN 21); (c) AD membrane (RUN 23).

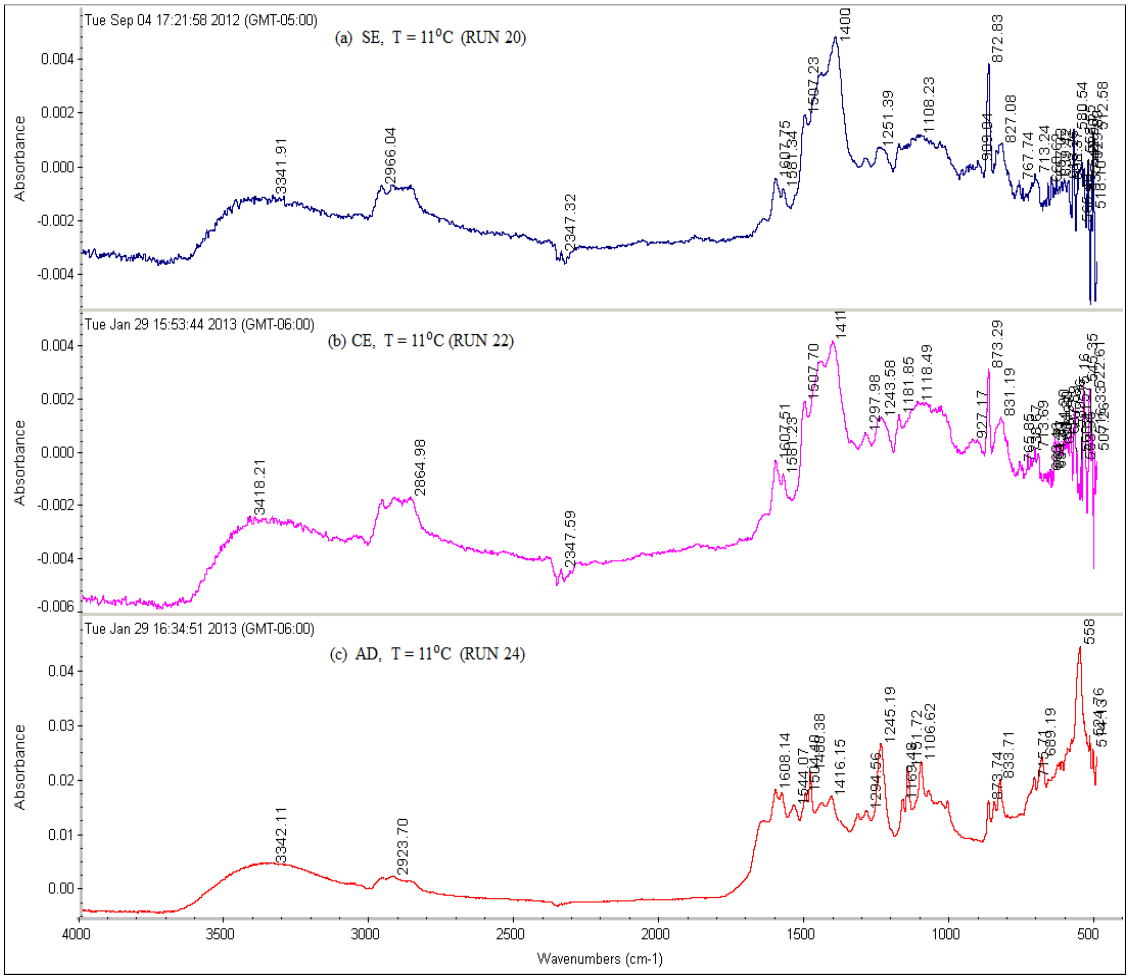

Figure 5.16. FTIR spectra for the RO membrane fouled by the feed water of location 5 at 11°C: (a) SE membrane (RUN 20); (b) CE membrane (RUN 22); (c) AD membrane (RUN 24).

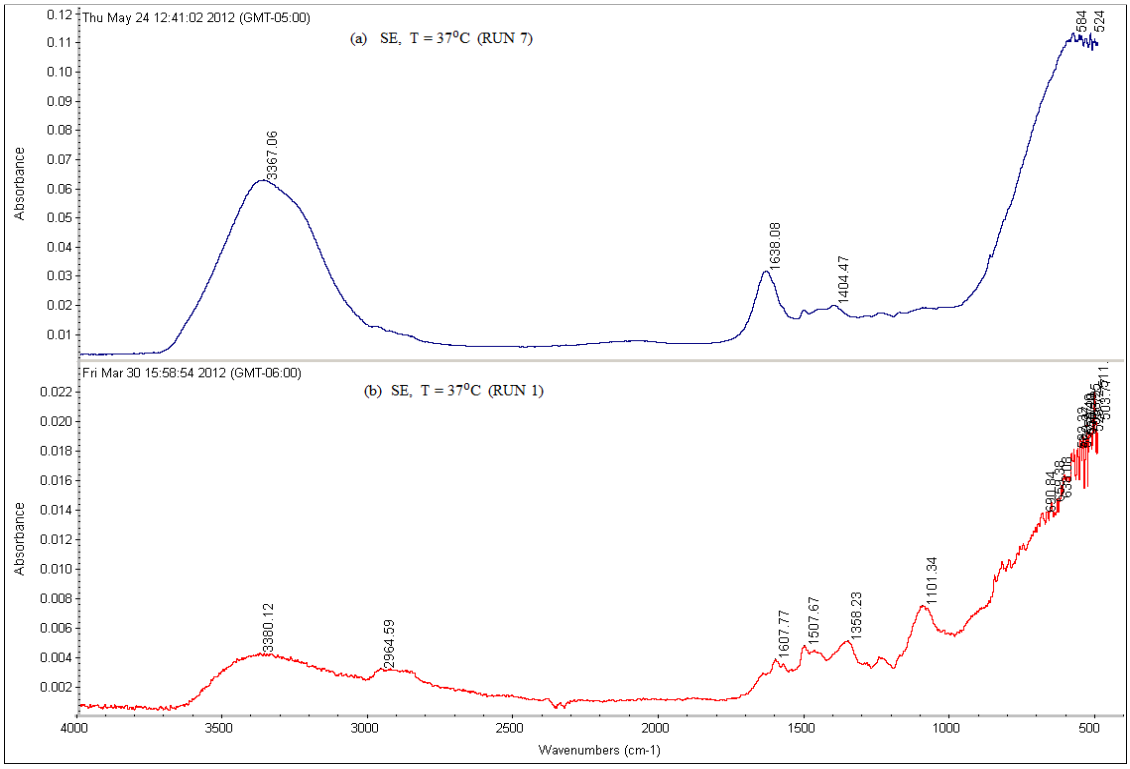

Figure 5.17. FTIR spectra for the SE membrane fouled by the feed water of location 6 at 37°C (RUN 7 with MF pretreatment and RUN 1 without MF pretreatment).

5.2.4. SEM/EDXS Analyses of Fouled Membranes

As mentioned before, a Zeiss NEON High Resolution Scanning Electron Microscope (SEM) operating at 10 kV in conjunction with Energy-Dispersive X-ray Spectroscopy (EDXS) and Secondary Ion Beam (FIB) (Samuel Roberts Noble Electron Microscopy Laboratory, University of Oklahoma) was used to directly observe the fouling materials deposited on the surface of the RO membranes. Samples from different fouled membranes were cautiously cut to preserve the biomass material in its original deposited condition. Then, the samples were sputter-coated with iridium (Ir) prior to the SEM imaging to prevent the charge up of the material surface which can cause a high brightness and result in a weak contrast in the image (JEOL, 2012). In general, for most of the runs, two spectra were taken to show the variation of the morphology of the scale formation on the surface of the RO membranes.

Both surfaces of the unused membranes and the fouled membranes were observed. First of all, samples from the clean CE, SE, and AD membranes were imaged by the SEM, and corresponding EDXS spectra were taken to reveal the morphology of the membrane surfaces and to also compare them to the fouled membranes surfaces. The SEM images of the unused membranes show that the surface of the CE membrane had a very smooth morphology, as shown in Figure 5.18, compared to a rough surface morphology of the SE and AD membranes, as shown in Figures 5.19 and 5.20, respectively. The EDXS spectra of the three membranes show that all membranes had a high percentage of carbon which can be caused by the aliphatic functional group in the cellulose acetate (CE) membrane, aromatic functional group in the polyamide (AD) membrane, and aliphatic and aromatic functional groups in the thin film composite (SE) membrane (Kucera, 2010; Kumar et al., 2006). A considerable percentage of sulfur is present in the spectra of both the SE and AD membranes as a result of the micro-porous substrate, which is typically polysulphone.

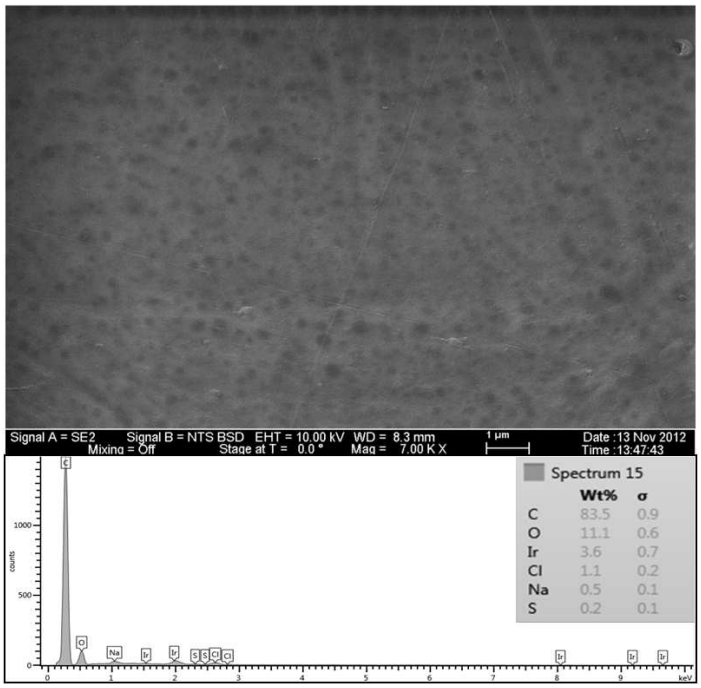

Figure 5.18. SEM image and EDSX spectrum of unused CE membrane.

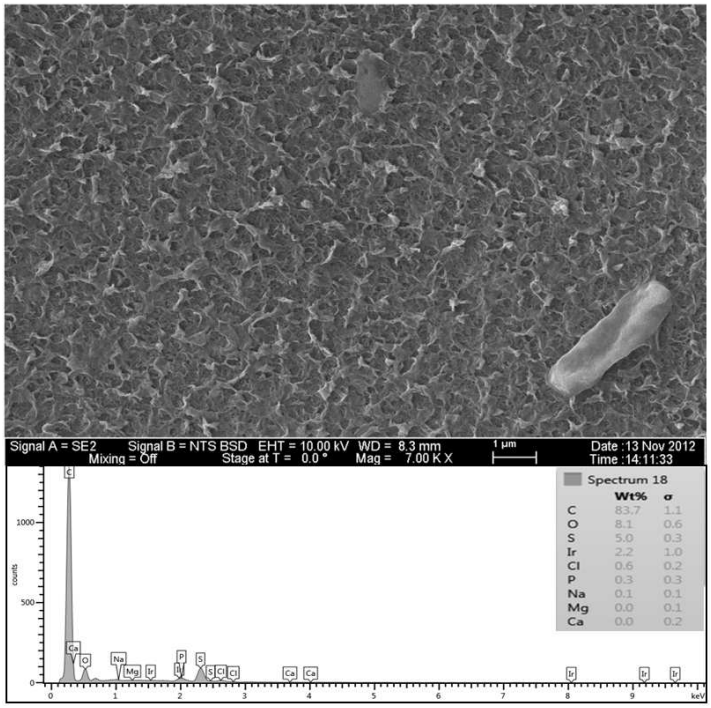

Figure 5.19. SEM image and EDSX spectrum of unused SE membrane.

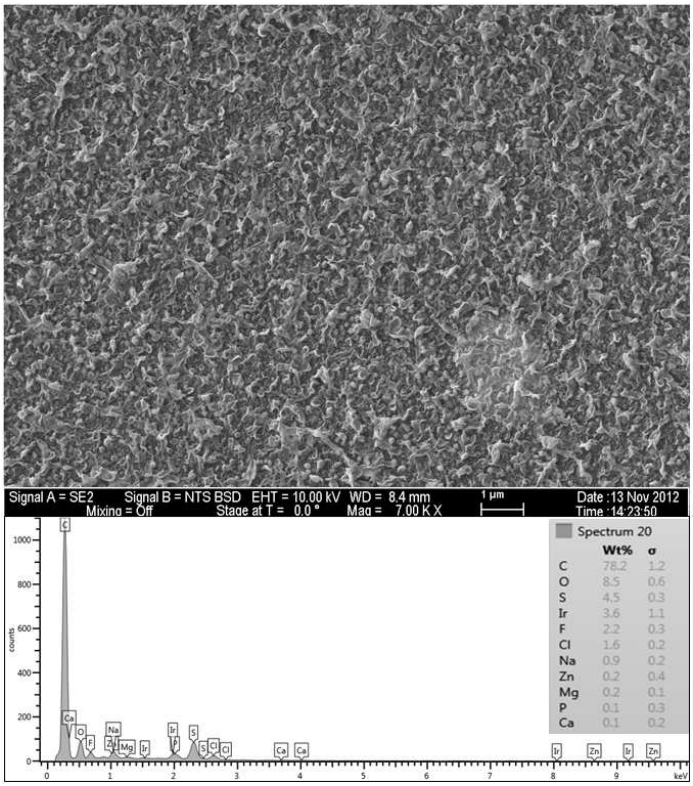

Figure 5.20. SEM image and EDSX spectrum of unused AD membrane.

Figure 5.21 elucidates a comparison of the extent of scale formation across the SE membrane surface for the three feed waters at the temperature of 37^{o}C using two levels of magnification (200 X and 1.0 KX). Sub-Figures 5.21 (a) and (b) show that a thick layer of the fouled material from the feed water of location 6 (run 1), where the highest TDS (2569 - 2657 mg/L) and the highest TOC (4.55 – 4.8 mg/L) existed, almost evenly covered the entire SE membrane surface. In addition, sub-Figures 5.21 (c) and (d) display that a thinner layer of the fouled material from the feed water of location 1 (run 13), where the TDS ranged between 1338 and 1428 mg/L and the TOC ranged between 1.4 and 2.3 mg/L, almost covered the entire surface of the SE membrane. Moreover, sub-Figures 5.21 (e) and (f) show that the fouled material from the feed water of location 5 (run 19), where the lowest TDS (679 - 742 mg/L) and the lowest TOC (1.2 – 1.4 mg/L) were present, partially covered the surface of the SE membrane. However, the results of the additional SEM images of different runs, as they will be illustrated in this section, revealed that the distribution and the morphology of the fouled materials deposited on the RO membrane surface depend not only on the feed water quality, but also on the type of the membrane and the operating conditions, such as the feed water temperature.

To investigate the difference in the scale morphology among the three types of the membranes (SE, CE, and AD), three SEM images of these membranes were taken after the membranes were operated under identical conditions (i.e. feed water quality of location 6, temperature of 37^{o}C, feed pressure of 380 psi - 400 psi, and feed flow rate of 0.6 gpm). First, Figure 5.22 shows the SEM image and the EDSX spectrum of the fouled SE membrane (run 1). The EDSX analysis unexpectedly showed that the scale formation had high level of Ni and Fe which were not highly present in the feed water of location 6. As expected, O, C, Na^{+}, Ca^{+2}, Mg^{+2}, and Cl^{-} were present in the spectrum. The data suggest that the fouling was due to a combination of organic matter and inorganic material. The presence of Ni was apparently due to a mistake in detecting the ions by the EDSX, because it did not appear in the other spectra. On the

other hand, although Fe was observed in the feed water in low quantity, it was probably due to a leaching from the system parts. For example, some rust was seen on the submerged part of the heated immersion circulator indicating a leach of iron into the feed water.

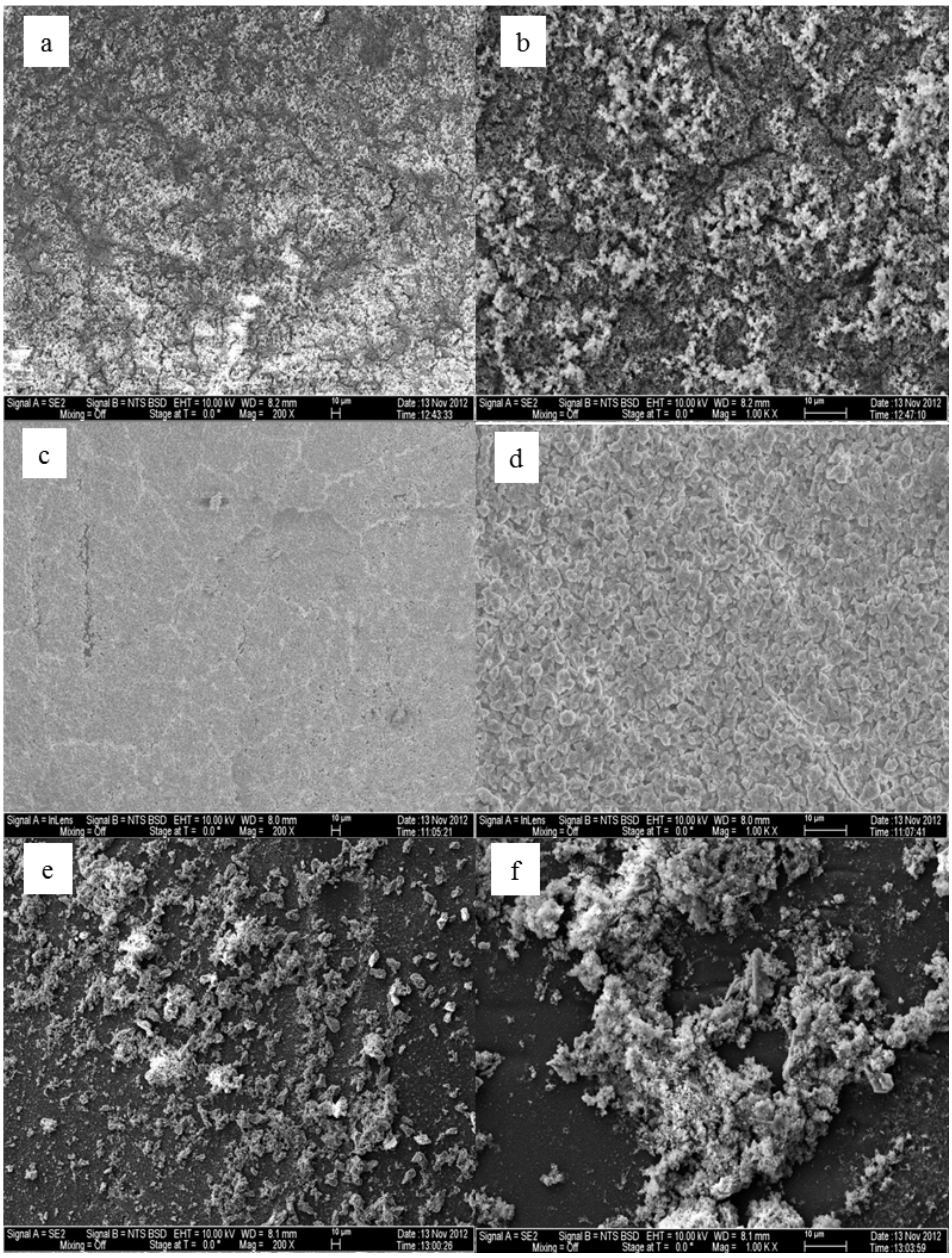

Figure 5.21. SEM image and EDSX spectra of (a) run 1 at magnification of 200 X; (b) run 1 at magnification of 1 KX; (c) run 13 at magnification of 200 X; (d) run 13 at magnification of 1 KX; (e) run 19 at magnification of 200 X; (f) run 19 at magnification of 1 KX.

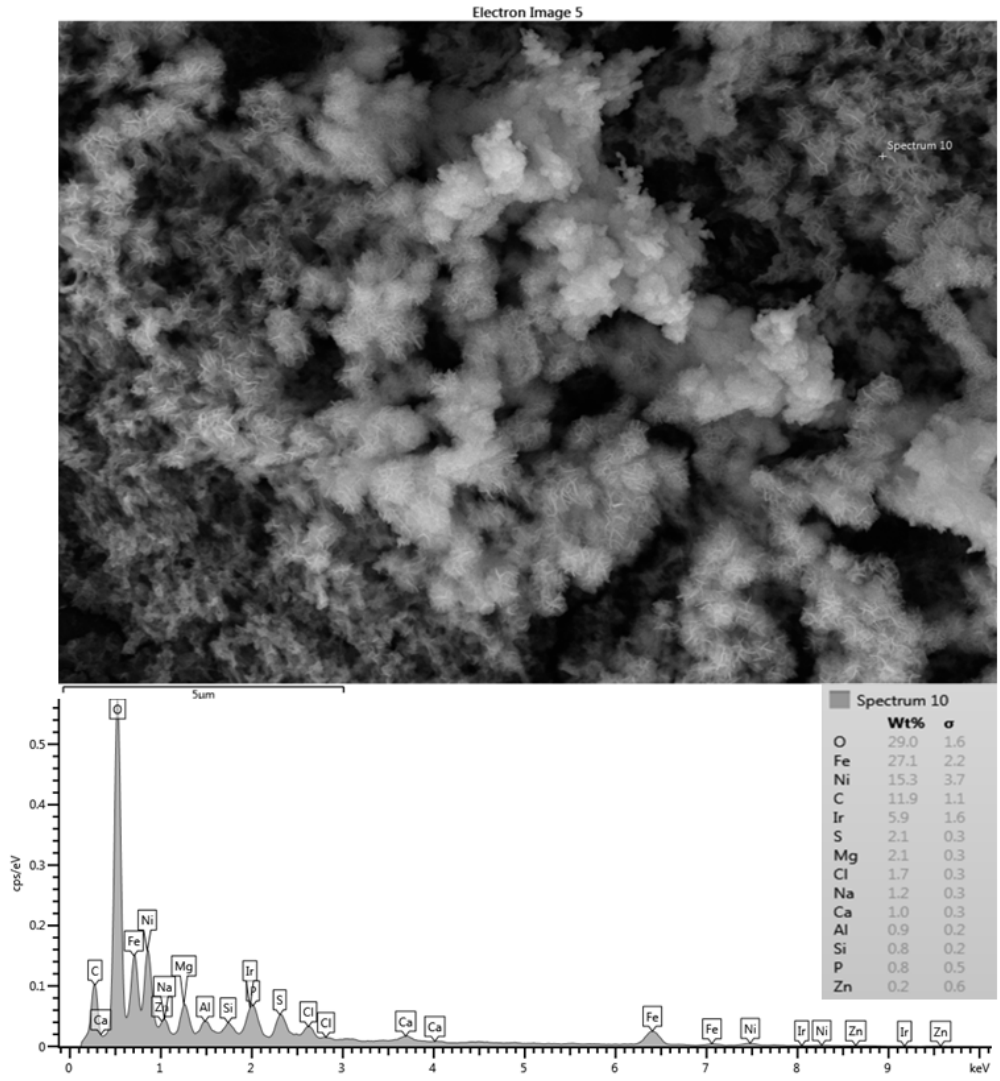

Figure 5.22. SEM image and EDSX spectrum of fouled SE membrane for location 6 (run 1). Run 1 was conducted at a feed flow rate of 0.6 gpm (2.27 Lpm), a temperature of 37°C, and a range of feed pressure of 380 psi - 400 psi (2,620 kPa – 2,757 kPa).

However, the deposited material on the CE membrane surface (run 3) which was conducted with the same water quality in location 6 at the temperature of 37°C mostly covered the membrane surface with a crystal structure (flowers) and lesser amounts of nonuniform shapes, as illustrated in Figure 5.23. To investigate both structures, spectra were taken in both places. Spectrum 8, which was located on the flower structure, shows that a high level of Ca^{+2} (38.1%) was present compared to a lower level (4.8%) in spectrum 9. Both spectra show high levels of C

and O. Moreover, spectrum 9 also shows a high level of Fe^{+2} (26.3%). The high peaks of O, C, and Ca^{+2} that exist in spectrum 8 suggest that the structure of the deposited material was calcium carbonate ($CaCO_3$) which is exactly consistent with that observed by Tzotzi et al. (2007) on a thin film composite polyamide membrane surface. The data presented in spectrum 9 suggest that the crystal forms (flower structure) were accompanied by a small amount of a mixture of organic matter and inorganic materials. In addition, the black smooth spots on the SEM image in Figure 5.23 are parts of the CE membrane surface. Therefore, the fouled material of run 3 partially covers the CE membrane surface compared to that of run 1 which apparently covers the entire surface of the SE membrane, as illustrated in Figure 5.22. This provides one potentially reasonable cause for the rapid decline in the permeate flux of run 1 compared to that of run 3. This observation agrees with the hypothesis that the permeate flux decline increases linearly with the increase of the scale formation on the membrane surface (Antony et al., 2011; Tzotzi et al., 2007).

Figure 5.24 shows that the fouled layer deposited on the AD membrane surface (run 5) has different shapes. Some large crystal shapes exist as part of the scale formation on the membrane surface. Also, two spectra were taken to investigate the morphology of the two different shapes of the fouled material on the membrane surface. Similar to the observation in spectrum 8 of run 3, spectrum 6 which was taken on the crystal shape shows a high level of Ca^{+2} (27.3%) compared to a lower level of Ca^{+2} (1.8%) on the nonuniform shaped material, as shown by spectrum 5. Likewise, both spectra show a high level of C and O as well as a high level of Fe^{+2} (24%) on the nonuniform shaped material. In addition, spectrum 5 shows a low level of silica present in the deposited material, and spectrum 6 shows a high peak of Cl^{-} on the crystal shape. The SEM image and the data of spectra 5 and 6 suggest that the fouling materials deposited on the AD membrane surface have different configurations, including crystals of different shapes and a mixture of organic and inorganic matter. As a result of high levels of O, C, and Ca^{+2}, the

large crystal form is also possibly due to the formation of $CaCO_3$ which was reported as a common scale with all feed types by Antony et al. (2011), Kucera (2010), and Greenlee et al. (2009).

The flower crystals of $CaCO_3$ seen in Figure 5.23 and the large and elongated crystals seen in Figure 5.24 are probably due to the high TOC (4.55-4.8 mg/L) and carbonate (72-82.42 mg/L) concentrations of the feed water in location 6, and $CaCO_3$ is likely a calcite crystal form as suggested by Koyuncu and Wiesner (2007). Also, they claimed that the ratio of the organic matter/calcium has an effect on the shape of the $CaCO_3$ crystal in the cake formation. Moreover, Koyuncu et al. (2006) proposed that organic matter may play a role in reducing calcium diffusivity in the cake formation. In addition, Lee et al. (2005) reported that natural organic matter (NOM) can reduce free calcium ions by producing NOM-calcium complexes on the membrane surface. Also, they claimed that NOM-calcium complexes form a compressed layer on the membrane surface which severely decreases the permeate flux. Therefore, some spectra did not show high peaks of calcium, particularly when the scale formation on the membrane surface was a more sludge-like deposit than crystal formation, such as those of runs 1(see Figure 5.22) and 4 (see Figure C7). The results of the various configurations of the scale formations deposited under the same conditions on the three types of the RO membrane indicate that the surface roughness and the material of the membrane itself affect the scale formation which ultimately impacts the permeate flux (Roever and Huisman, 2007; Tzotzi et al., 2007).

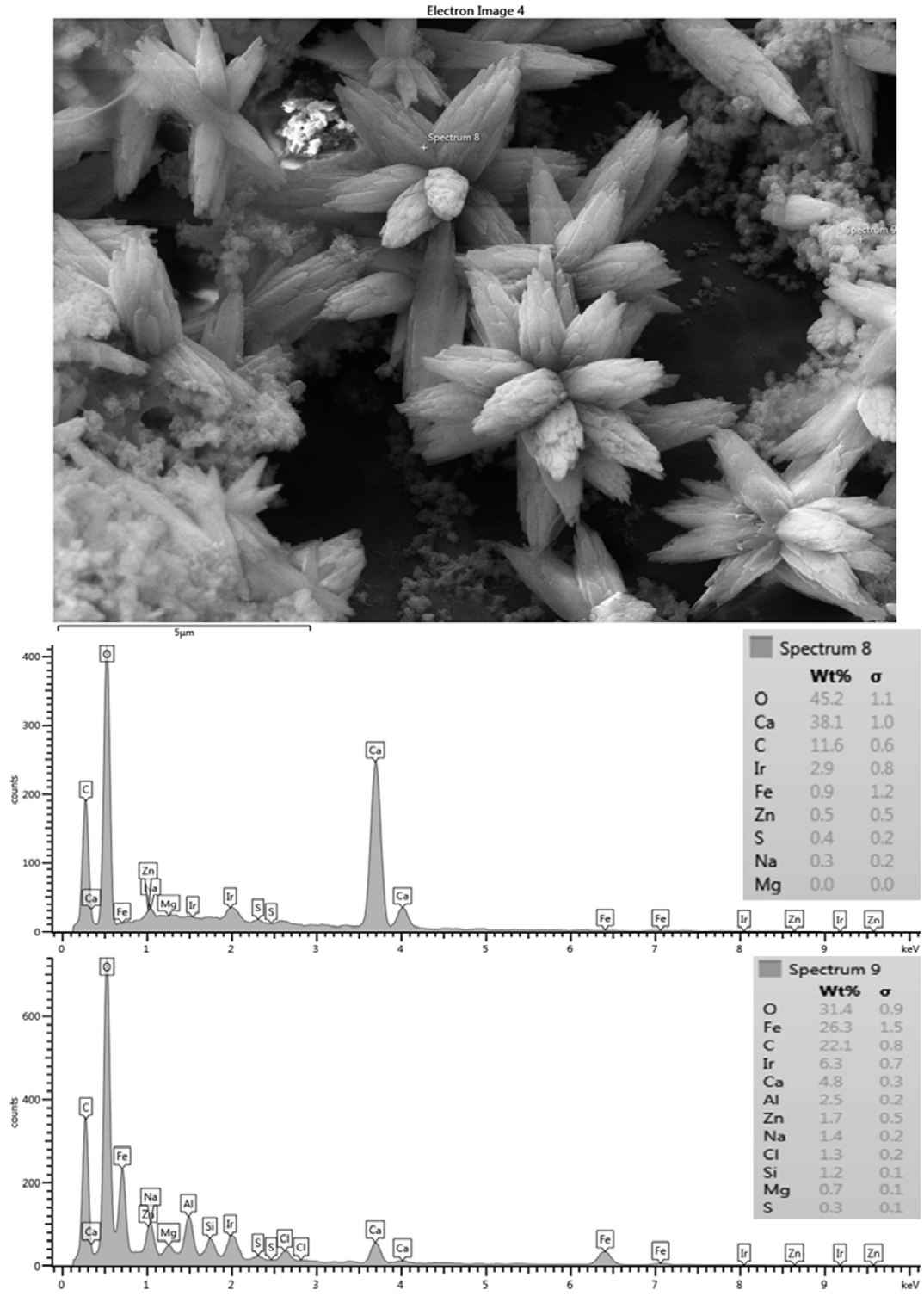

Figure 5.23. SEM image and EDSX spectrum of fouled CE membrane for location 6 (run 3). Run 3 was conducted at a feed flow rate of 0.6 gpm (2.27 Lpm), a temperature of 37^{o}C, and a range of feed pressure of 380 psi - 400 psi (2,620 kPa – 2,757 kPa).

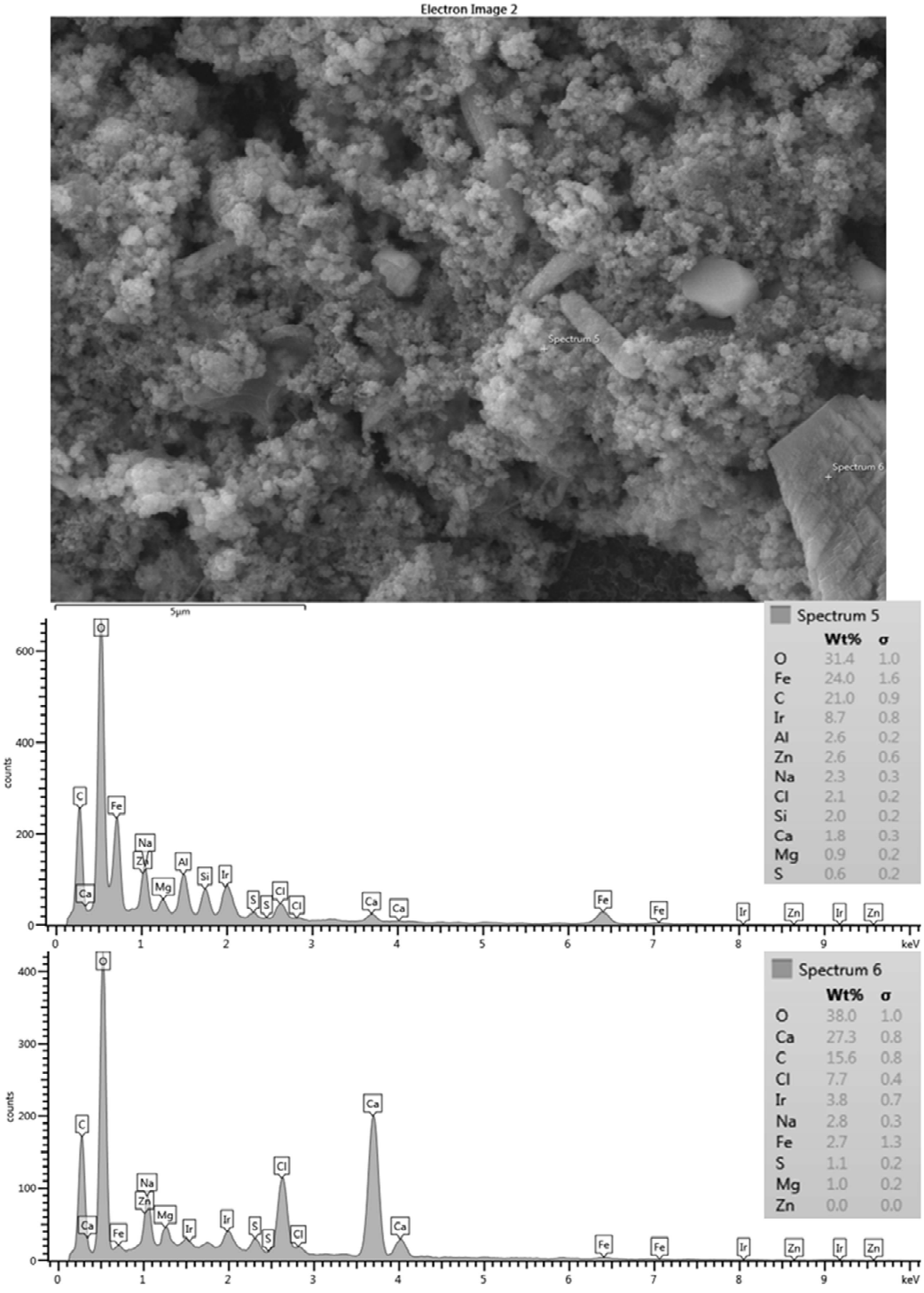

Figure 5.24. SEM image and EDSX spectrum of fouled AD membrane for location 6 (run 5). Run 5 was conducted at a feed flow rate of 0.6 gpm (2.27 Lpm), a temperature of 37^{o}C, and a range of feed pressure of 380 psi - 400 psi (2,620 kPa – 2,757 kPa).

The effect of feed water temperature on the formation of the fouled material deposited on the membrane surface was also examined in this study. The SEM images in Figure 5.25 show a comparison between the scale formations on the surface of several RO membranes at high and low temperatures. The SEM images focus on the densest accumulated materials on the selected RO membrane surfaces. The scale formation on the CE membrane at the temperature of 11^{o}C (run 4) is quite different from that at 37^{o}C (run 3), as shown in sub-Figures 5.25 (a) and (b). The morphology of the fouled material on the CE membrane surface of run 3, as previously mentioned, is more in crystalline shape which is mostly $CaCO_3$, while the morphology is a sludge-like deposit on the membrane surface of run 4. It is obvious that low temperature (11^{o}C) affected the deposited material on the CE membrane and resulted in the sludge layer. Jawor and Hoek (2009) reported that high temperatures (25 to 35^{o}C) of brackish feed water can enhance the crystal formation of the deposited material on the RO membrane surface, which agrees with what has been observed in run 3. The EDSX spectrum of fouled membrane of run 4 (see Figure C7, appendix C) shows that high levels of C and O, lesser amounts of Fe, Cl^{-}, Zn, Na^{+}, and Ca^{+2}, and a small amount of P, Mg^{+2}, and S were present in the scale formation. The results suggest that the scale formation on the CE membrane surface of run 4 is mostly organic matter or carbonaceous which can be attributed to the high levels of TOC and carbonate of the feed water, and is accompanied by inorganic materials. It can be assumed that the higher total permeate flux drop of run 4 (42.8%) compared to that of run 3 (34.7%) is a consequence of the blockage of the CE membrane surface as a result of the sludge layer formation.

In lower TOC feed water (1.4 - 2.3 mg/L), the effect of the temperature on the morphology of the deposited material on the membrane surface is not the same as the one seen in the high TOC feed water (4.55 – 4.8 mg/L). The SEM images of the fouled SE membrane of run 13 and run 14 shown in sub-Figures 5.25 (c) and (d) revealed that the formation of the fouled material from the feed water in location 1 deposited on the membranes surface is mostly in crystal

shapes at both temperatures (37 and 11°C). In addition, the results exhibited that the EDSX spectra of both fouled membranes (see Figures C10 and C11, appendix C) are nearly identical. Both spectra have high peaks of C, O, and Ca^{+2} indicating that the formed crystal on the membrane surface is likely $CaCO_3$. The relatively low TOC and high Ca^{+2} (77.4-82 mg/L) and carbonate (73-94.2 mg/L) concentrations in feed water in location 1 apparently resulted in the uniform crystal shapes of $CaCO_3$. This observation is consistent with the findings noted by Koyuncu and Wiesner (2007).

Moreover, the SEM images of the deposited material from the feed water in location 5 at the temperature of 37°C (run 19) and 11°C (run 20), are shown in sub-Figures 5.25 (e) and (f), respectively. Both images show that the fouling materials extend across the entire surface of the SE membranes with a more crystalline morphology of the fouling developed on the membrane surface of run 20 at a low temperature (11°C). The EDSX spectra shown in Figures C12 and C13 (appendix C) revealed a high peak of Ca^{+2} in addition to the high peaks of O and C on the fouled membrane surface of run 20, which indicate that most of the crystal morphology is $CaCO_3$. Also, the EDSX spectra display that the fouling of run 19 and run 20 have a combination of organic matter and inorganic material. In addition, Inductively Coupled Plasma (ICP) spectrometer analysis showed that the Ca^{+2} concentration of the permeate at low temperature (run 20) was higher than that at high temperature (run 19), as shown in Figure 5.26. The Ca^{+2} concentration is a consequence of more calcium deposits on the SE membrane surface which resulted in forming more crystal morphology like $CaCO_3$.

Sub-Figures 5.25 (g) and (h) show the SEM images of the scale formation of the fouled material from feed water in location 5 deposited on the CE membrane surface at the temperatures of 37°C (run 21) and 11°C (run 22), respectively. Similar to those of run 19 and run 20, the scale formation also extended across the entire surface of the CE membrane of runs 21 and 22. The

fouling form of the high feed water temperature is apparently sludge-like deposit on the membrane surface, while the fouling form of low feed water temperature is a combination of both sludge and crystalline shapes. The EDSX spectra in Figure C14 show that the cake formation of run 21 has the carbon range of 77.6% – 79.1% and oxygen of 13.8% - 14.4%, suggesting that the majority of the fouled material is organic matter. However, the EDSX spectra of Figure C15 exhibit a high range of calcium (25.5% – 59.1%), besides the high ranges of the carbon (7.9% - 22.7) and the oxygen (23.8% - 43.6%) in the fouled material of run 22, suggesting that the large particles of the cake formation are similar to those of run 20, which are $CaCO_3$. Again, the low TOC and high carbonate concentrations of the feed water in location 5 were likely the main reason behind the formation of the $CaCO_3$ crystals. This observation agrees with what found by Koyuncu and Wiesner (2007). Contradictory to the morphology observation of the high TOC and TDS feed water runs (for instance runs 3 and 4), the low temperature (11^{o}C) with the low TOC and TDS feed water (for instance runs 21 and 22) enhances the crystal formation of the deposited material on the RO membrane surface (see Figure 5.25).

Overall, the results of the SEM images and EDSX spectra of the previously discussed runs revealed that the selected RO membranes have high rejection of organic matter, carbonate, and calcium, as also observed by Antony et al. (2011), Koyuncu & Wiesner (2007), Tran et al. (2007), and Koyuncu et al. (2006).

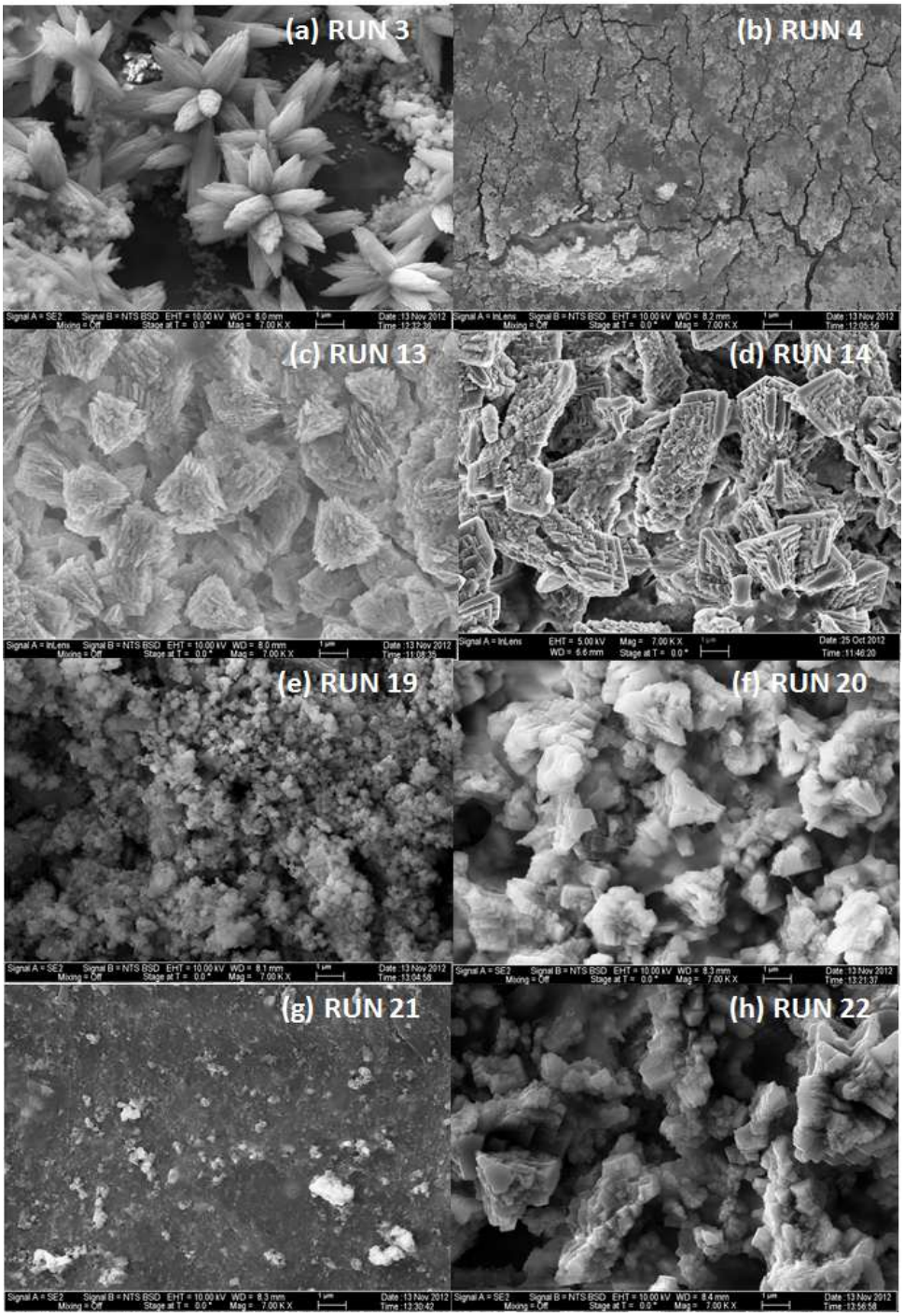

Figure 5.25. SEM images of fouled RO membranes: (a) CE membrane at 37^{o}C for location 6 (run 3), (b) CE membrane at 11^{o}C for location 6 (run 4), (c) SE membrane at 37^{o}C for location 1 (run 13), (d) SE membrane at 11^{o}C for location 1 (run 14), (e) SE membrane at 37^{o}C for location 5 (run 19), (f) SE membrane at 11^{o}C for location 5 (run 20), (g) CE membrane at 37^{o}C for location 5 (run 21), and (h) CE membrane at 11^{o}C for location 5 (run 22).

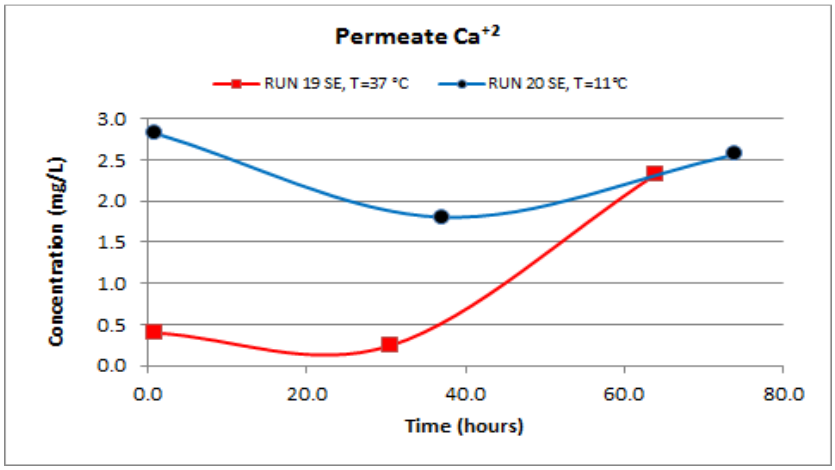

Figure 5.26. Evolution of the permeate calcium concentration of run 19 at 37°C and run 20 at 11°C. Runs 19 and 20 were conducted at a feed flow rate of 0.6 gpm (2.27 Lpm) of location 5 and a range of feed pressure of 380 psi - 400 psi (2,620 kPa – 2,757 kPa).

Another observation is that although the feed waters in locations 1 and 6 had high concentrations of sulfate (312-320 mg/L and 681-687.4 mg/L, respectively), sulfur peaks were at very low levels, as shown in some of the spectra of the runs, indicating that some potentially low level of $CaSO_4$ precipitated on the membrane surface. The low level of the precipitated sulfate is due to the high rejection of the RO membranes for the carbonate which outcompetes the sulfate ion, as interpreted by Koyuncu and Wiesner (2007). It is also noted that the concentration of the sulfate in the concentrate stream of all conducted runs was very high when the desired water recovery was achieved. For example, the final sulfate concentrations in the concentrate stream of runs 1, 3, and 5 in location 6 were 2280, 1813.3, and 1917.1 mg/L, respectively. Another example is that the final sulfate concentrations in the concentrate stream of runs 19, 21, and 23 in location 5, which is a relatively low sulfate feed water (88.8 - 91.4 mg/L) compared to locations 1 and 6, were 331.4, 548.8, and 466.94 mg/L, respectively. This observation provides additional evidence that only small amounts of sulfur precipitated on the surface of the fouled RO membranes.

The effect of using 0.1 micron MF membrane, which is considered as the most appropriate method to remove larger particulates as a pretreatment unit of the feed water in

advance of the RO membrane (Greenlee et al., 2009), on the precipitated material on the membrane surface was also investigated. Figure 5.27 shows an SEM image comparison of the fouled material of the un-pretreated (run 3) and pretreated (run 9) feed water in location 6 on the CE membrane surface. The SEM images in Figure 5.27 display that the extent of the fouling across the surface of the CE membrane conducted without the MF membrane covers more than 70% of the membrane surface, compared to about 25% of that of the CE membrane conducted with the MF membrane. This gives a reasonable cause to justify the high initial permeate flux of run 9 (0.716 Lpm/m^2) compared to the lower initial permeate flux of run 3 (0.481 Lpm/m^2). Additionally, the formation of the fouled materials from the pretreated feed water by the MF membrane on the CE membrane surface (run 9) is apparently in clusters, and the EDSX of run 9 (Figure C9) shows high peaks of C and O indicating that most of the fouling is organic matter. Furthermore, the EDSX spectra of run 3 and run 9, shown in Figures C6 and C9, elucidate that the precipitated calcium level on the membrane surface decreased from 38.1% to 0.4%. In addition, the permeate calcium concentration of run 9 conducted with the MF membrane is lower than that of run 3 conducted without an MF membrane, as shown in sub-Figure 5.28 (a), while the final concentration of the calcium in the concentrate stream of run 9 is higher than that of run 3, as shown in sub-Figure 5.28 (b). The results suggest that more organic matter, which plays an important role in reducing calcium diffusivity in the fouled layer (Koyuncu and Wiesner 2007; Koyuncu et al., 2006; Lee et al., 2005), deposited on the RO membrane surface of run 9, and also more inorganic material was captured by the MF membrane. Therefore, the precipitated calcium on the surface of the fouled CE membrane was considerably reduced, and consequently the concentration of the calcium in the permeate stream of run 9 reduced as well. However, the concentrations of the sulfate and chloride in the permeate stream of run 3 are higher than those of run 9. As a result, the permeate conductivity of run 9, as previously mentioned and illustrated in sub-Figure 5.9 (b), is slightly lower than that of run 3.

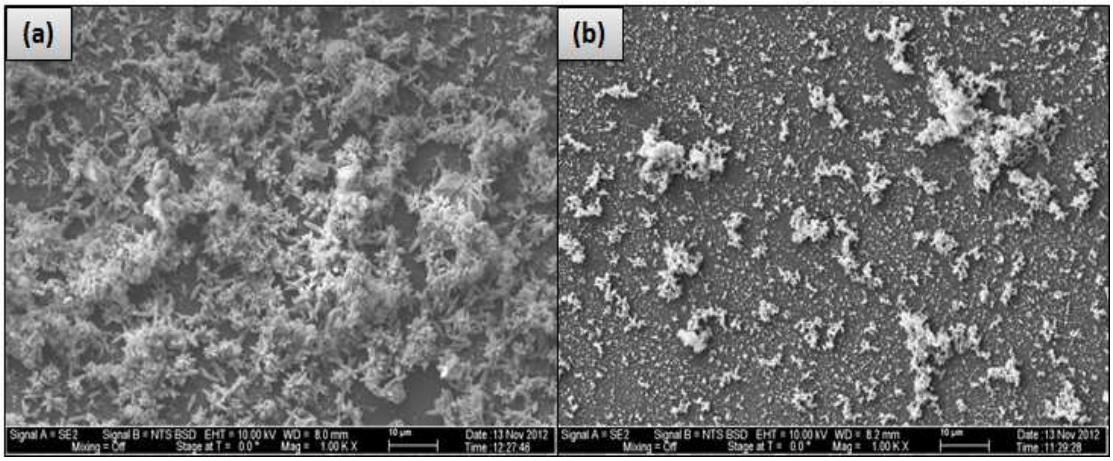

Figure 5.27. SEM image of (a) the fouled CE membrane by the un-pretreated feed water of location 6 by MF membrane (run 3) and (b) the fouled CE membrane by the pretreated feed water of location 6 by MF membrane (run 9). Both runs were conducted at a feed flow rate of 0.6 gpm (2.27 Lpm), a temperature of 37^{o}C, and a range of feed pressure of 380 psi - 400 psi (2,620 kPa – 2,757 kPa).

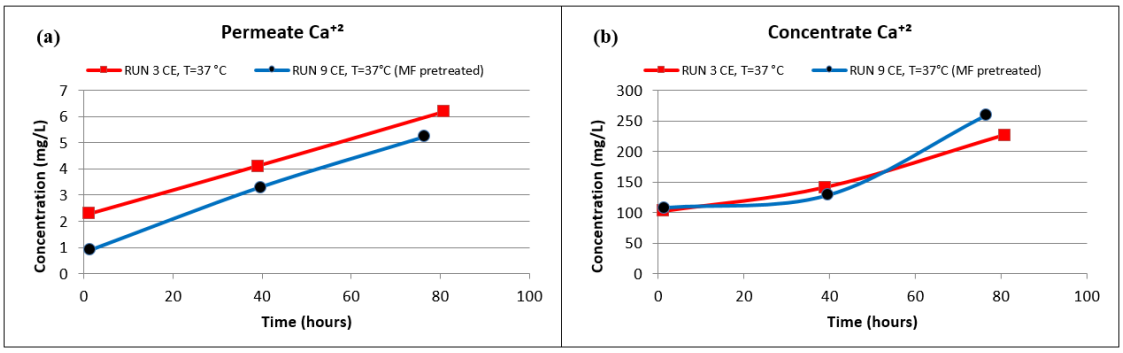

Figure 5.28. Evolution of the permeate (a) and concentrate (b) calcium concentration of runs 3 (without MF pretreatment) and 9 (with MF pretreatment). Runs 3 and 9 were conducted at a temperature of 37^{o}C, feed flow rate of 0.6 gpm (2.27 Lpm) of location 6 and a range of feed pressure of 380 psi - 400 psi (2,620 kPa – 2,757 kPa).

Furthermore, the SEM/EDSX investigation of the cross-section of the fouling layer on the SE membranes from the three water qualities was also done in this study. As previously mentioned, the clean SE membrane has three distinct layers, as shown in Figure 5.29. The top one is the effective layer which has a thickness of about 2.7 µm, and the two others are supporting layers. The spectrum of the clean membrane showed some peaks of Ir which was used to coat the

membrane samples to prevent the charge-up of the material surface. The results revealed that there were no distinct layers present through the formation of the fouling, such as those observed by Tran et al. (2007). Therefore, the associated EDSX spectra were represented by area instead of using spots. Figure 5.30 illustrates the thickness and the morphology of the scale formation of the fouling on the SE membrane from the feed water of location 6 (high TOC and high TDS). The EDSX spectrum of run 1, shown in Figure 5.30, displayed that, as previously observed in the plan view SEM image (Figure 5.22), the scale formation was due to a combination of organic matter and inorganic material. However, a higher level of Ca^{+2} was noticed in the cross-section SEM image than that of the plan view SEM image. Also, a high level of Ni and Fe was noted in the fouling layer. Figure 5.31 displays the SEM images of the cross-section of the fouling on the SE membrane from location 1 (moderate TOC and moderate TDS). Similar to the observation seen in run 1, the spectrum of run 13, shown in Figure 5.31, indicated that the fouling layer contained both organic and inorganic materials. However, the level of Ca^{+2} of the cross-section SEM image was lower than that of the plan view SEM image (Figure C10). In addition, Figure 5.32 illustrates the thickness and the formation of the fouled materials from location 5 (low TOC and low TDS) on the SE membrane. Moreover, similar to the observation seen in the plan view SEM image (Figure C12), the spectrum of the cross-section SEM image of the fouling of run 19, illustrated in Figure 5.32, exhibited high organic matter and lower inorganic material. Generally, the SEM images of the cross-section of the scale formation showed that the composition of the fouled material was about the same through the entire thickness.

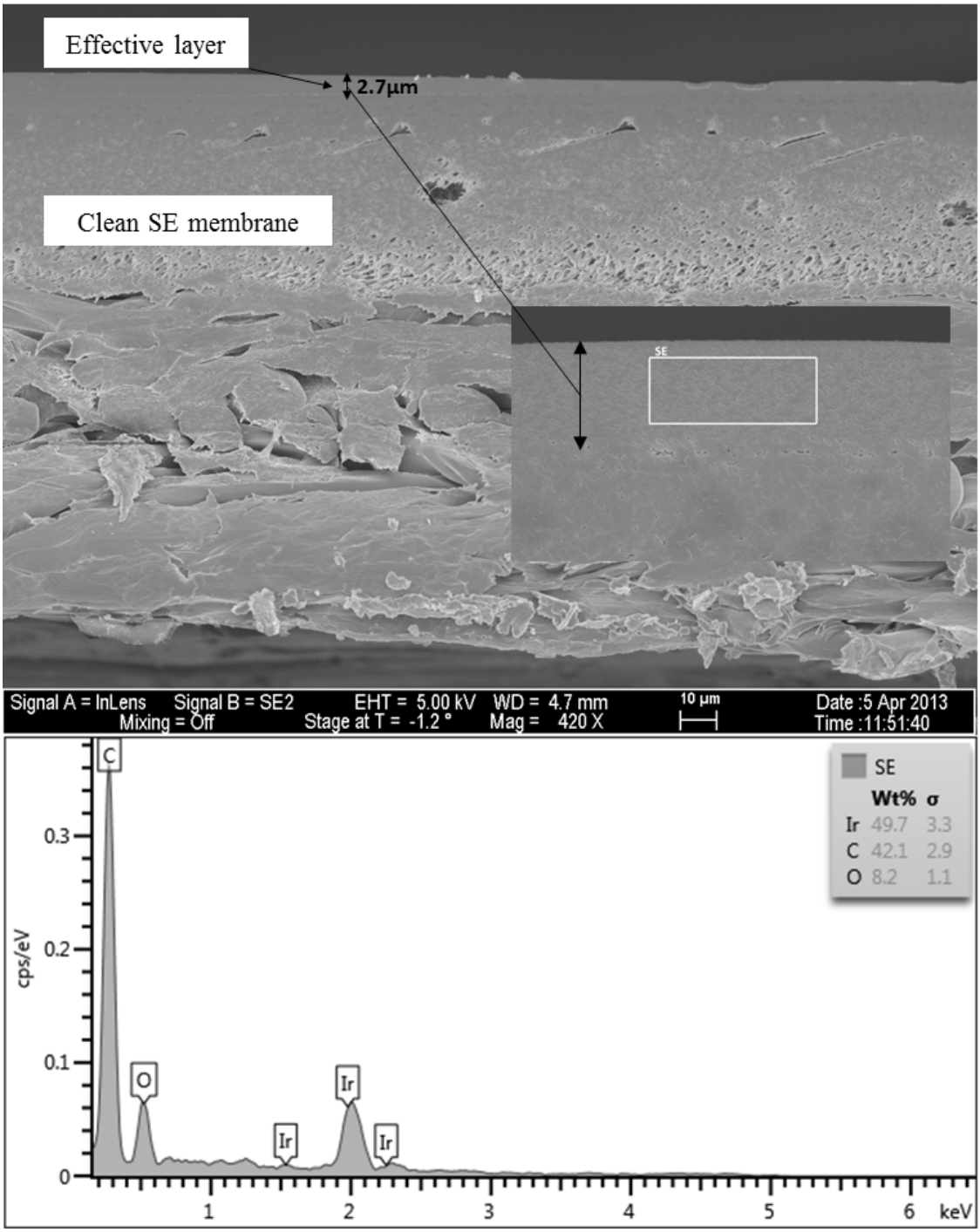

Figure 5.29. SEM images and EDSX spectrum of the cross-section of the clean SE membrane.

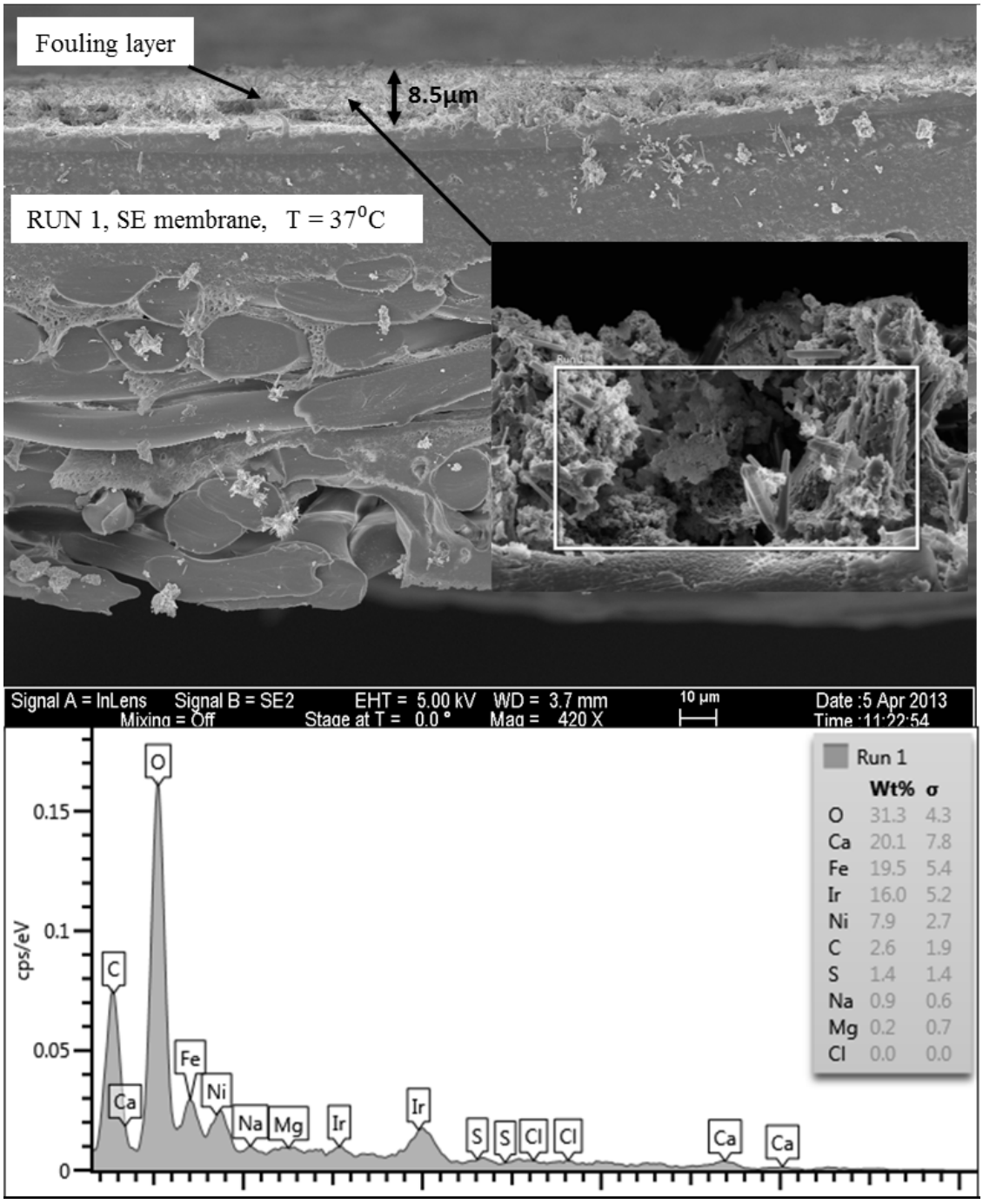

Figure 5.30. SEM images and EDSX spectrum of the cross-section of the fouled SE membrane for location 6 (run 1).

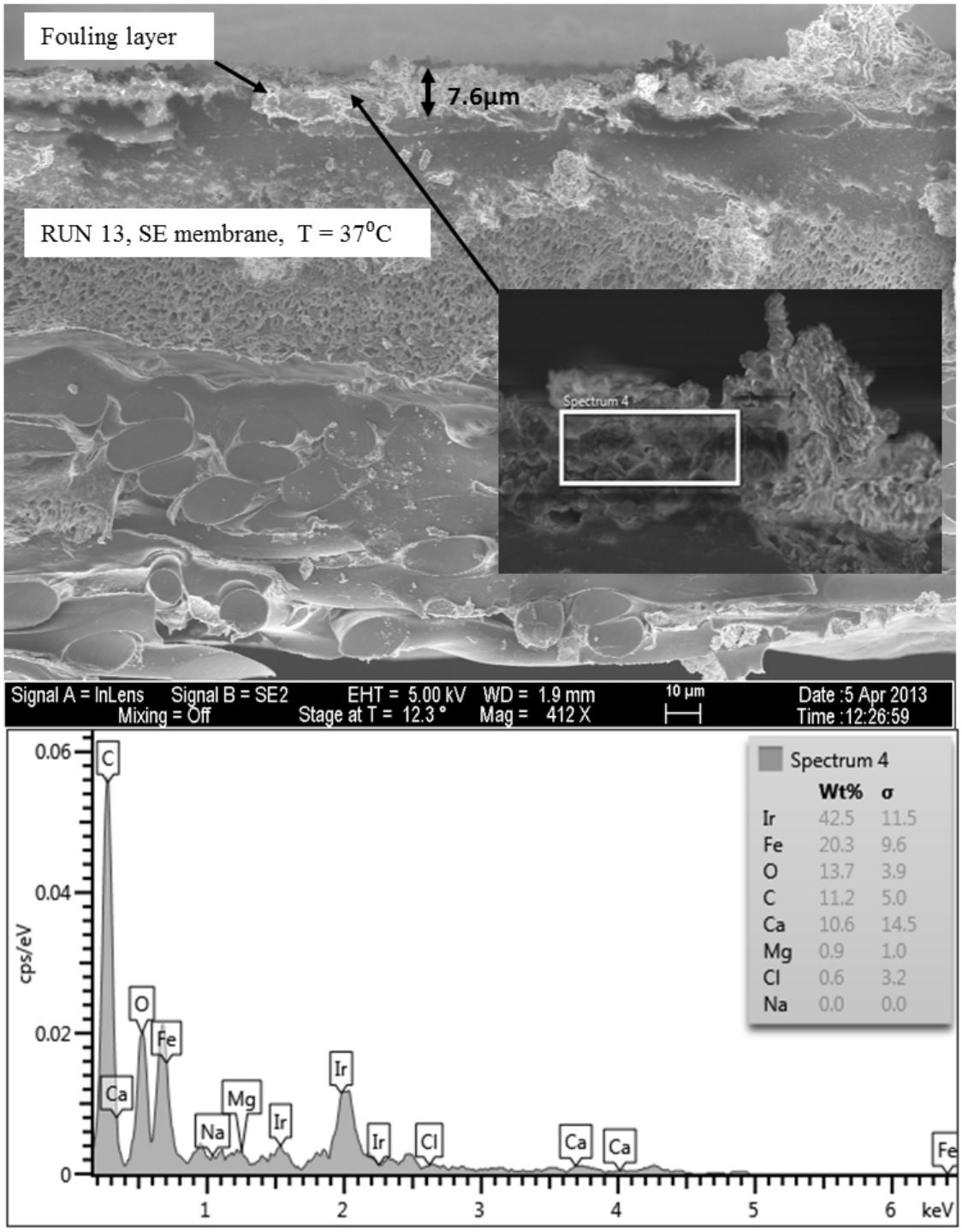

Figure 5.31. SEM images and EDSX spectrum of the cross-section of the fouled SE membrane for location 1 (run 13).

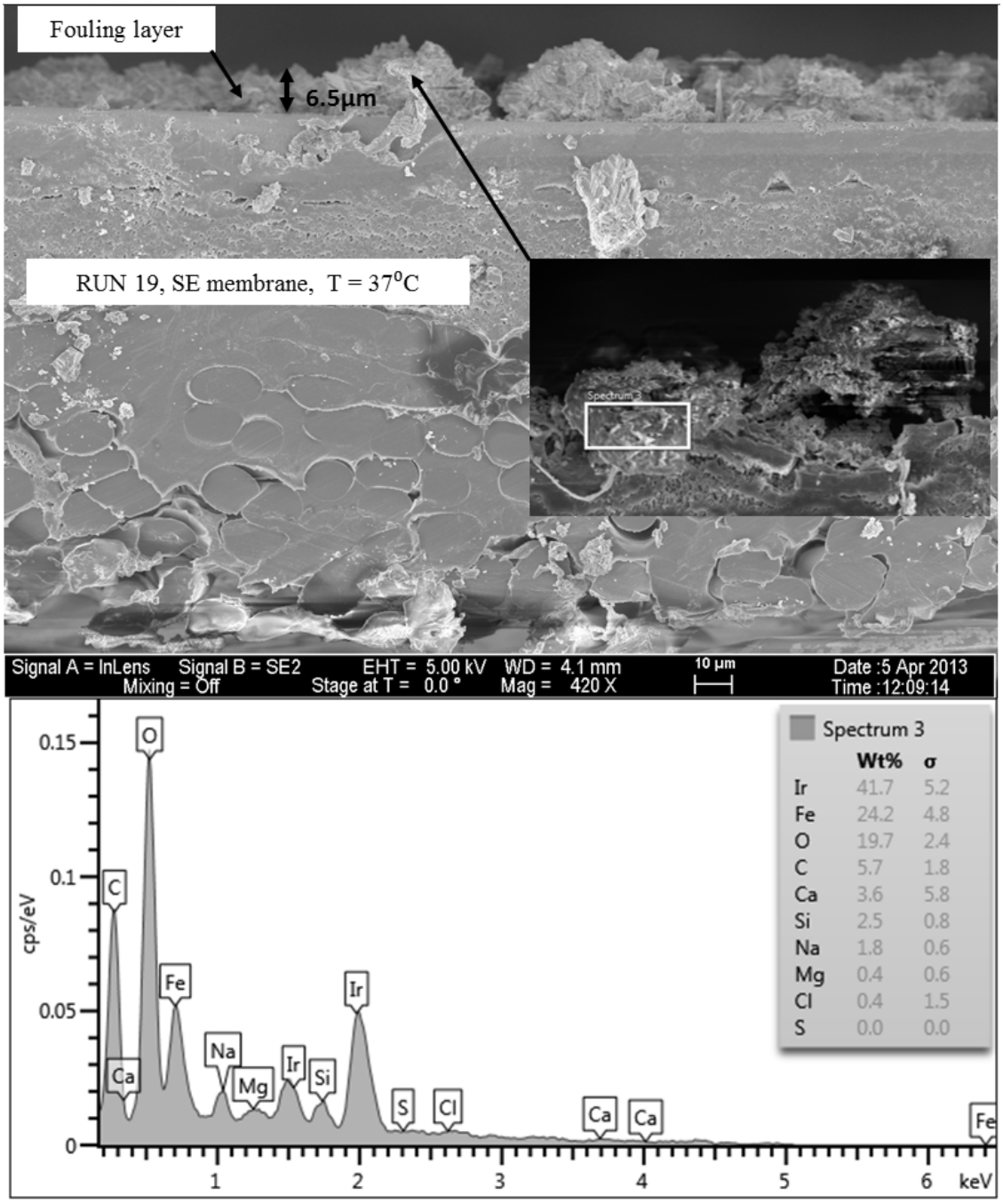

Figure 5.32. SEM images and EDSX spectrum of the cross-section of the fouled SE membrane for location 5 (run 19).

CHAPTER VI

CONCLUSIONS AND RECOMMENDATIONS

6.1. Summary

The main objective of this research was to develop an overview concerning the performance of the reverse osmosis membrane in desalinating simulated brackish surface water, which was similar to the water quality existed in the Iraqi marshes. Three different flat sheet RO membrane types (SE, CE, and AD), were tested utilizing three different simulated brackish surface water qualities. The quality of the simulated feed waters was classified into low TDS (679 - 742 mg/L) and low TOC (1.2 – 1.4 mg/L) feed water and represented by location 5, moderate TDS (1338 - 1428 mg/L) and moderate TOC (1.4 - 2.3 mg/L) feed water and represented by location 1, and high TDS (2569 - 2657 mg/L) and high TOC (4.55 – 4.8 mg/L) feed water and represented by location 6. A bench-scale cross-flow filtration unit was used to conduct all fouling experiments in this study. A total of 24 runs were conducted by repeating the same experimental procedures. Three different feed waters, three different RO membranes, and two temperature values were used as primary variables to run the experiments. In addition, several runs were conducted with pretreated feed water using a 0.1 micron MF membrane. All runs were conducted at a feed flow rate of 0.6 gpm (2.27 Lpm) and a range of feed pressures for 380 psi - 400 psi (2,620 kPa – 2,757 kPa).

The permeate flux and permeate conductivity of the three RO membranes were examined. The effect of the high and low feed water temperature (37^{o}C and 11^{o}C) on the operation efficiency of the three RO membranes was also investigated. In addition, using the Microfiltration (MF) membrane to pretreat the feed water and its effect on the performance of the RO membranes was examined as well. Moreover, the main foulants and the scale formation on the used RO membrane surfaces from the simulated feed waters were diagnosed using SEM images and EDXS spectra. Also, the effect of the feed water temperature on the morphology of the deposited material layer on the RO membrane surfaces was inspected. Lastly, FTIR analysis was used to identify the functional groups of the organic matter deposited on the RO membrane surfaces.

6.2. Conclusions

The permeate fluxes of the high TDS and high TOC feed water (location 6) produced by all the RO membrane types started in the range of 0.36 to 0.66 Lpm/m^2 and ended in the range of 0.254 to 0.334 Lpm/m^2 to achieve the desired water recovery percentage. In addition, the initial permeate fluxes of the moderate TDS and moderate TOC feed water (location 1) were in the range of 0.50 to 0.991 Lpm/m^2, and the final permeate fluxes were in the range of 0.307 to 0.514 Lpm/m^2. However, the permeate fluxes of the low TDS and low TOC feed water (location 5) treated by the three types of the RO membranes started in the range of 0.439 to 0.949 Lpm/m^2 and ended in the range of 0.296 to 0.439 Lpm/m^2. In general, a gradual decrease in the permeate flux produced by all membranes over time was observed for all runs. The observed permeate flux decline in all runs was due to the scale formation from the feed water on the RO membrane surface, which reduced the available filtration area. The high permeate fluxes observed in the runs of locations 1 and 5, compared to those of location 6, were apparently due to a lesser scale formation on the membrane surface from the feed water with lower TOC and TDS concentrations.

In all locations, the results elucidated that the SE membranes generally produced the highest permeate flux and moderate salt ion rejection among the three RO membrane types. The SE membrane achieved more than 97.5%, 99.3%, 99.4%, 99.5%, and 97.9% removal of Na^{+}, Ca^{+2}, Mg^{+2}, SO_4^{-2}, and Cl^{-}, respectively. On the other hand, the AD membranes had the least permeate flux and the highest salt ions rejection. The AD membrane exhibited more than 99%, 99.2%, 99.5%, 99.4%, and 99.4% removal of Na^{+}, Ca^{+2}, Mg^{+2}, SO_4^{-2}, and Cl^{-}, respectively. However, the CE membranes achieved the least salt ions rejection and a moderate permeate flux. The CE membrane showed more than 95.6%, 98.4%, 99%, 99.2%, and 95.1% removal of Na^{+}, Ca^{+2}, Mg^{+2}, SO_4^{-2}, and Cl^{-}, respectively.

Moreover, for most of the runs, the permeate flux levels produced by the RO membranes at a low temperature were lower than those at a high temperature (see appendix E). Also, it was found that, when the temperature was increased from 11^{o}C to 37^{o}C, the rejection levels of the RO membranes for most of the ions decreased throughout the fouling runs. At high temperature, the feed water viscosity decreased and the membrane material swelled, thus the diffusivity of water and salt ions through the RO membranes increased. Therefore, the productivity of the RO membranes at high temperatures rose but its water quality declined.

Generally, employing the MF membrane as a pretreatment unit for the feed water to operate the RO system considerably increased the initial permeate flux, particularly of the runs conducted with a high temperature. Subsequently, the total time of each run was distinctly reduced to achieve the same desired water recovery percentage compared to those of the corresponding runs conducted without the MF membrane. In addition, using the MF membrane as a pretreatment process for the feed water slightly improved salt ions rejection percentages by the RO membranes. The improvement of the salt ions rejection varied among the three used RO membranes.

The FTIR spectra of the fouled RO membranes showed that the main functional groups of the organic matter were aromatic hydrocarbons, aliphatic alcohols, aromatic ethers, aliphatic hydrocarbons, inorganic carbonate and lower amounts of olefins.

The SEM images and the EDSX spectra of the fouled RO membranes surfaces revealed that the distribution and the morphology of the deposited materials varied according to the feed water quality, the RO membrane type, and the operation conditions, such as the feed water temperature. The scale formation, for instance, on the RO membranes from the feed water of location 6 (2569 - 2657 mg/L TDS and 4.55 – 4.8 mg/L) almost covered the entire surface of the used RO membranes with a thick layer. However, the fouled material from the feed water of location 5 (679 - 742 mg/L TDS and 1.2 – 1.4 mg/L TOC) partially covered the surface of the used RO membranes. Also, it was seen that, at a high temperature, the deposited materials from the high TDS and high TOC feed water (location 6) on the RO membranes had crystal shapes (mostly $CaCO_3$), while the formation of the deposited materials, at a low temperature, was a sludge-like deposit (mostly organic matter). On the contrary, the formation of the deposited materials from the low TDS and low TOC feed water (location 5) on the surface of the RO membranes, at a low temperature, had more crystal shapes than that of the deposited materials at a high temperature.

The EDSX spectra of the scale formation on the surface of most of the fouled RO membranes showed a high level of C and O compared to the other elements recorded by the scan. This plus the absence or minimal amount of the inorganic cations indicated that the major fouling was the organic matter. In addition, calcium carbonate ($CaCO_3$) was the predominant compound of the crystal formation present on the surface of several RO membranes. The results of the various configurations of the scale formations deposited under the same conditions on the three types (SE, CE, and AD) of the RO membrane indicated that the surface roughness and the material of the membrane itself affected the scale formation. Moreover, although the feed waters

in locations 1 and 6 had high concentrations of sulfate (312-320 mg/L and 681-687.4 mg/L, respectively), only some potentially low level of $CaSO_4$ precipitated on the membrane surface.

Also, the SEM images of the fouled RO membranes revealed that using the MF membrane as a pretreatment process for the feed water reduced the extent of the fouling across the surface of the RO membranes by more than 45%. For example, the fouling layer of the CE membrane conducted without the MF membrane covered more than 70% of the membrane surface, compared to about 25% of that of the CE membrane conducted with the MF membrane. Supporting this idea was the fact that the initial permeate flux of the run conducted with the MF membrane was higher than the initial permeate flux of the run conducted without using the MF membrane.

The SEM images of the cross-section of the scale formation, from the three water qualities (locations 1, 5, and 6), on the SE membranes showed that the composition of the fouled material was about the same through the entire thickness. The average thickness of the fouling layer from high TDS high TOC (location 6), moderate TDS moderate TOC (location 1), and low TDS and low TOC (location 5) feed water was 8.5, 7.6, and 6.5 **μ**m, respectively.

6.3. Recommendations Based on This Study

If the membrane treatment technology were implemented in the Iraqi marshes, the following recommendations, based on this study, should be considered:

1. The Thin-Film Composite RO membrane (SE) is a better performance type of the RO membrane.

2. The total organic carbon (TOC) of the feed water may need to be treated.

3. Based on the membrane process performance characteristics, the ultrafiltration membrane needs to be considered as an option to pretreat the feed water from these marshes before conducting it with the RO membrane.

4. Further studies are needed on a pilot scale or bench scale to produce process variables about using this type of membrane.

5. Further study on the overall economics and process of using the RO membrane technology in this area is needed.

REFERENCES

Abbas, A. (2005). “Simulation and analysis of an industrial water desalination plant.” Chemical Engineering and Processing, 44, 999-1004.

Abbas, A. and Al-Bastaki, N. (2001) “Performance decline in brackish water FilmTec spiral wound RO membranes.” Desalination, 136, 281-286.

Afonso, M. D., Jaber, J. O., and Mohsen, M. S. (2004). “Brackish groundwater treatment by reverse osmosis in Jordan.” Desalination, 164, 157-171.

Al-Dabbas, M. A. M. and Manii, J. K. (2007). “Assessment of Surface Water, and Groundwater Quality of Haur Al-Hammar after Restoration /Southern Iraq.” < http://www.scbaghdad.edu.iq/index.php?option=com_content&view=article&id=236>.

Al-Saad, H.T., Al-Hello, M.A., Al-Taein, S.M. and DouAbul, A.A.Z. (2010). “Water quality of the Iraqi southern marshes.” Mesopotamian Journal of Marine Science, 25 (2): 79 – 95.

Alspach, B., Zachman, B., Johnson, B., and Stevens, C. (2011). “Characterizing RO fouling potential of brackish surface water.” International Desalination Association (IDA) Journal, 3(1), 36-42.

American Public Health Association (APHA), American Water Works Association (AWWA), and Water Environment Federation (WEF). (2005). “Standard methods for the examination of water and wastewater, No. 5310C.” American Public Health Association, Washington, DC.

Amiri, M.C. and Samiei, M. (2007). “Enhancing permeate flux in a RO plant by controlling membrane fouling.” Desalination 207, 361–369.

Amjad, Z., Pugh, J. and Harn, J. (1996). “Membranes: antiscalants and dispersants in reverse osmosis systems.” UltrapureWater, 48–52.

Antony, A., Low, J. H., Gray, S., Childress, A. E., Le-Clech, P., and Leslie, G. (2011). “Scale formation and control in high pressure membrane water treatment systems: A review.” Journal of Membrane Science, 383, 1– 16.

ArabHunter.com (2012) “Wetlands: Iraq.” http://www.arabhunter.com/index.php/iraq (October 16, 2012).

Avlonitis, S., Hanbury, W. T. and Boudinar, B. M. (1993). “Spiral Wound Modules Performance: An Analytical SolutionsPart II.” Desalination, 89, 227-246.

American Water Works Association (AWWA) Membrane Technology Research Committee (2005). “Committee Report: Recent advances and research needs in membrane fouling.” Journal/American Water Works Association, 97 (8), 79-89.

Bartels, C., Franks, R., Rybar, S., Schierach, M. and Wilf, M. (2005). “The effect of feed ionic strength on salt passage through reverse osmosis membranes.” Desalination, 184, 185 -195.

Boerlage, S., Kennedy, M., Aniye, M. P., Abogrean, E., El-Hodali, D., Tarawneh, Z. and Schippers, J. (2000). “Modified fouling index ultrafiltration to compare pretreatment processes of reverse osmosis feed water.” Desalination 131, 201–214.

Brian, P. L. T. (1966). “Mass transfer in reverse osmosis. In Desalination by Reverse Osmosis.” U. Merten, editor. The M.I.T. Press, Cambridge, Mass. 101.

Cath, T. Y., Childress, A. E. and Elimelech, M. (2006). “Review; Forward osmosis: Principles, applications, and recent developments.” Journal of Membrane Science 281, 70–87.

Cheah, SM (2000). Separation processes; Distillation. http://www.separationprocesses.com/Distillation/DT_Chp07b.htm (June, 7, 2011).

Chu, H.P. and Li, X.Y. (2005). “Membrane fouling in a membrane bioreactor (MBR): sludge cake formation and fouling characteristics.” Biotechnology and Bioengineering, 90(3), 323–331.

Cohen, .R. D. and Probstein, R. F. (1986). “ Colloidal Fouling of reverse osmosis membranes.” Journal of Colloid and Interface Science, 114(1), 194-207.

Conlon, W. J. and McClellan, S. A. (1989). “Membrane softening: treatment process comes of age.” Journal AWW 81 (11), 47 – 51.

Cooley, H., Gleick, P. H. and Wolff, G. (2006). “Desalination, with a grain of salt: A California perspective.” Pacific Institute.

Cotruvo, J., Voutchkov, N., Fawell, J., Payment, P., Cunliffe, D., and Lattemann, S. (2010). “Desalination technology: health and environmental impacts.” International Water Association (IWA) Publishing, London, UK.

Delgado, D.J. and Moreno. P. (2008). Desalination research progress, Nova Science Publishers, Inc. New York. USA Nova Biomedical books.

Dolnicar, S. and Schafer, A. I., (2006). “Puplic perception of desalinated water versus recycled water in Australia, AWWA Desalination Symposium.

Eriksson, P. (1988). “Nanofiltration extends the range of membrane filtration.” Environmental Progress, 7(1), 58 – 62.

Eriksson, P. (1998). “New design feed channel spacer in spiral wound elements for pretreatment cost reduction” Final Technical Report. Desalination Research and Development Program Report No. 45. Desalination Systems, Inc. Escondido, CA

Escobar, I. and Schafer, A. (2010). “Sustainable water for the future: water recycling versus desalination.” Sustainability Science and Engineering, volume 2, 1st edition, Elsevier.

Frenkel, V. and Gourgi, T. (1995). “Brackish water RO desalination plant in the Gaza Strip.” Desalination, 101, 47-50.

Geise, G. M., Park, H. B., Sagle, A. C., Freeman, B. D., and McGrath, J. E. (2011). “Water permeability and water/salt selectivity tradeoff in polymers for desalination.” Journal of Membrane Science, 369, 130–138.

Geraldes, V., Pereira, N. E. and de Pinho, M. N. (2005). “Simulation and optimization of medium-sized seawater reverse osmosis processes with spiral-wound modules” Ind. Eng. Chem. Res. 44, 1897-1905.

Greenlee, L. F., Lawler, D. F., Freeman, B. D. Marrot, B. and Moulin, P. (2009) “Reverse osmosis desalination: Water sources, technology, and today’s challenges.” Water Res., 43, 2317–2348.

GWI (Global Water Intelligence), (2006). 19th IDA Worldwide desalting plant Inventory. Oxford, UK: Media Analytics Ltd.

GWI, (2007). A Global Industry Forecast (CD ROM), Global Water Intelligence, Media Analytics Ltd., Oxford, UK, 2007, www.globalwater intel.com

Hamdan, M. A., Asada, T., Hassan, F. M., Warner, B. G., Douabul, A., Al-Hilli, M. R. A., and Alwan, A. A. (2010). “Vegetation response to re-flooding in the Mesopotamin welands, southern Iraq.” Society of Wetland Scientists.

HCTAB (Hydranautics Company: Technecal Application Bulletin), (2005). “RO/NF polyamide membrane feedwater requirements.” TAB 116. www.membranes.com.

Hessami, M. A., Hall, N. and Robb, A. (2009). “An overview of reverse osmosis water desalination and the solution diffusion mathematical model.” ASME International Mechanical Engineering Congress and Exposition, IMECE 2009-1559, November 13-19, Lake Buena Vista, Florida, USA P67-75.

Hoek, E. M. V., Allred, J., Knoell, T. and Jeong, B. H. (2008). “Modeling the effects of fouling on full-scale reverse osmosis processes.” Journal of Membrane Science, 314, 33–49.

Hoek, E. M.V. and Elimelech, M. (2003). “Cake-Enhanced concentration polarization: a new fouling mechanism for salt-rejecting membrane.” Environmental Science and Technology, 37 (24), 5581-5588.

Hoek, E. M.V., Kim, A. S. and Elimelech, M. (2002). “Influence of crossflow membrane filter geometry and shear rate on colloidal fouling in reverse osmosis and nanofiltration separations.” Environmental Engineering Science, 19 (6), 357-372.

Holmes, K. (2010). Map Talker. < http://www.maptalker.com/map-gallery/iraq/> (Aug. 5, 2011).

IDA and GWI, (2008). IDA Worldwide Desalting Plant Inventory, Report No. 20 in MS Excel Format, Media Analytics Ltd., Oxford, UK.

Jawor, A. and Hoek, E. M.V. (2009). “Effects of feed water temperature on inorganic fouling of brackish water RO membranes.” Desalination, 235, 44–57.

Jenkins, D., Snoeyink, V. L., Ferguson, J. F., and Leckie, J. O. (1980a) “Water chemistry: laboratory manual.” John Wiley and Sons, third edition, 36–43.

Jenkins, D., Snoeyink, V. L., Ferguson, J. F., and Leckie, J. O. (1980b) “Water chemistry: laboratory manual.” John Wiley and Sons, third edition, 51–55.

JEOL, (2012). “A Guide to Scanning Microscope Observation.” JEOL, Serving Advanced Technology (2006-2012) JEOL USA, Inc.

Jin, X., Jawor, A., Kim, S. and Hoek, E. M.V. (2009). “Effects of feed water temperature on separation performance and organic fouling of brackish water RO membranes.” Desalination, 239, 346–359.

Karime, M., Bouguecha, S., and Hamrouni, B. (2008). “RO membrane autopsy of Zarzis brackish water desalination plant.” Desalination, 220, 258-266.

Kim, S. and Hoek, E. M. V. (2007). “Interactions controlling biopolymer fouling of reverse osmosis membranes.” Desalination, 202, 333-342.

Koyuncu, I. and Wiesner, M. R. (2007). “Morphological variations of precipitated salts on NF and RO membranes.” Environmental Engineering Science, 24(5), 602-614.

Koyuncu, I., Wiesner, M. R., Bele, C., Coriton, G., Djafer, M. and Cavard, J. (2006). “Bench-scale assessment of pretreatment to reduce fouling of salt-rejecting membranes.” Desalination, 197, 94-105.

Kucera, J. (2010). “Reverse osmosis industrial applications and processes.” John Wiley and Sons, Inc. Hoboken, New Jersey and Scrivener, LLC, Salem, Massachusetts.

Kumar, M., Adham, S. S. and Pearce, W. R. (2006). “Investigation of seawater reverse osmosis fouling and its relationship to pretreatment type.” Environmental Science & Technology, 40(6), 2037-2044.

Lashkaripour, G. R. and Zivdar, M. (2005). “Desalination of brackish groundwater in Zahedan city in Iran.” Desalination, 177, 1-5.

Lee, K. P., Arnot, T. C., and Mattia, D. (2011). “ A review f reverse osmosis membrane materials for desalination-development to date and future potential.” Journal of Membrane Science, 370, 1-22.

Lee, S., Cho, J. and Elimelech, M. (2005). “A novel method for investigating the influence of feed water recovery on colloidal and nom fouling of RO and NF membranes.” Environmental Engineering Science, 22(4), 496-509.

Li, N. N., Fane, G. A., Winston Ho, W. S. and Matsuura (2008). “Advanced membrane technology and applications.” John Wiley and Sons, Inc. Hoboken, New Jersey.

Lonsdale, H., Merten, U., and Riley, R. L. (1965). “Transport properties of cellulose acetate osmotic membranes.” J. Appl. Poly. Sci., 9, 1341.

Magara, Y., Kawasaki, M., Sekino, M. and Yamamura, H.,(2000). “Development of reverse osmosis seawater desalination in Japan.” Water Science and Technology 41 (10–11), 1–8.

Malaeb, L. and Ayoub, G. M. (2011). “ Reverse osmosis technology for water treatment: State of the art review.” Desalination, 267, 1 -8.

Mickley, M. C. (2001). “Membrane concentrate disposal: practices and regulation.” U.S. Department of the Interior, Bureau of Reclamation, Mickley and Associates.

Morenski, F. (1992). “Current pretreatment requirements for reverse osmosis membrane applications.” In: Official Proceedings of the 53rd International Water Conference, pp. 325–330.

Nakamura, K., Miyamoto, J. and Nakamura, T. (2009). “A fouling index reflecting statistical aspects of fouling process with reverse osmosis desalination.” Proceedings of the World Congress on Engineering and Computer Science 2009 Vol II, WCECS 2009, October 20-22, 2009, San Francisco, USA.

Norberg, D., Hong, S., Taylor, J. and Zhao, Y. (2007). “Surface characterization and performance evaluation of commercial fouling resistant low-pressure RO membranes.” Desalination, 202, 45-52.

NRC (National Research Council), (2008). “Desalination a national perspective.” Committee on Advancing Desalination Technology , Water Science and Technology Board, Division on Earth and Life Studies, Washington, D. C.

Ouki, M. (2010). “Middle east gas: adapting to new market realities.” 14th Annual Middle East Gas Summit, 29-31 March 2010, Abu Dhabi, UAE.

Oveolia (2010). “Membrane filtration, microfiltration, ultrafiltration, reverse osmosis.” Veolia Water Solutions and Technologies, < http://www.veoliawaterst.com/learn-about-water-treatment/980,membrane-filtration-reverse-osmosis-micro-nano-ultra.htm> (Jan. 23, 2011).

Patel-Predd, P. (2006). “Water desalination takes a step forward.” Environmental Science Technology 40 (11): 3454-5.

Paul, D. and Abanmy, A. R. M. (1990). “Reverse osmosis membrane fouling – the final frontier.” Ultra-Pure Water, 7(3), 25-36.

Personal Communication (2013). Dr. Mark Fishbein, Department of Botany, Oklahoma State University.

Reverter, J. A., Talo, S., Alday, J. (2001). “Las Palmas III – the success story of brine staging.” Desalination 138, 207–217.

Ribeiro, J. (1996). “Desalination technology survey and prospects.” European Commission, Joint Research Center, Institute for Prospective Technological Studies, EUR 16434 EN.

Richardson, C. J. and Hussain, N. A. (2006). “Restoring the garden of Eden: An ecological assessment of the marshes of Iraq.” BioScience, 56 (6), 477-489.

Roever, E. W. F. and Huisman, I. H. (2007). “Microscopy as a tool for analysis of membrane failure and fouling.” Desalination, 207, 35–44.

ROplant's photostream, (2009a). “Multi-stage flash distillation (MSF).” (Uploaded on May 29, 2009). <http://www.flickr.com/photos/21182585@N07/with/3869985256/>.

ROplant's photostream, (2009b). “Spiral Wound Reverse Membrane.” (Uploaded on Oct 29, 2009). <http://www.flickr.com/photos/21182585@N07/with/3869985256/>.

Sablani, S. S., Goosen, M. F. A., Al-Belushi, R., and Gerardosb, V. (2002). "Influence of spacer thickness on permeate flux in spiral-wound seawater reverse osmosis systems." Desalination 146(1-3): 225-230.

Saehan, (2006). “Technical manual: reverse osmosis membrane.” Customer Satisfaction Membranes, Saehan Industries, Inc. Mapo-Gu, Seoul 121-710, Korea. http://www.saehancsm.com/

Sahachaiyunta, P., Koo, T. and Sheikholeslami, R. (2002). “Effect of several inorganic species on silica fouling in RO membranes.” Desalination, 144 (1-3), 373-378.

Sandia (2003). “Desalination and water purification roadmap- A report of the executive committee.” DWPR Program Report #95. U.S. Department of the Interior, Bureau of Reclamation and Sandia National Laboratories. Available from: http://wrri.nmsu.edu/tbndrc/roadmapreport.pdf.

Sheikholeslami, R. (1999). “Composite fouling-inorganic and biological: A review.” Environmental Progress, 18(2), 113-122.

Sheikholeslami, R. and Tan, S. (1999). “Effect of water quality on silica fouling of desalination plants.” Desalination, 126, 267-280.

Sheikholeslami, R. and Zhou, S. (2000). “Performance RO membranes in silica bearing waters.” Desalination, 132, 337-344.

Song, L., Hong, S., Hu, J. Y., Ong, S. L. and Ng, W. J. (2002). “Simulations of Full-Scale Reverse Osmosis Membrane Process.” Journal of Environmental Engineering, 128(10), 960-966.

Speth, T., Gusses, A. and Summers, R. (2000). “Evaluation of nanofiltration pretreatments for flux loss control.” Desalination, 130, 31–44.

Spiegler, K. S., and El-Sayed, Y. M. (1994). “A Desalination Primer.” L’Aquila, Italy: Balaban Desalination Publications. June, 1994. ISBN: 0866890343.

Sterlitech Corporation (2010). “Flat Sheet Membranes Specifications.” <http://www.sterlitech.com/flat-sheet-membranes-specifications.html> (Aug. 6, 2010).

TechCommentary, (1997). “Membrane Technologies for water and wastewater treatment.” EPRI Community Environmental Center and ProWrite Inc., California.

Tran, T., Bolto, B., Gray, S., Hoang, M. and Ostarcevic, E. (2007). “An autopsy study of a fouled reverse osmosis membrane element used in a brackish water treatment plant.” Water Research, 41, 3915–3923.

Tzotzi, C., Pahiadaki, T., Yiantsios, S.G., Karabelas, A.J., and Andritsos, N. (2007). “A study of $CaCO_3$ scale formation and inhibition in RO and NF membrane processes.” Journal of Membrane Science, 296, 171–184.

UNEP (United Nation Environment Program), (2007). “Completion report on drinking water and sanitation pilot projects and EST assessment of selected options.” Project No. 41243.

UNEP, (1999). Overview on land–based sources and activities affecting the marine environment in the ROPME sea area, UNEP Regional Seas Reports and studies No. 168, UNEP/GPA Coordination Officw, The Hague, The Netherlands and Regional Organization for the Protection of the Marine Environment (ROPME), Safat, Kuwait.

USBR (U.S. Bureau of Reclamation), (2003a). “Desalination and water purification research and development.” Desalting Handbook for Planners. 3rd Edition; Report No.72. Denver, Colorado: U. S. Department of the Interior, Bureau of Reclamation, Water Treatment Engineering and Research Group.

USBR (U.S. Bureau of Reclamation), (2003b). “Polyamide reverse osmosis membrane fouling and its prevention: oxidation- resistant membrane development, membrane surface smoothing and enhanced membrane hydrophilicity.” Report No. 1098-1. Denver, Colorado: U S Department of the Interior; Desalination Research and Development Program, Bureau of Reclamation.

Vrijenhoek, E., Hong, S. and Elimelech, M. (2001). “Influence of membrane surface properties on initial rate of colloidal fouling of reverse osmosis and nanofiltration membranes.” Journal of Membrane Science 188, 115–128.

Wade, N. M. (2001). “Distillation plant development and cost update.” Desalination, 136, 3 -12.

Wangnick, K., (2002). 2002 IDA Worldwide Desalting Plants Inventory. Report No. 17. Wangnick Consulting GMBH/International Desalination Association.

Weber, W. J. (1972). “Physicochemical processes for water quality control.” 1st Ed., Wiley and Sons, Inc, New York. Ch. 7. Membrane processes, p (307-362).

Wiley, D.E., Fletcher, D.F. and, Schwinge, J. (2002). “A CFD study of unsteady flow in narrow spacer-filled channels for spiral-wound membrane modules.” Desalination, 146, 195-201.
Williams, M. E. (2003). “A brief review of reverse osmosis membrane technology.” EET Corporation and Williams Engineering Services Company, Inc.
WRF (Water Research Foundation) , (2010). “Guidelines for implementing seawater and brackish water desalination facilities.” Water Research Foundation and Arsenic Water Technology Partnership.
Yang, H. L., Huang, C. and Pan, J. R. (2008). “Characteristics of RO foulants in a brackish water desalination plant.” Desalination, 220, 353–358.

APPENDIX A: REYNOLDS NUMBER CALCULATION

Reynolds No. (Re) = $\mathrm{u}d_h/v$

v= solution kinematic viscosity

u = cross flow velocity

dh = cross flow channel hydrodynamic diameter

dh =HW/(2H+2W)

H = 0.432 mm

W = 95 mm

dh = 0.215 mm = 0.215×10^{-2} m

Q = 0.6 gpm = 2.27 Lpm = $2.27 \times 10^{+2}$ mm^2/min

v = 0.7009×10^{-6} m^2/s (at 37 °C) Re = 282

Area (A) = HW = 41.04 mm^2

u = Q/A = 0.9217 m/s

v = 1.2767×10^{-6} m^2/s (at 11 °C) Re = 155

APPENDIX B: FTIR SPECTRAL INTERPRETATION

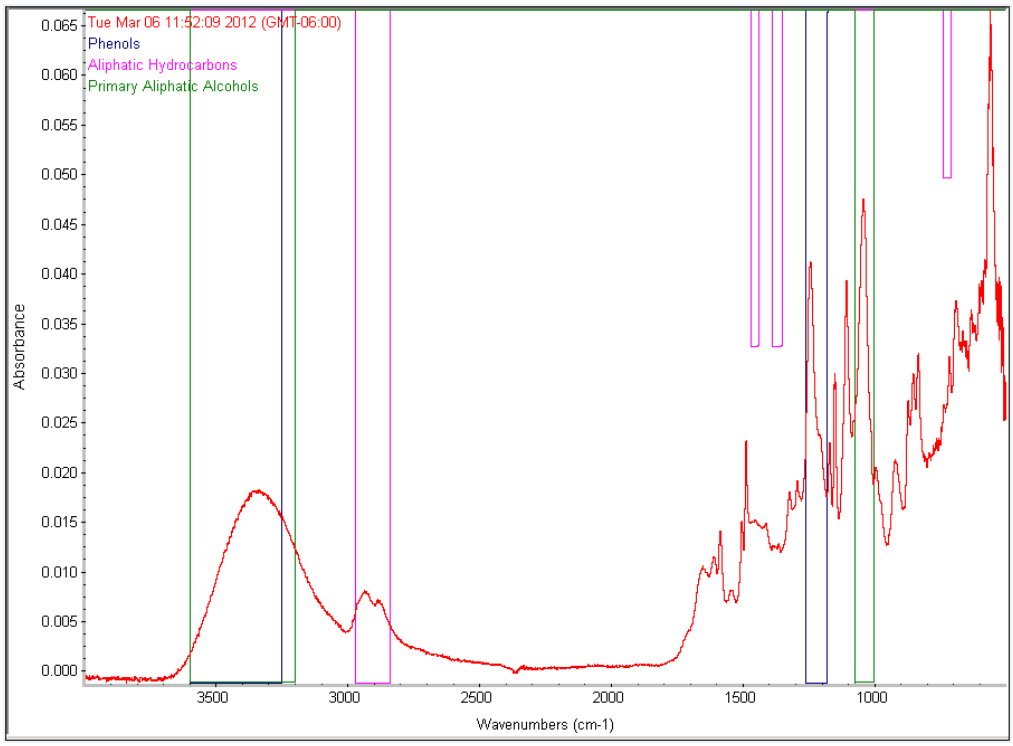

Figure B1. FTIR spectral interpretation for the unused SE membrane.

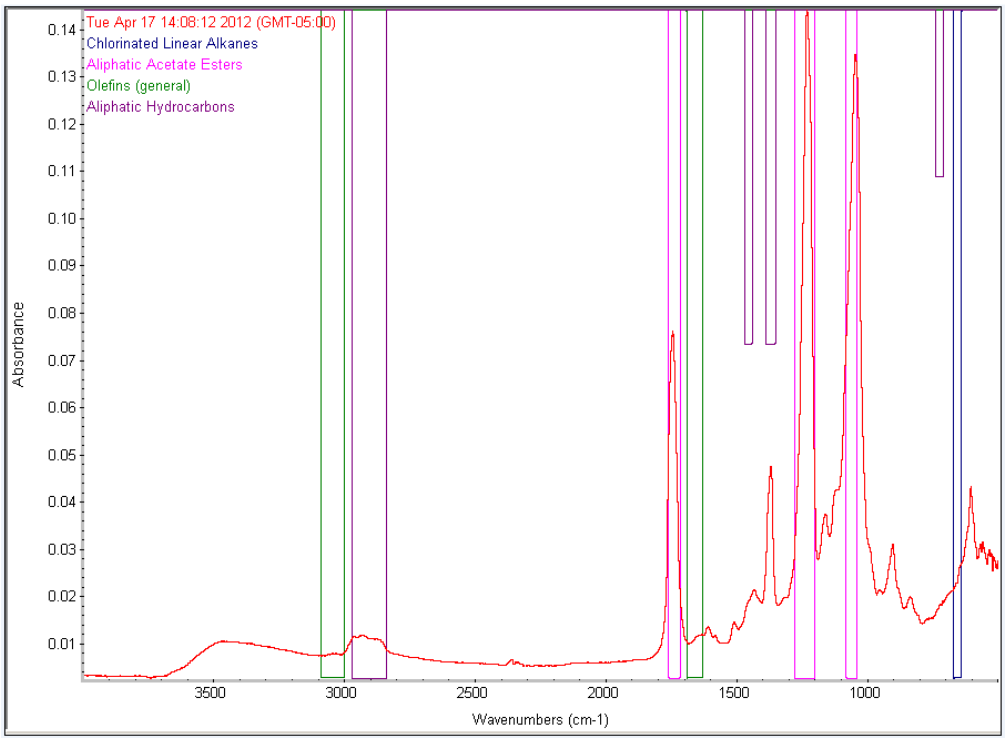

Figure B2. FTIR spectral interpretation for the unused CE membrane.

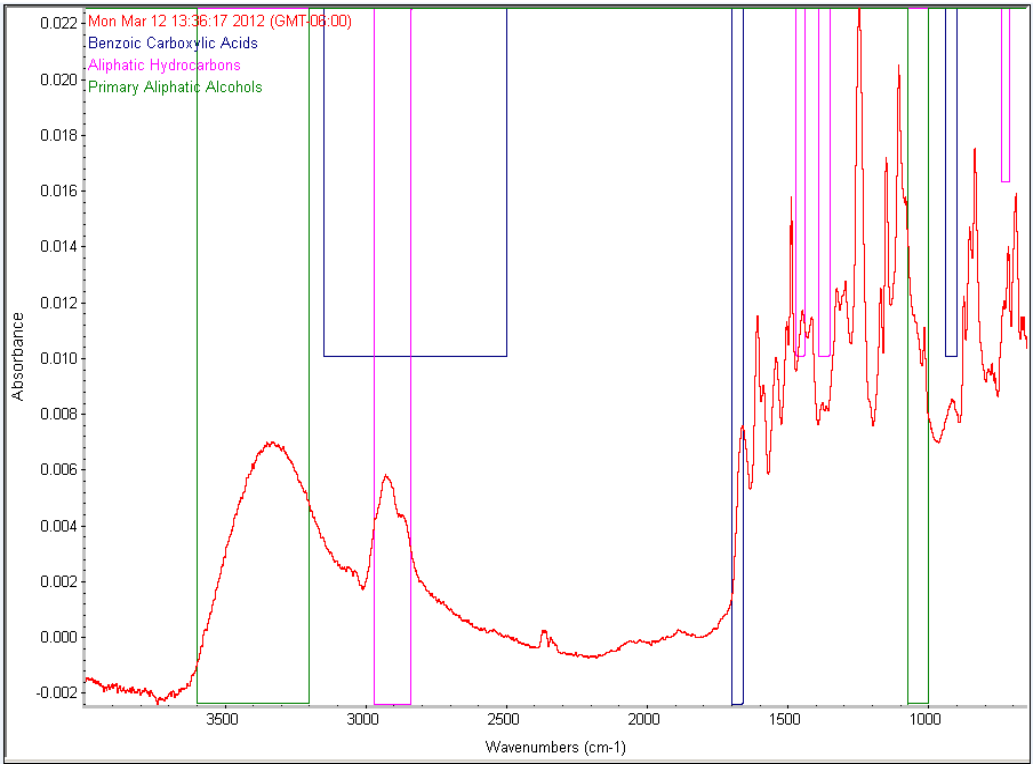

Figure B3. FTIR spectral interpretation for the unused AD membrane.

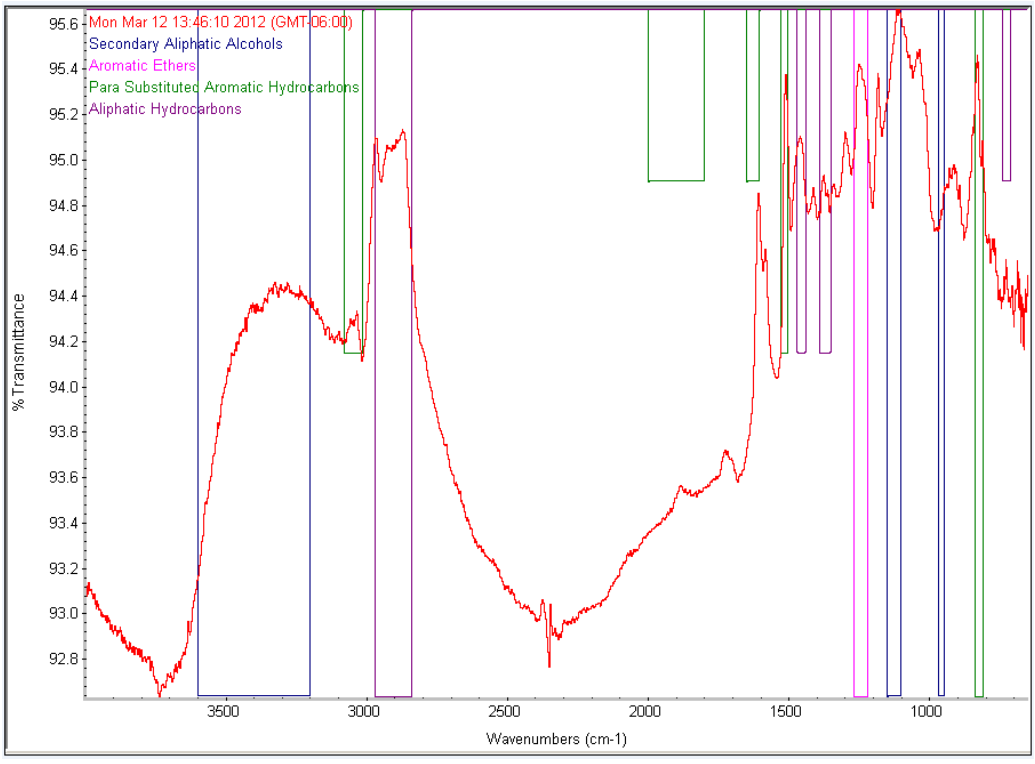

Figure B4. FTIR spectral interpretation of the total organic carbon (TOC) sample.

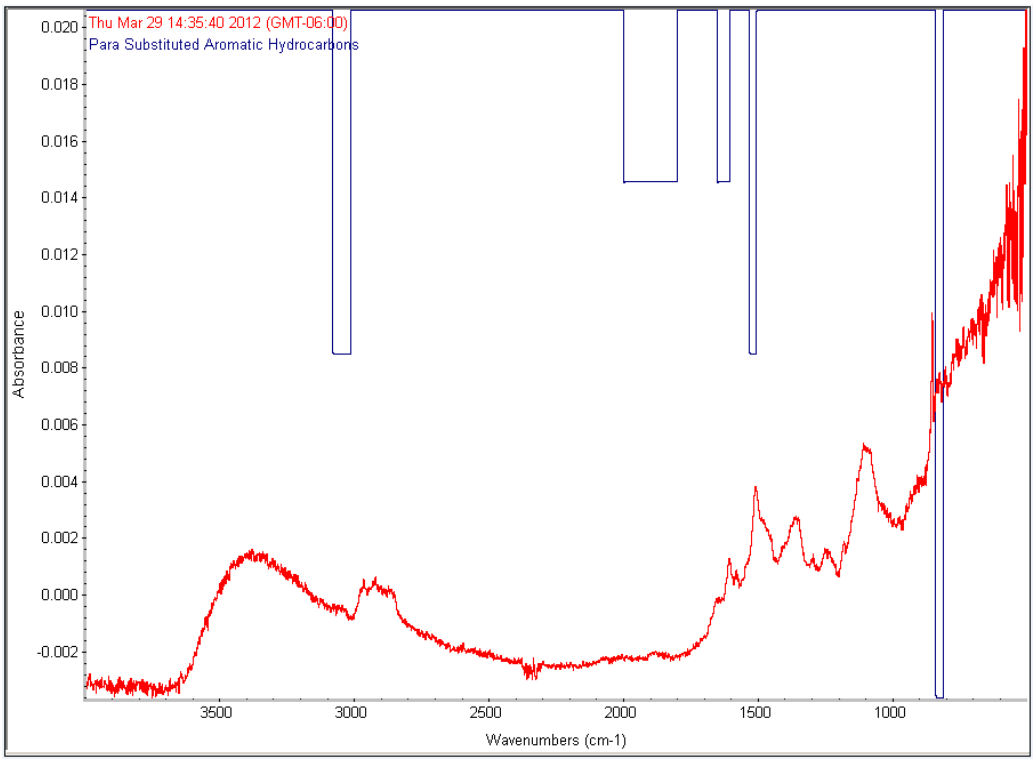

Figure B5. FTIR spectral interpretation of run 1.

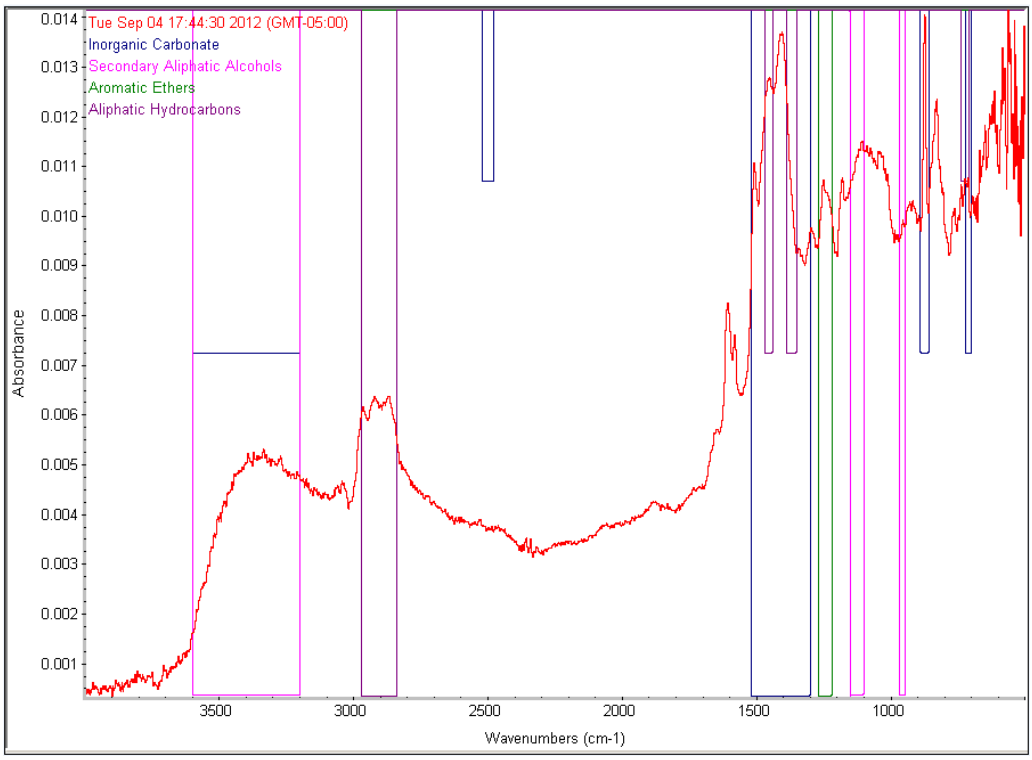

Figure B6. FTIR spectral interpretation of run 2.

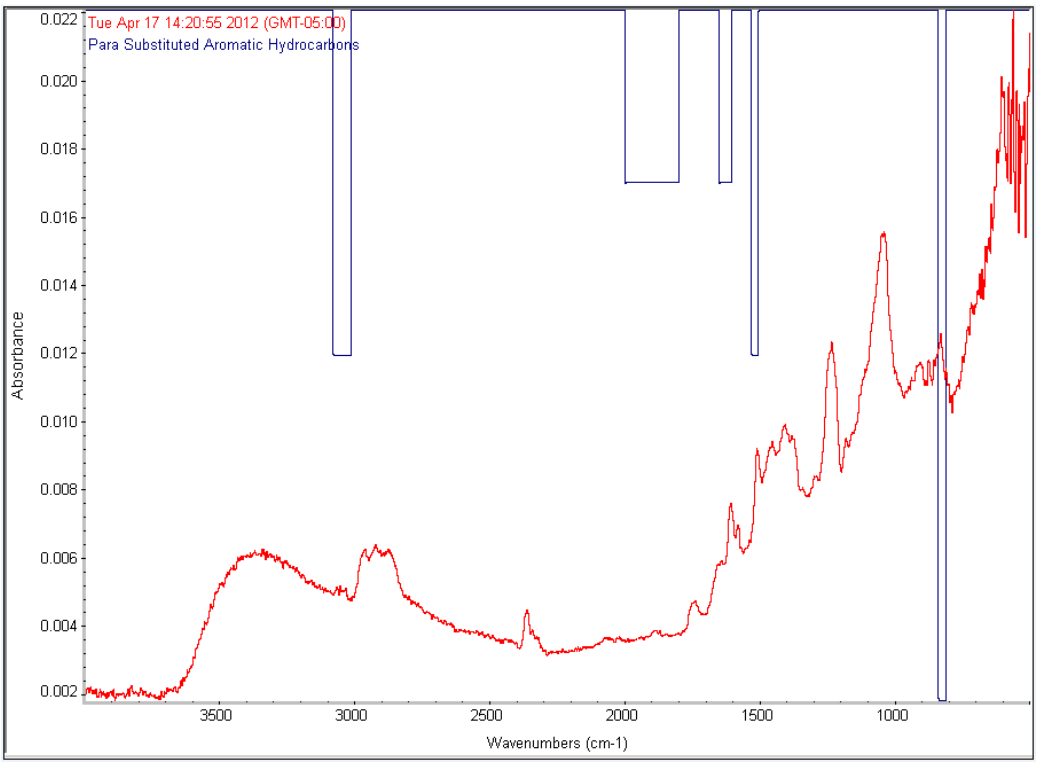

Figure B7. FTIR spectral interpretation of run 3.

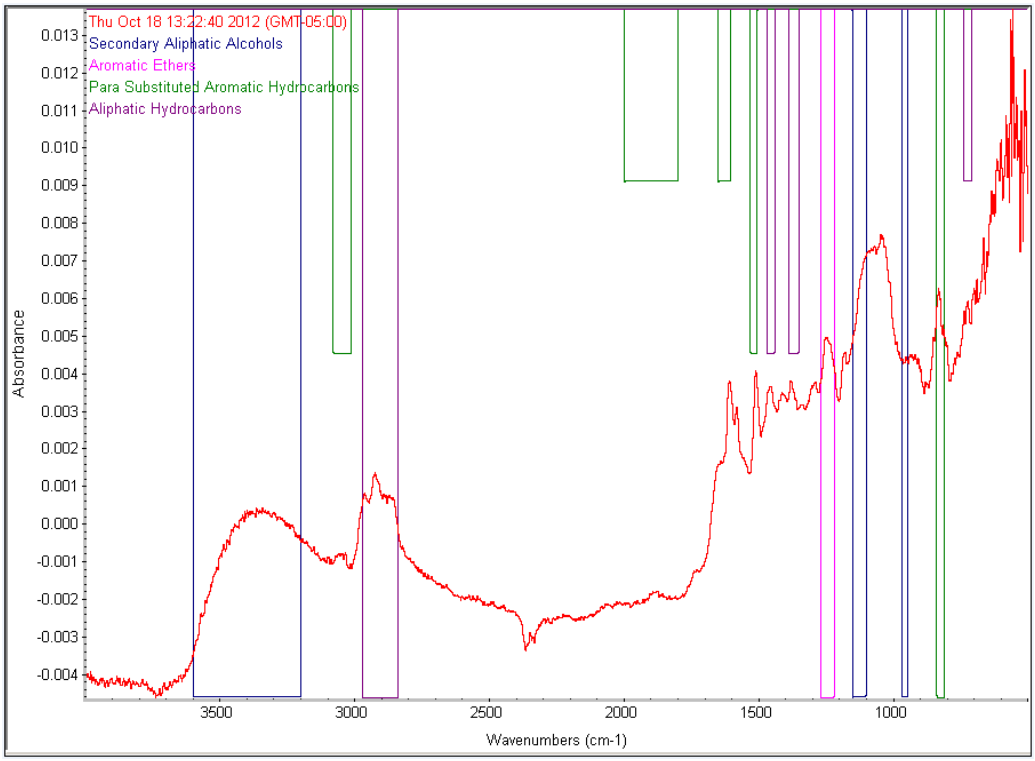

Figure B8. FTIR spectral interpretation of run 4.

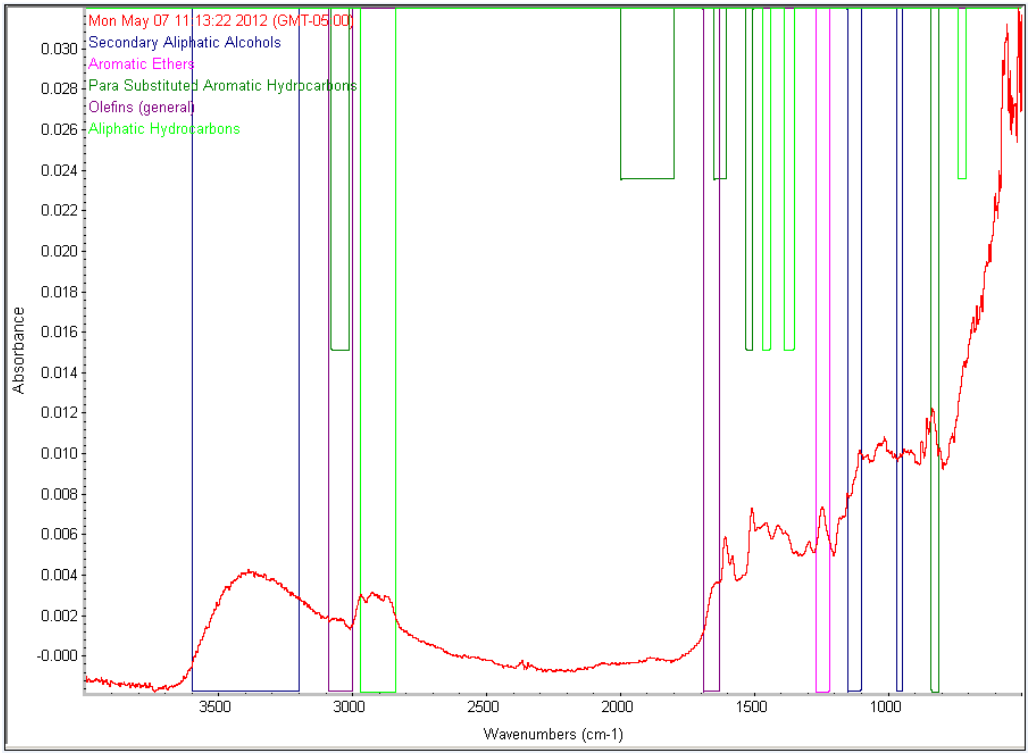

Figure B9. FTIR spectral interpretation of run 5.

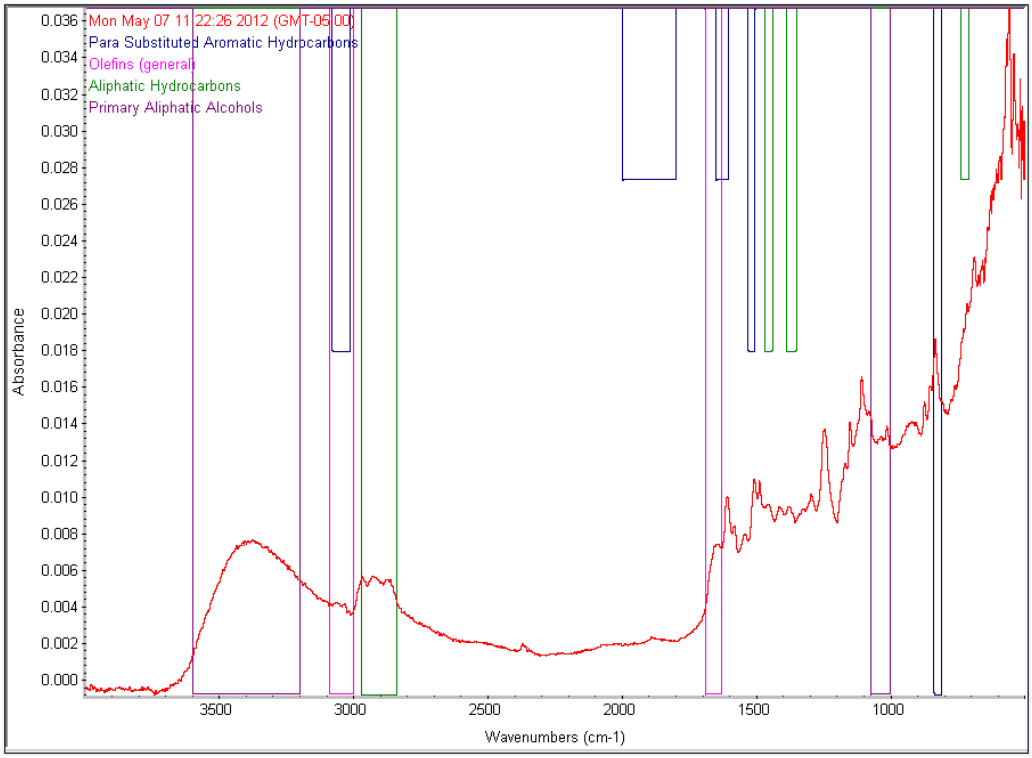

Figure B10. FTIR spectral interpretation of run 6.

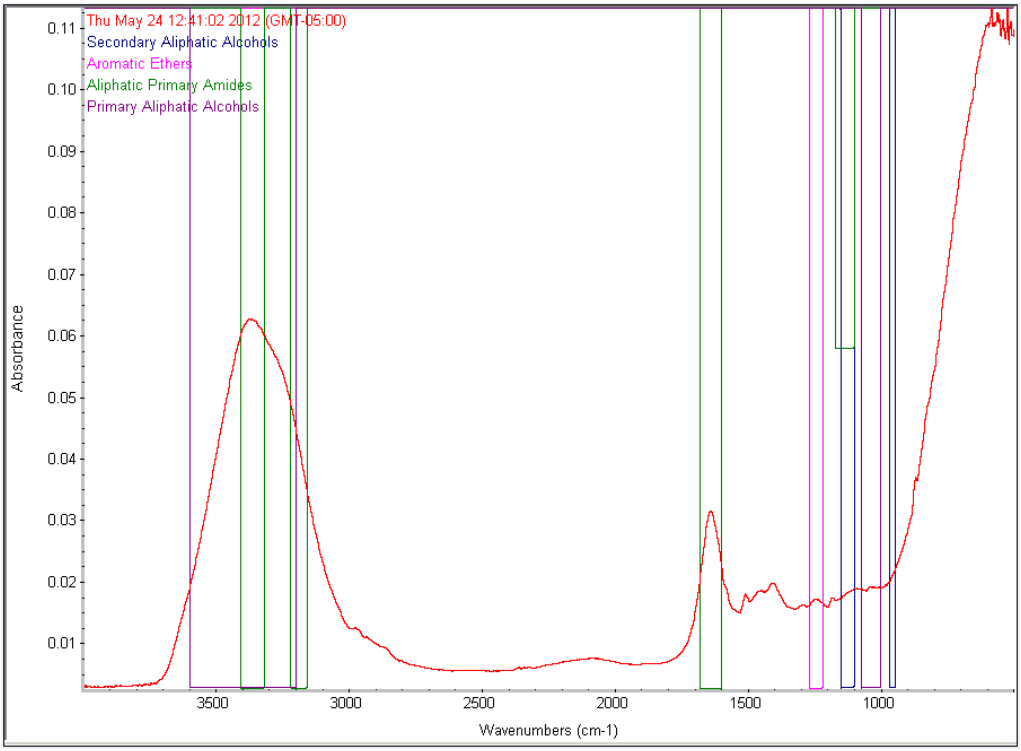

Figure B11. FTIR spectral interpretation of run 7.

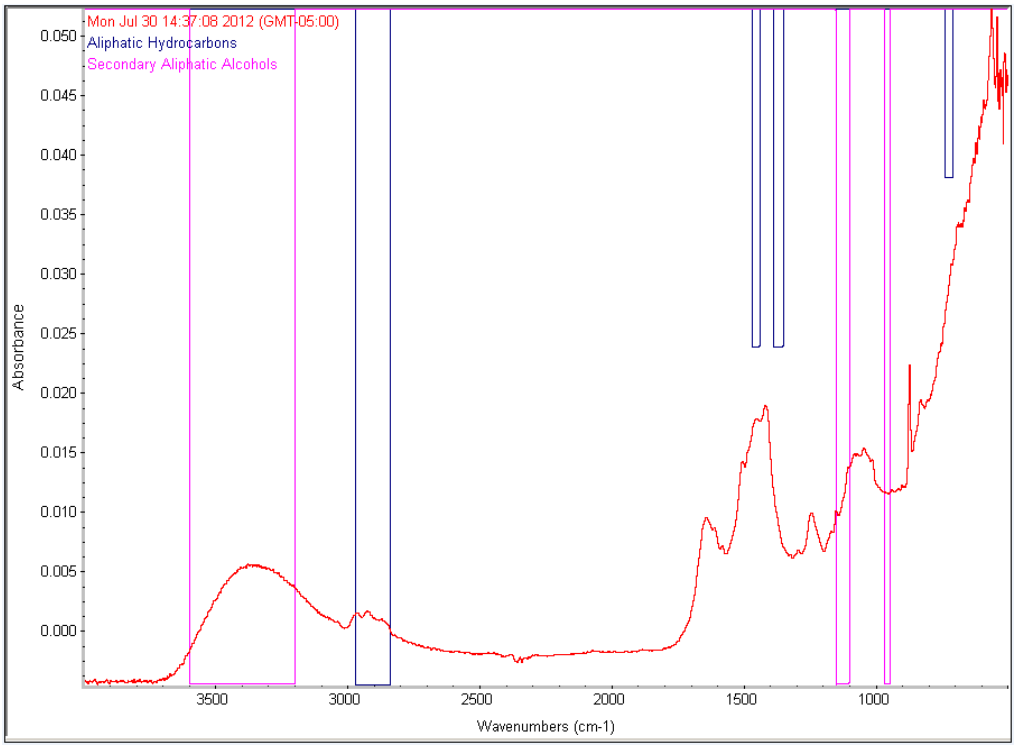

Figure B12. FTIR spectral interpretation of run 8.

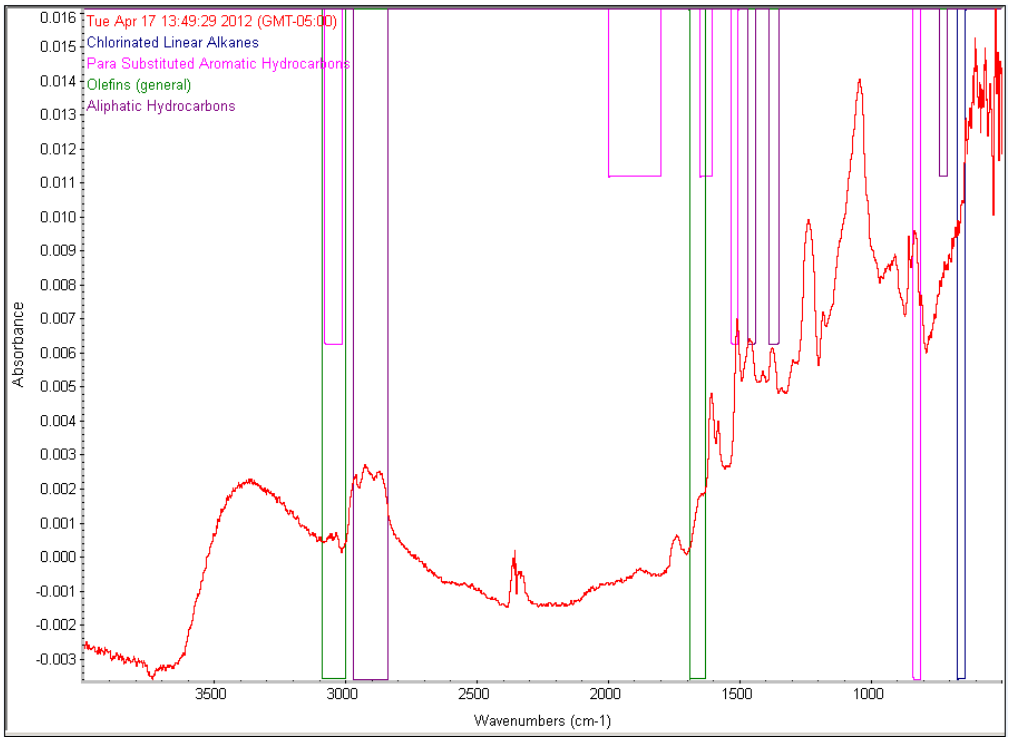

Figure B13. FTIR spectral interpretation of run 9.

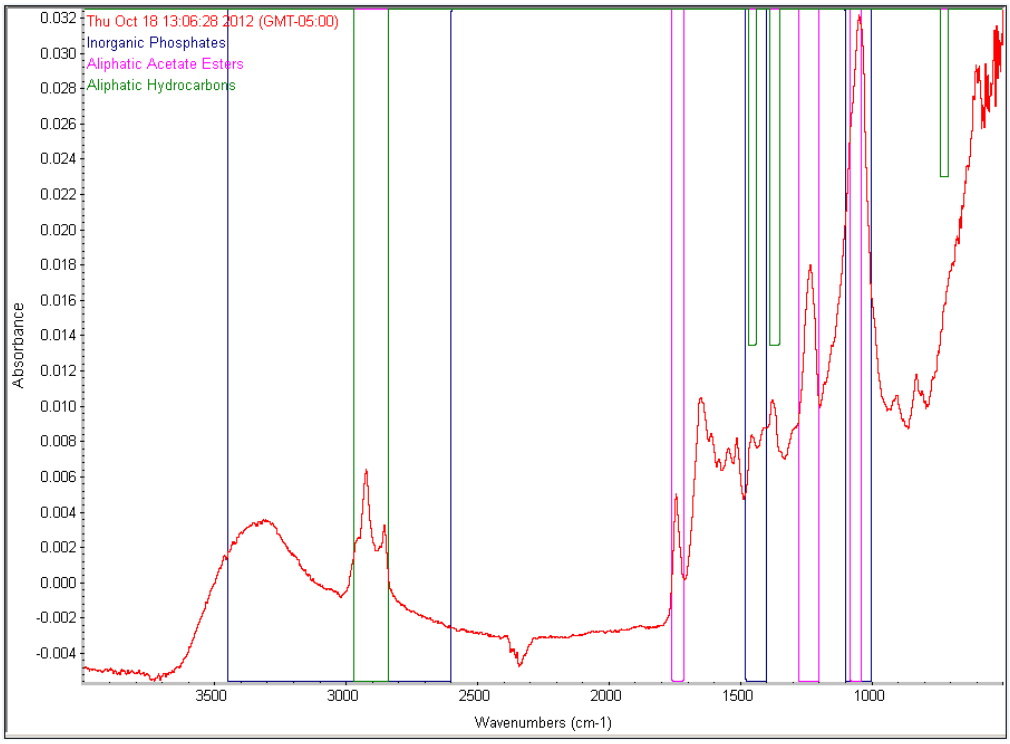

Figure B14. FTIR spectral interpretation of run 10.

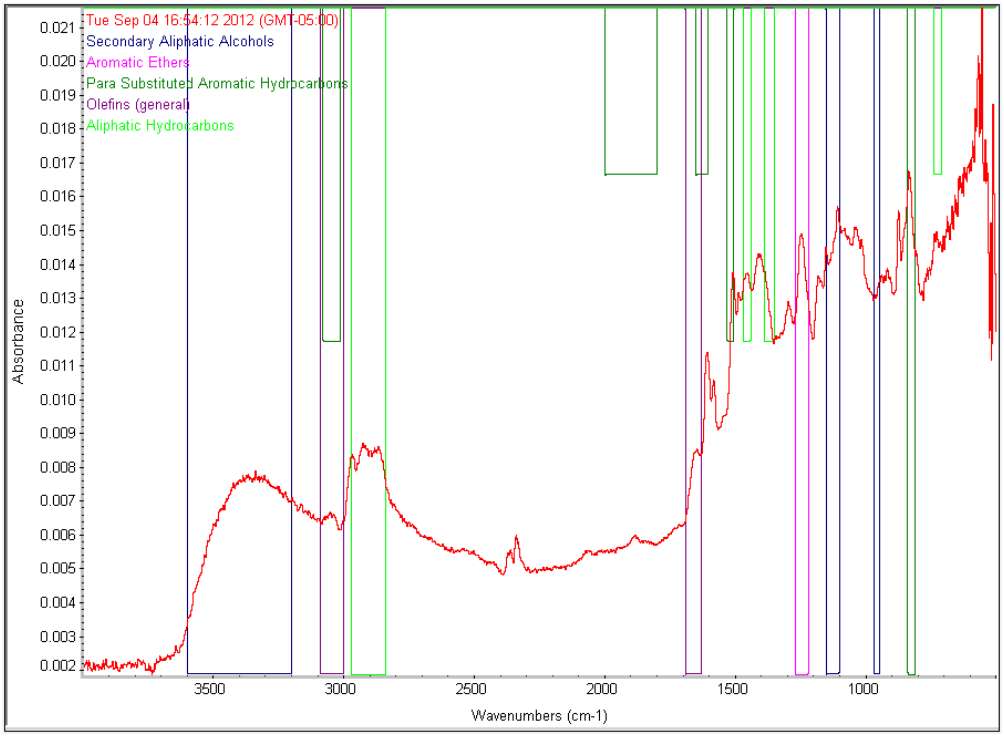

Figure B15. FTIR spectral interpretation of run 11.

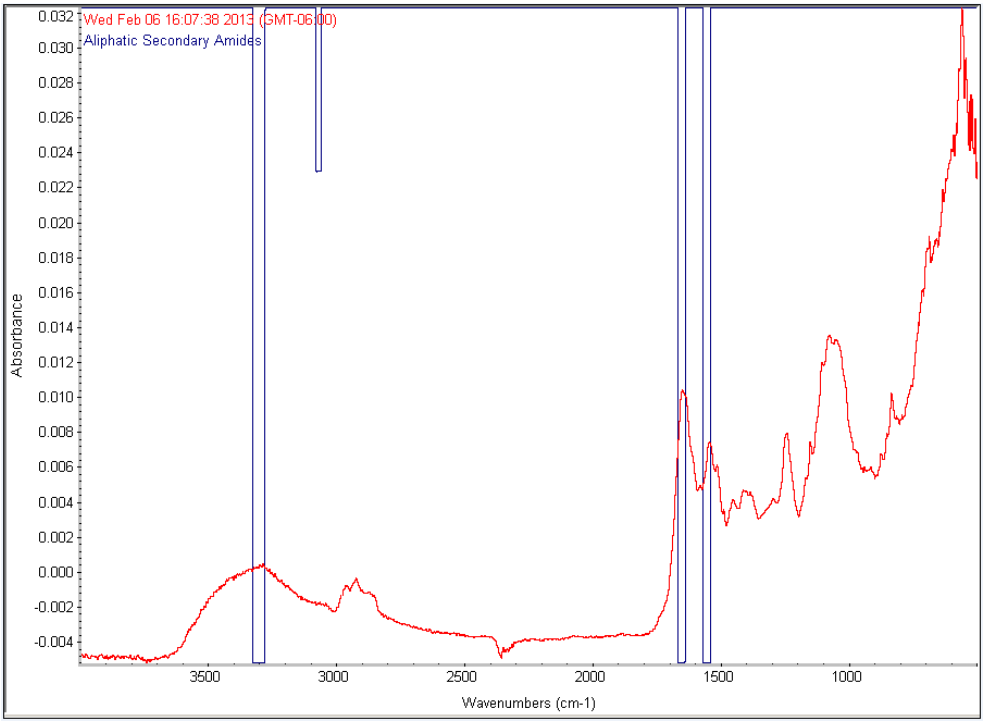

Figure B16. FTIR spectral interpretation of run 12.

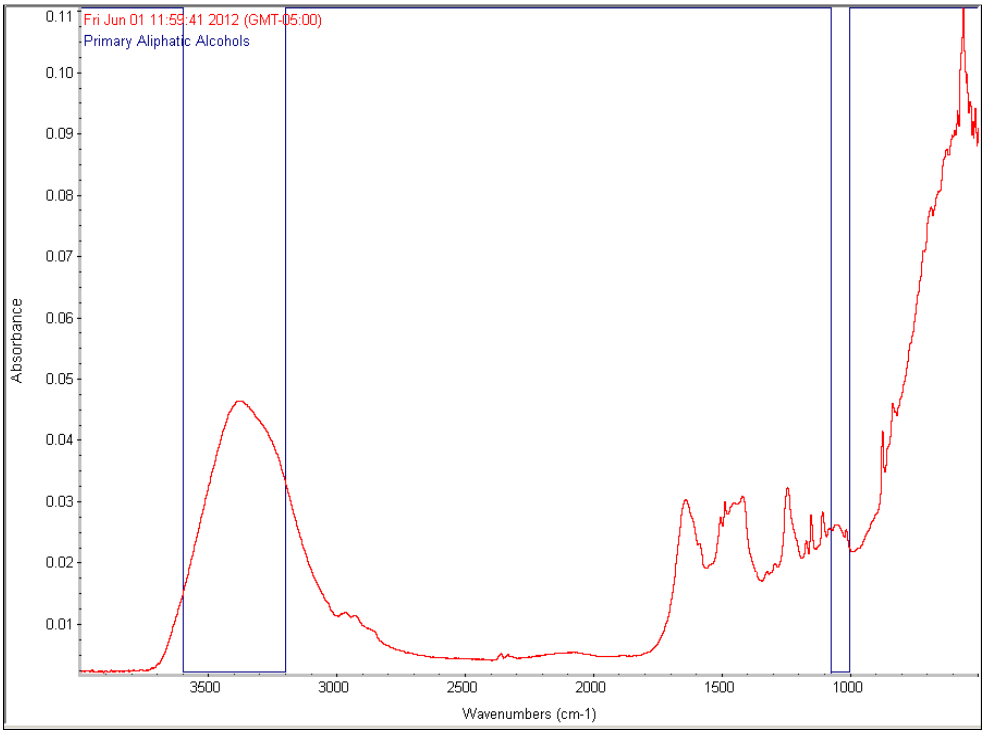

Figure B17. FTIR spectral interpretation of run 13.

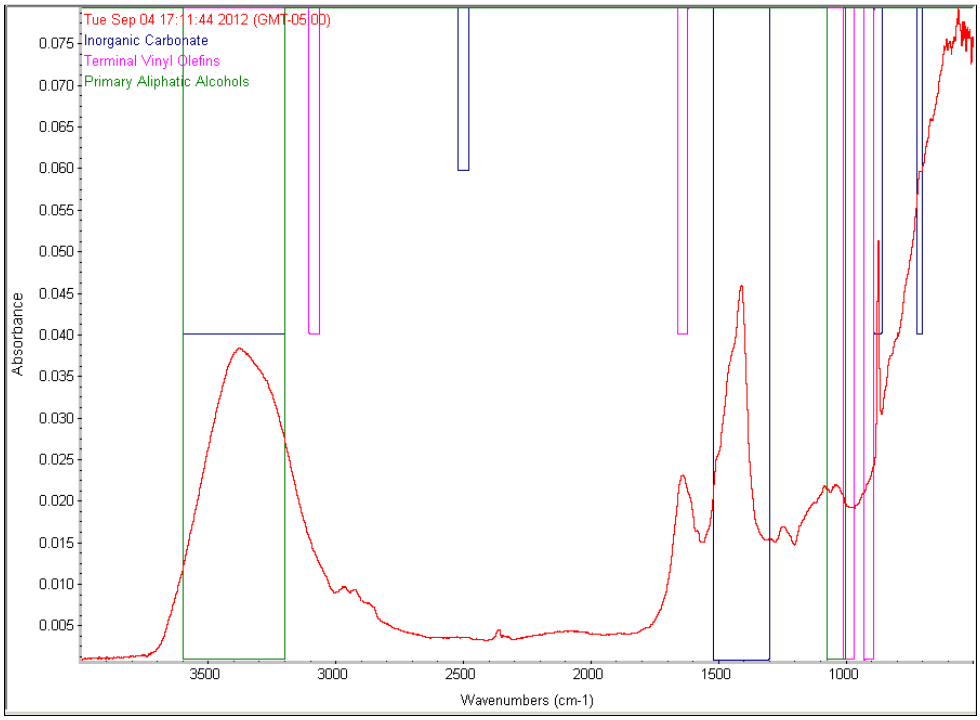

Figure B18. FTIR spectral interpretation of run 14.

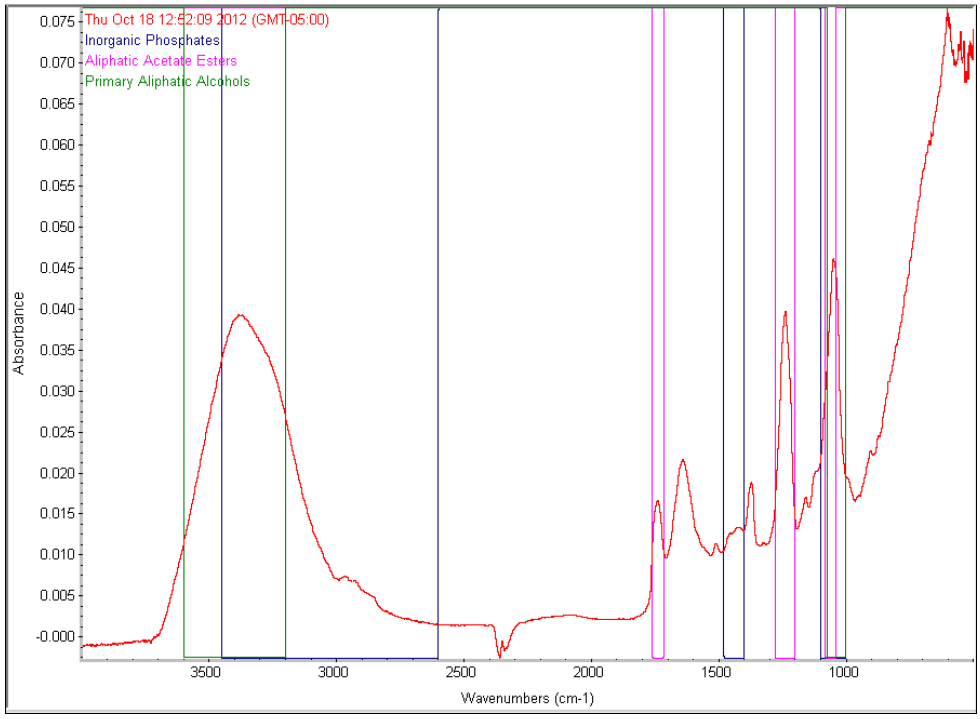

Figure B19. FTIR spectral interpretation of run 15.

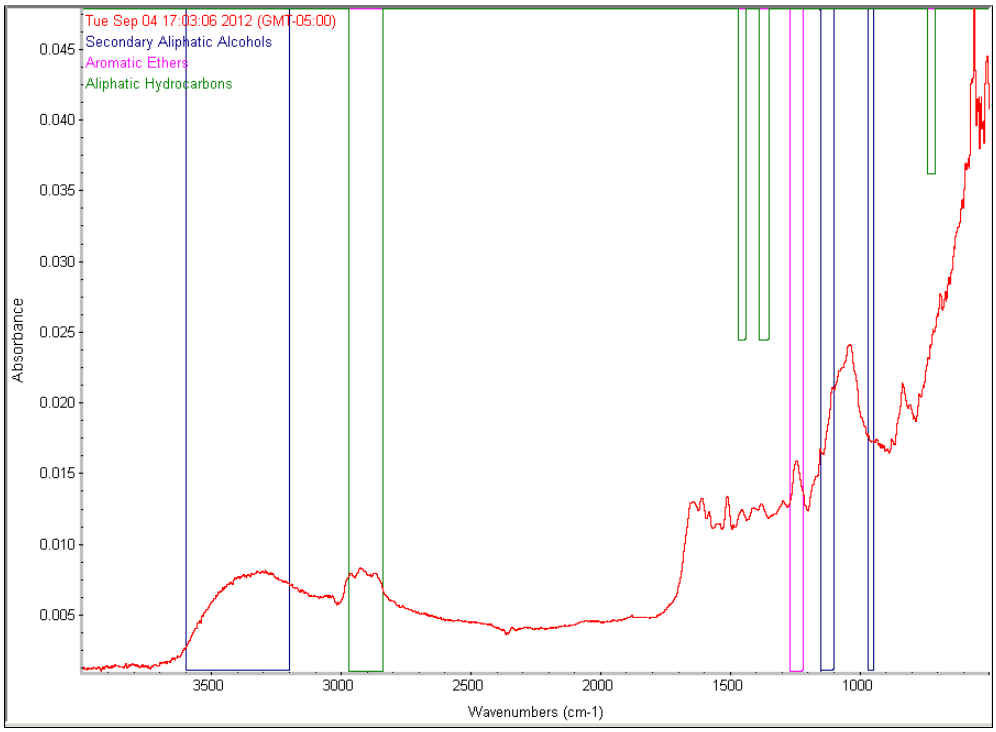

Figure B20. FTIR spectral interpretation of run 17.

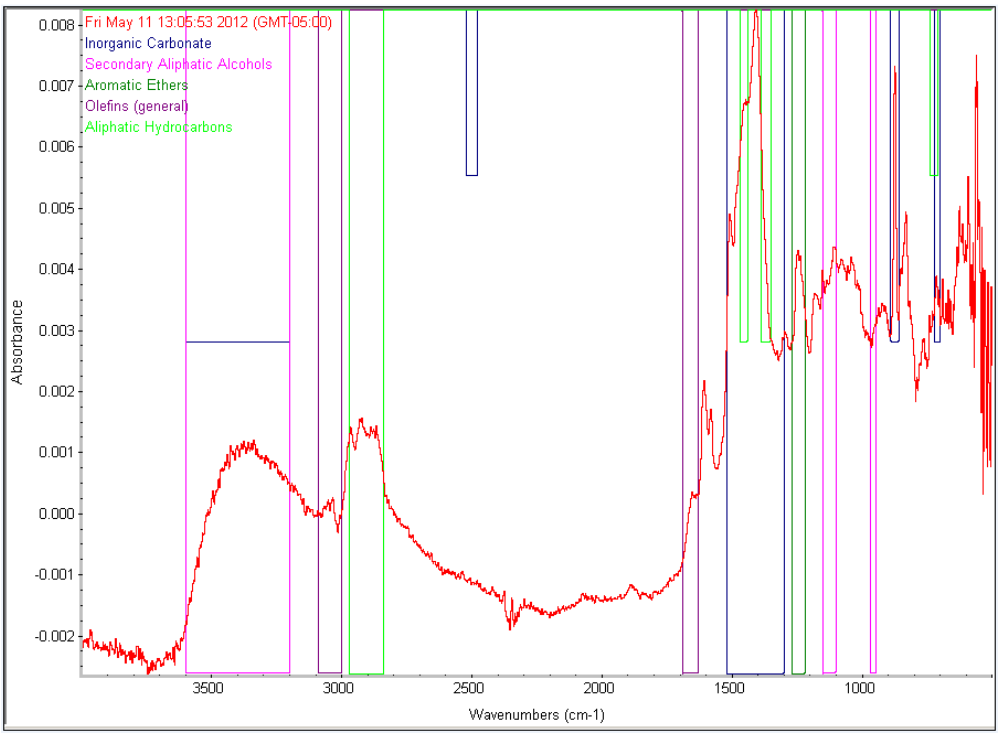

Figure B21. FTIR spectral interpretation of run 19.

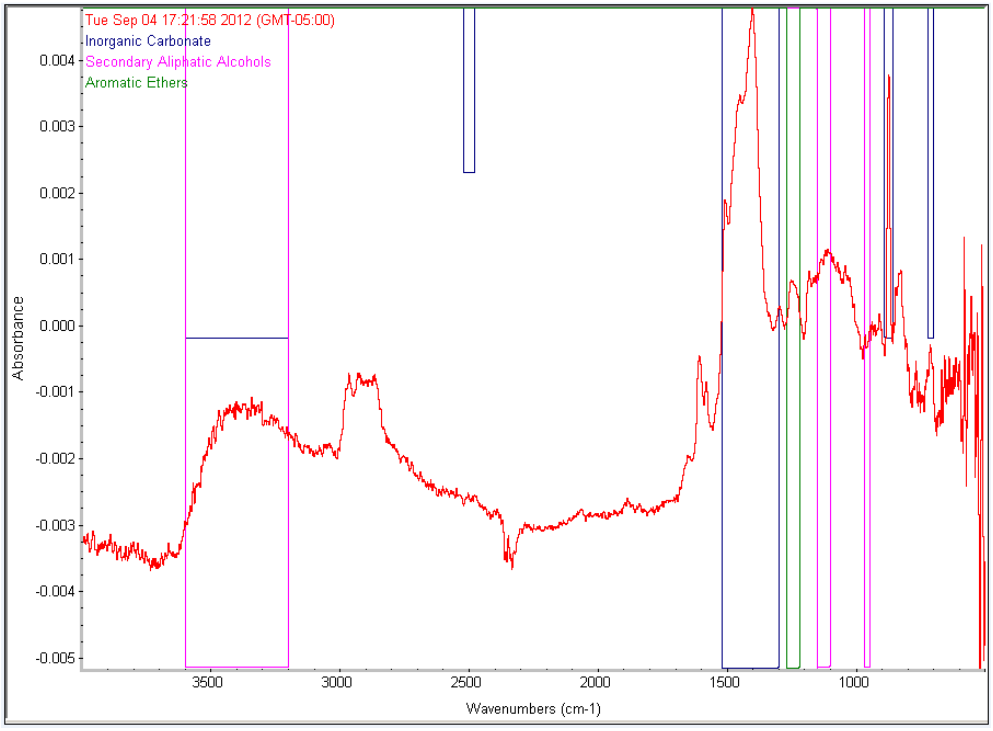

Figure B22. FTIR spectral interpretation of run 20.

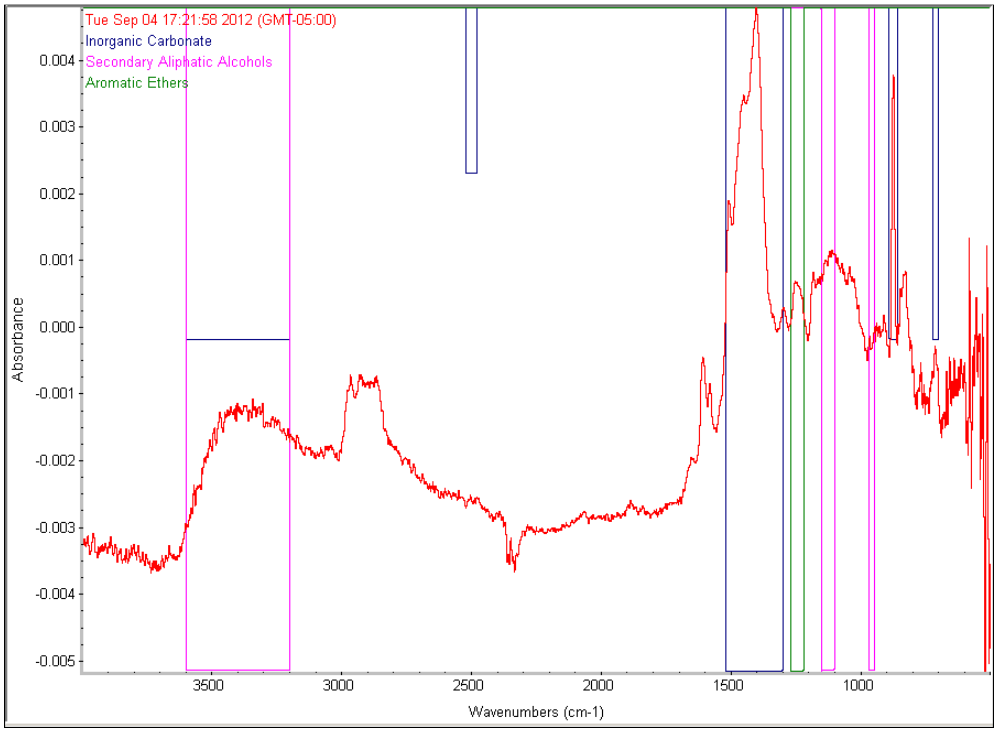

Figure B23. FTIR spectral interpretation of run 21.

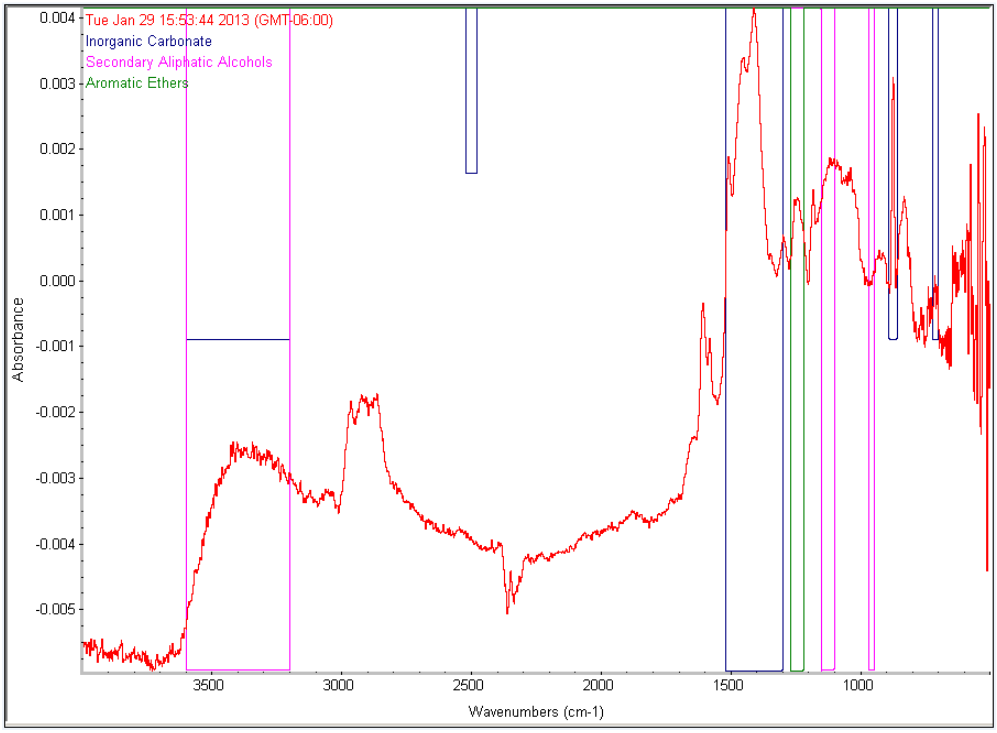

Figure B24. FTIR spectral interpretation of run 22.

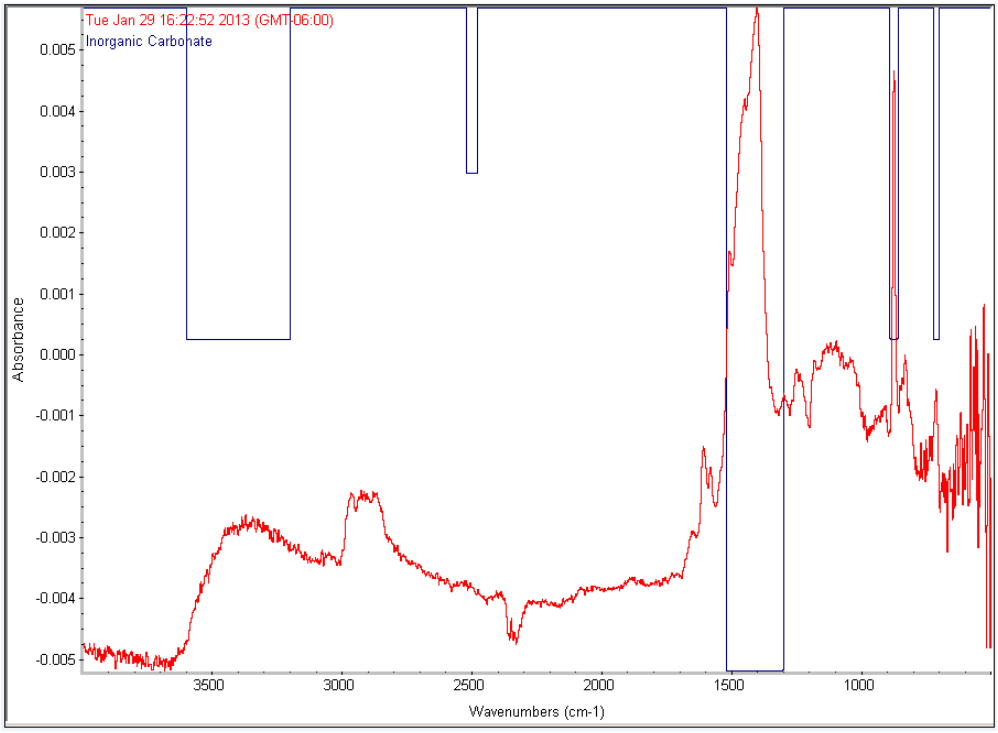

Figure B25. FTIR spectral interpretation of run 23.

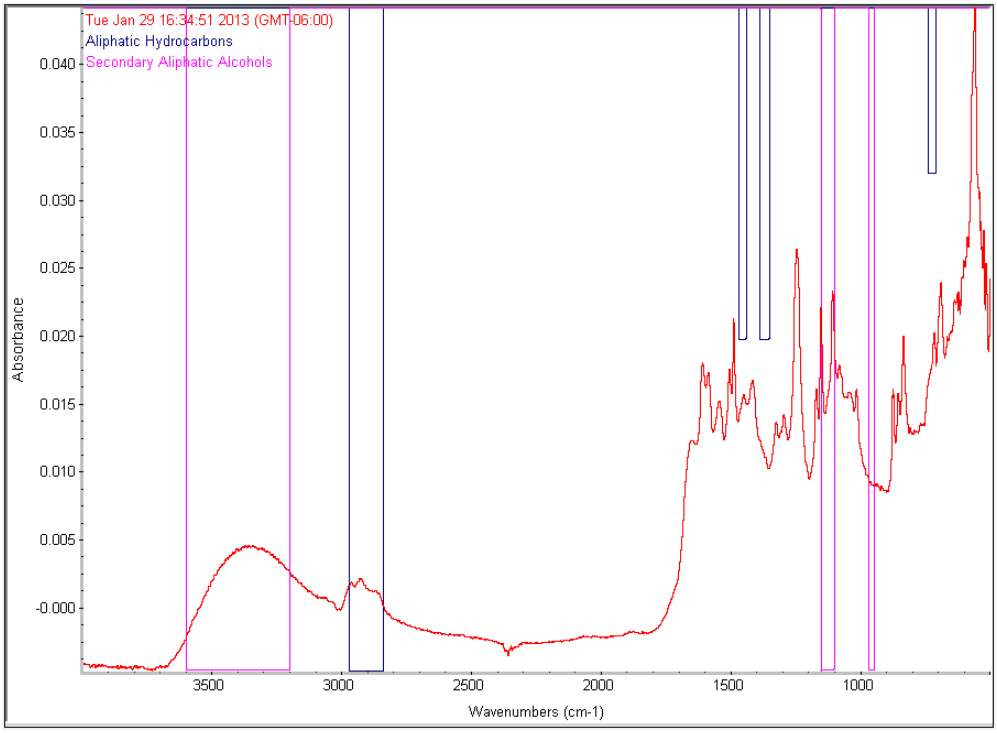

Figure B26. FTIR spectral interpretation of run 24.

APPENDIX C: SEM IMAGES AND EDSX SPECTRA

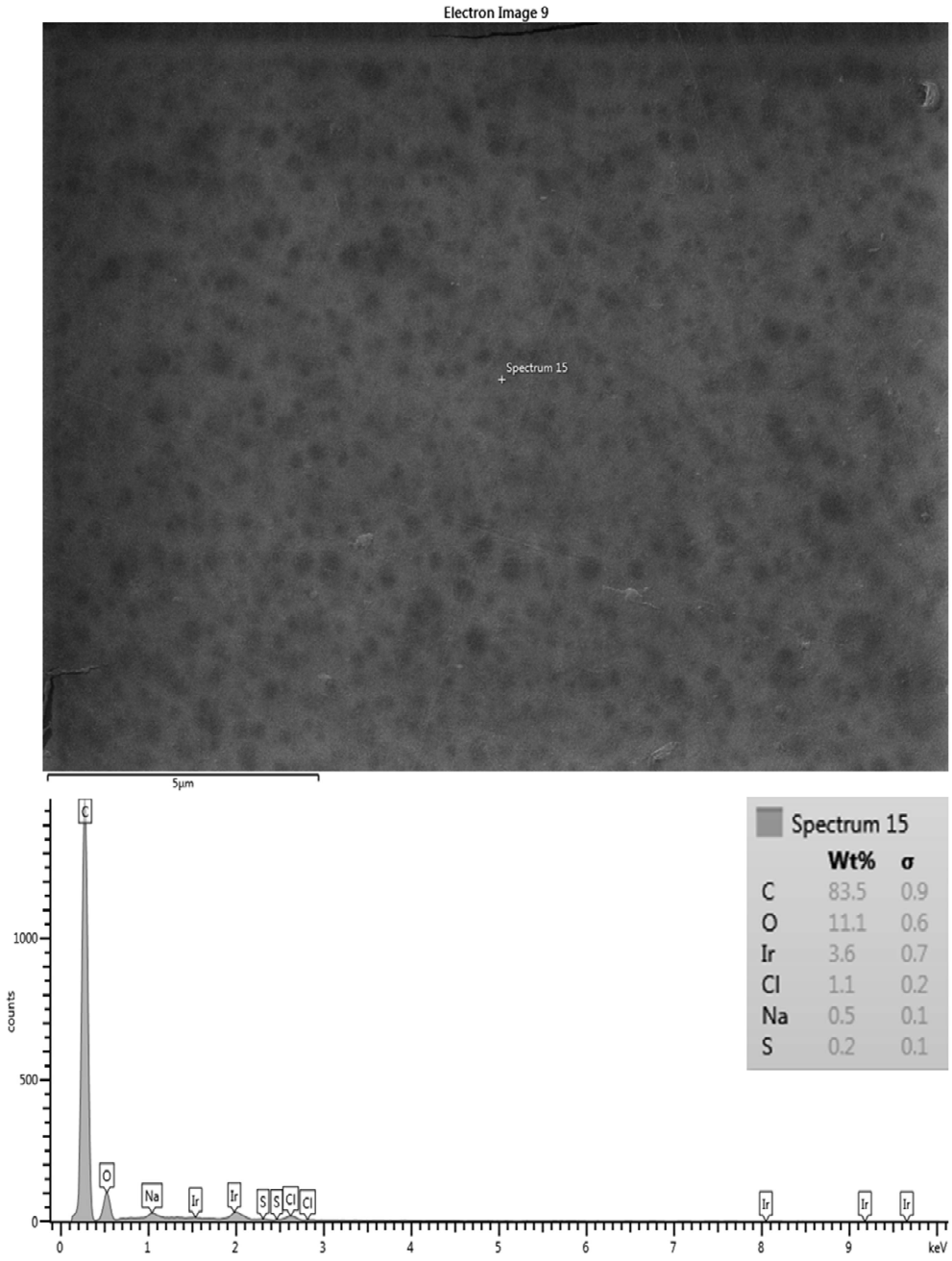

Figure C1. SEM image and EDSX spectrum of unused CE membrane.

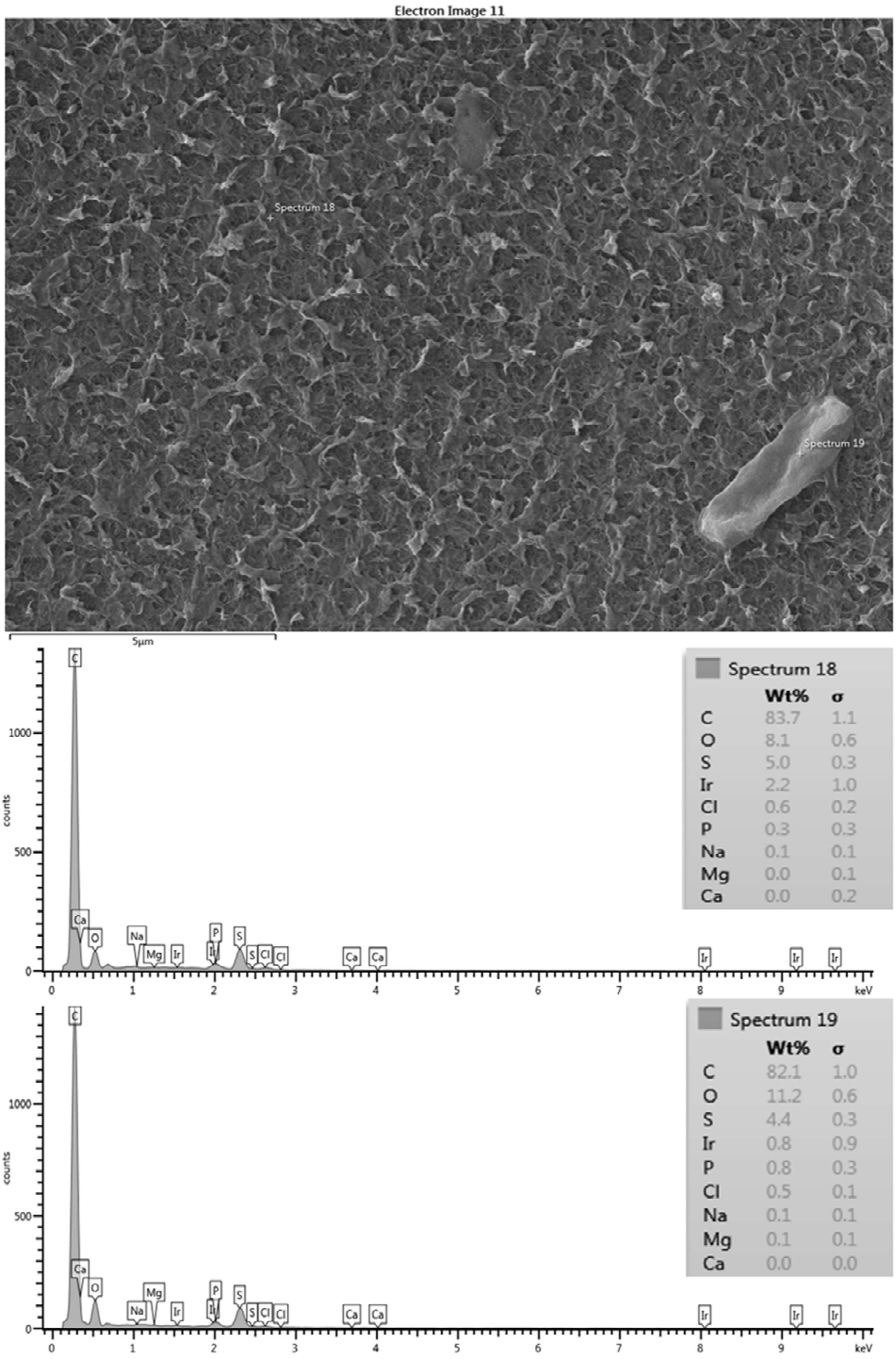

Figure C2. SEM image and EDSX spectra of unused SE membrane.

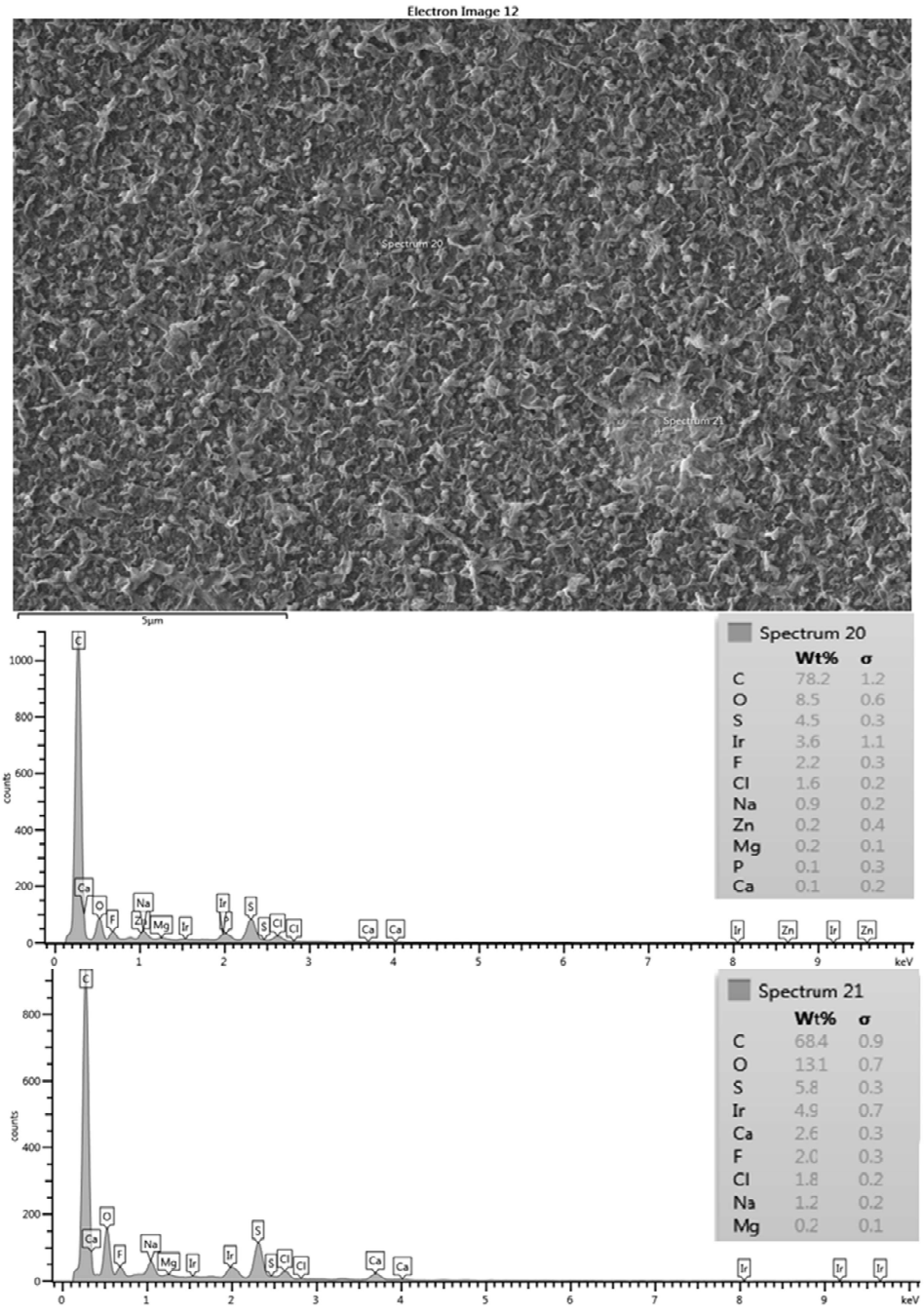

Figure C3. SEM image and EDSX spectrum of unused AD membrane.

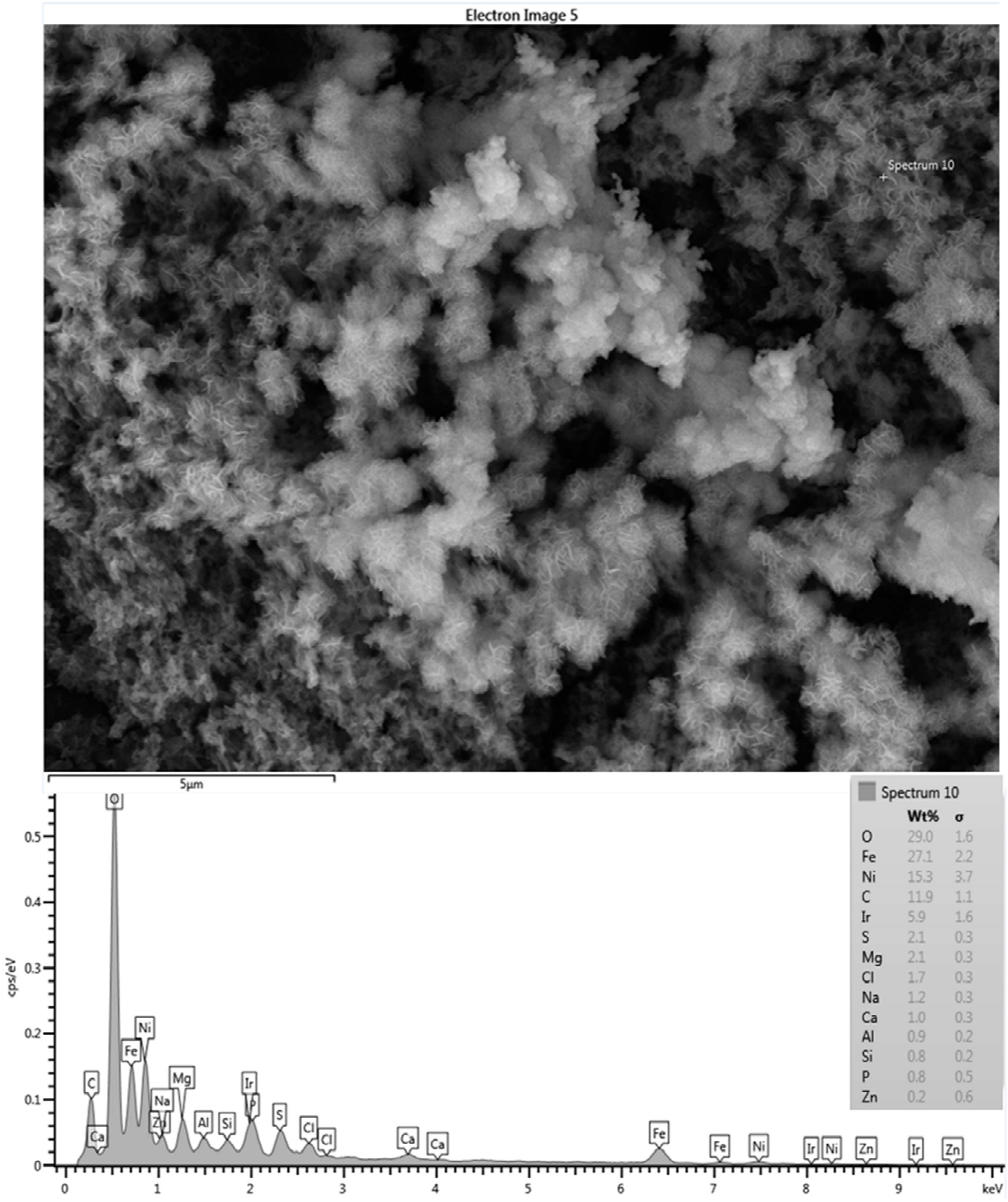

Figure C4 . SEM image and EDSX spectrum of run 1.

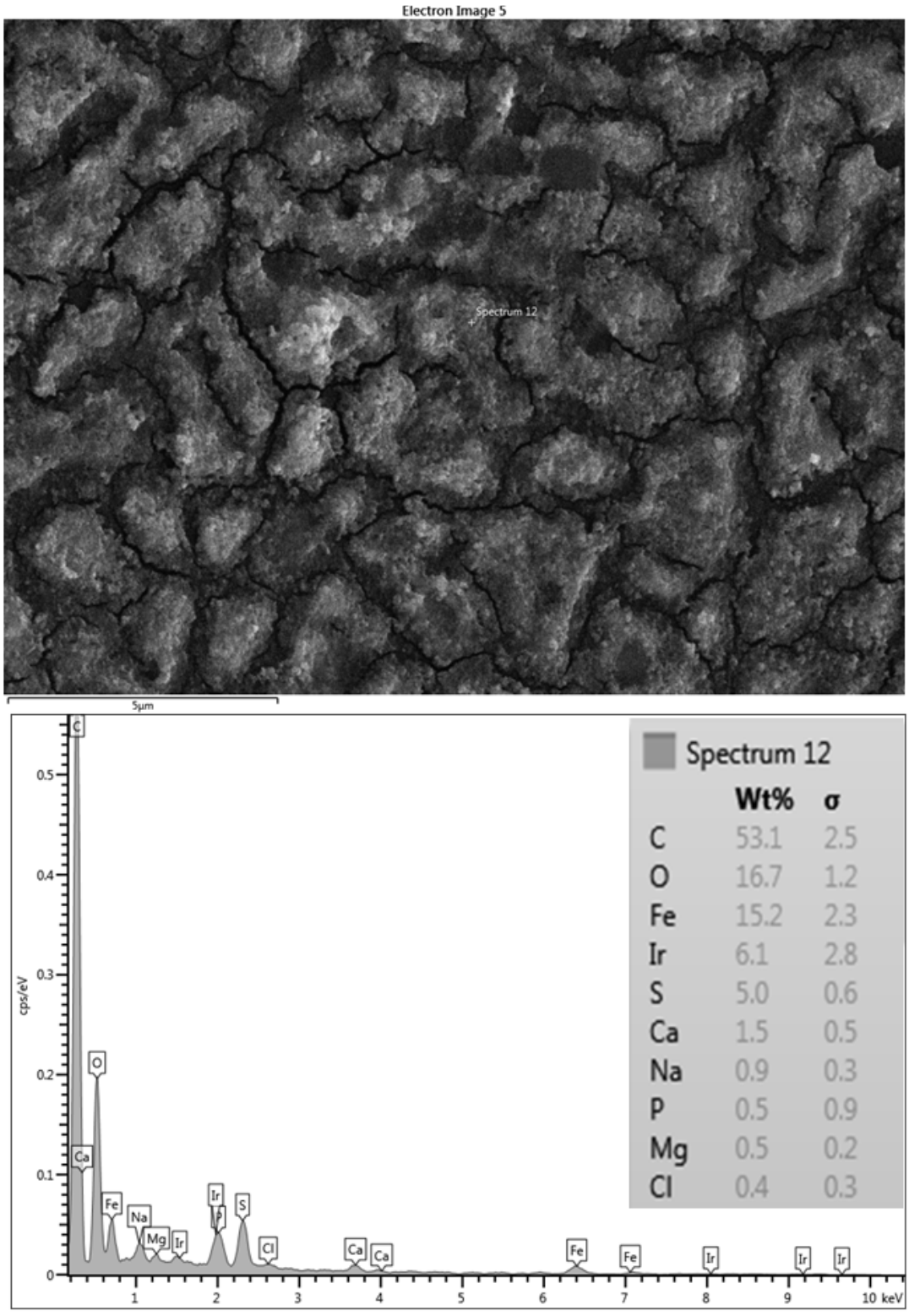

Figure C5. SEM image and EDSX spectra of run 2.

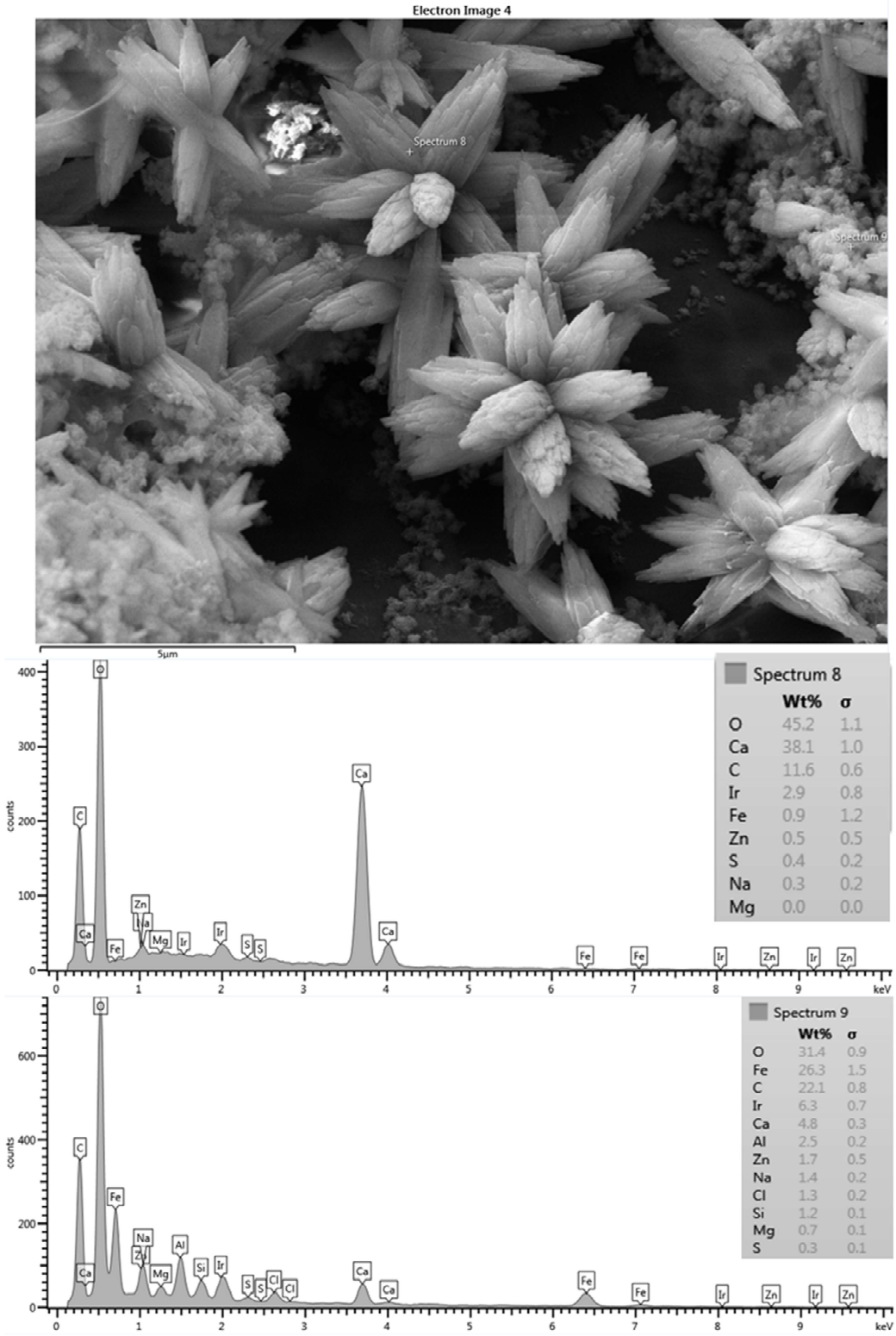

Figure C6. SEM image and EDSX spectra of run 3.

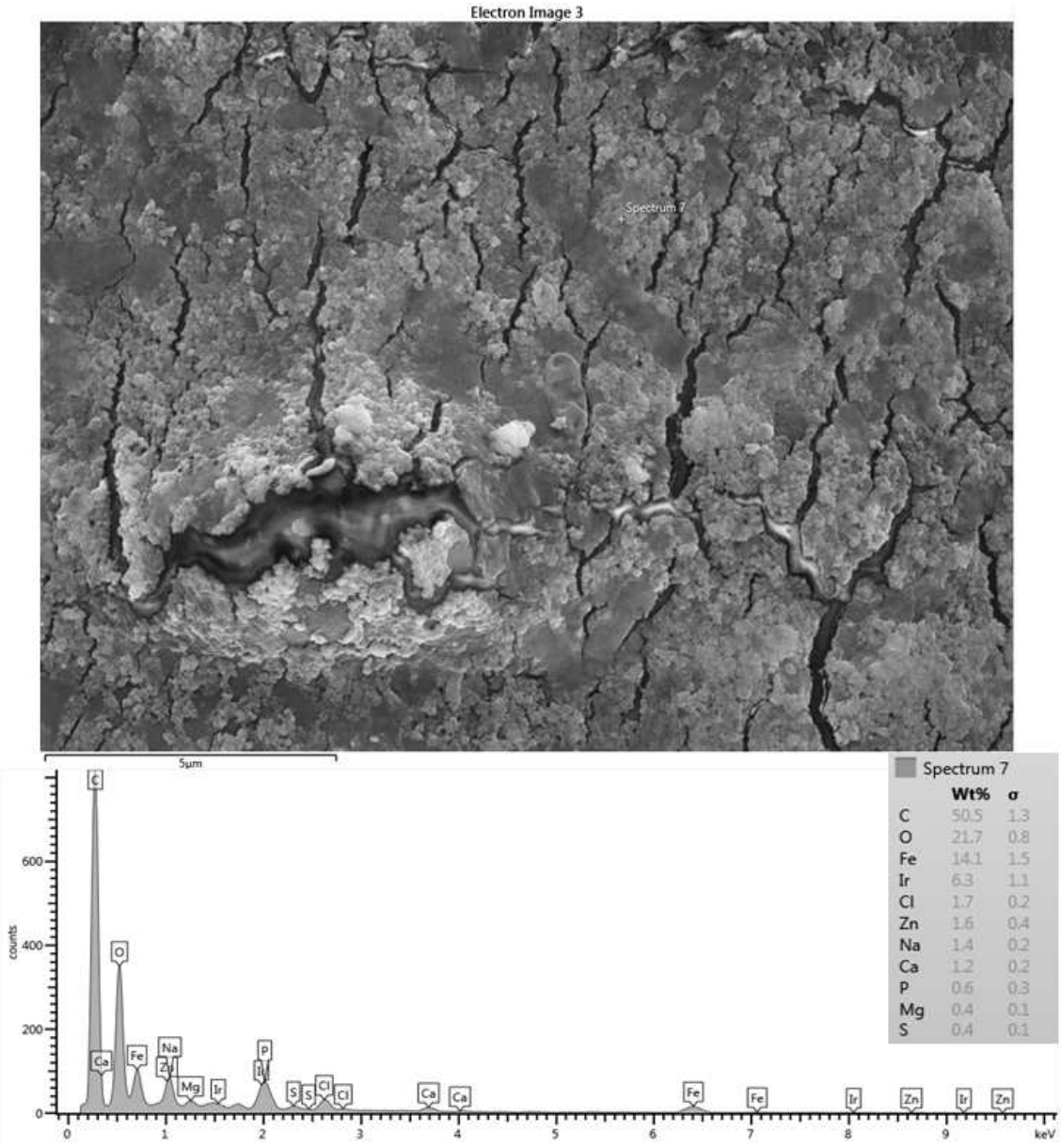

Figure C7. SEM image and EDSX spectrum of run 4.

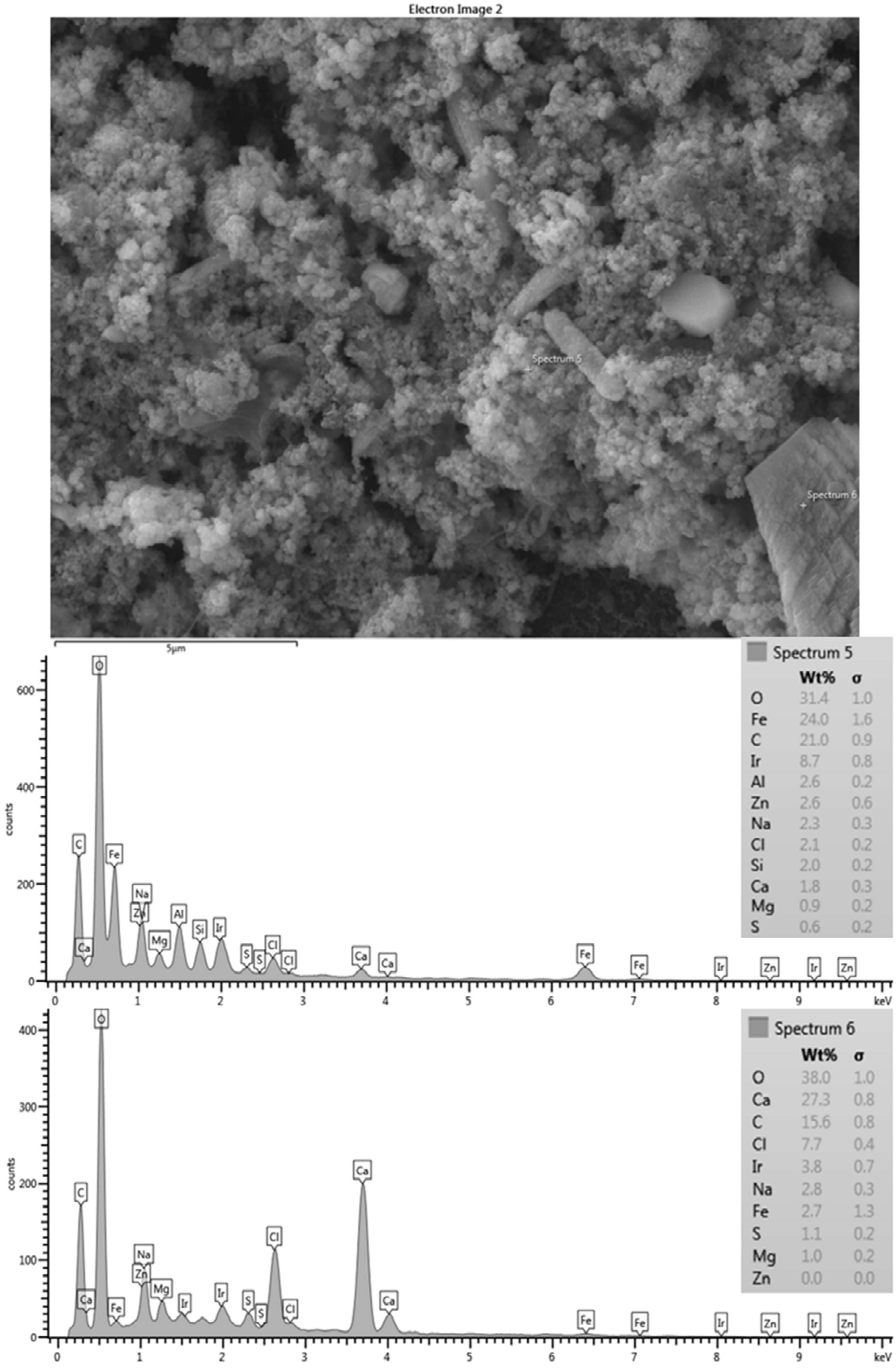

Figure C8. SEM image and EDSX spectra of run 5.

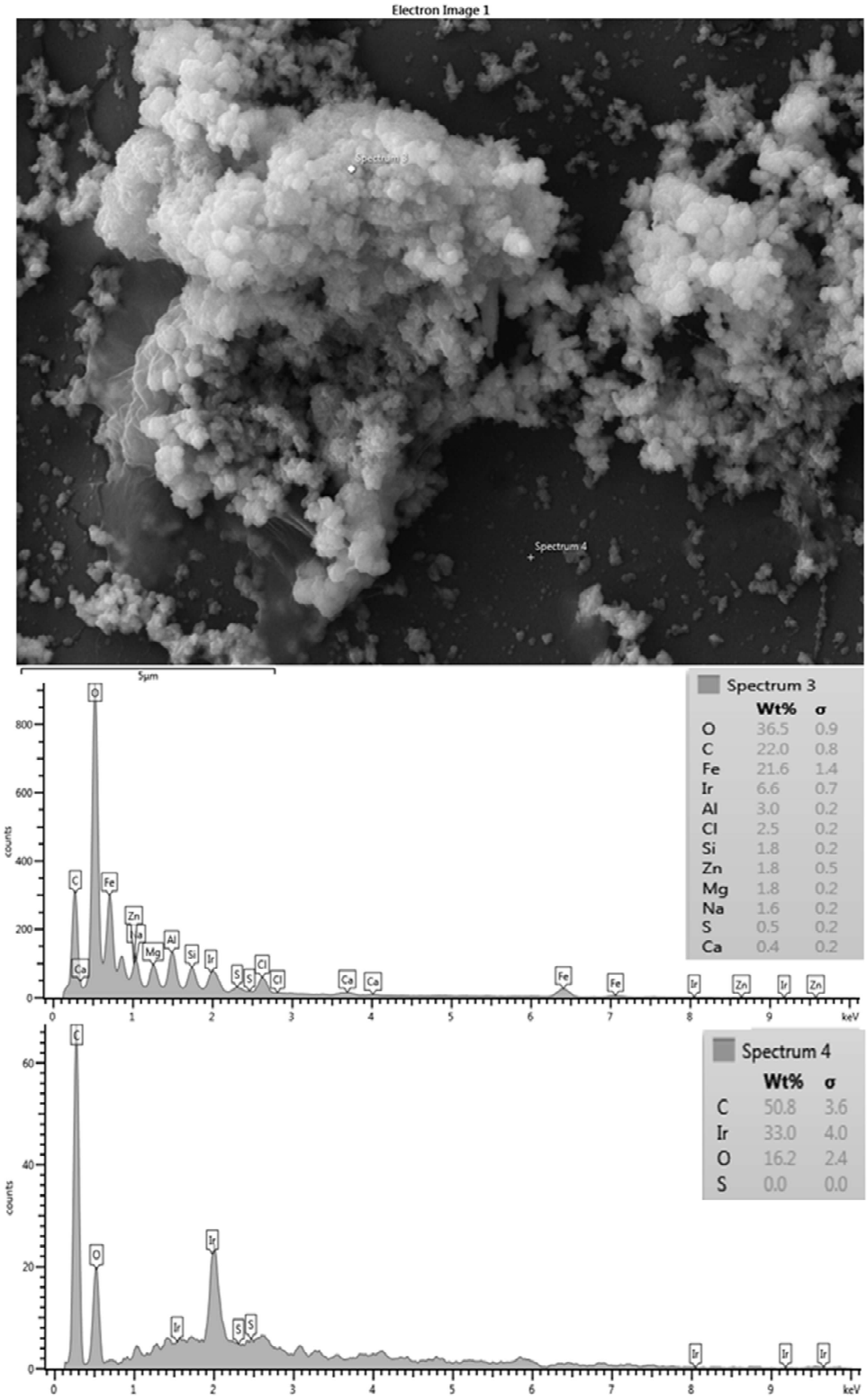

Figure C9. SEM image and EDSX spectra of run 9.

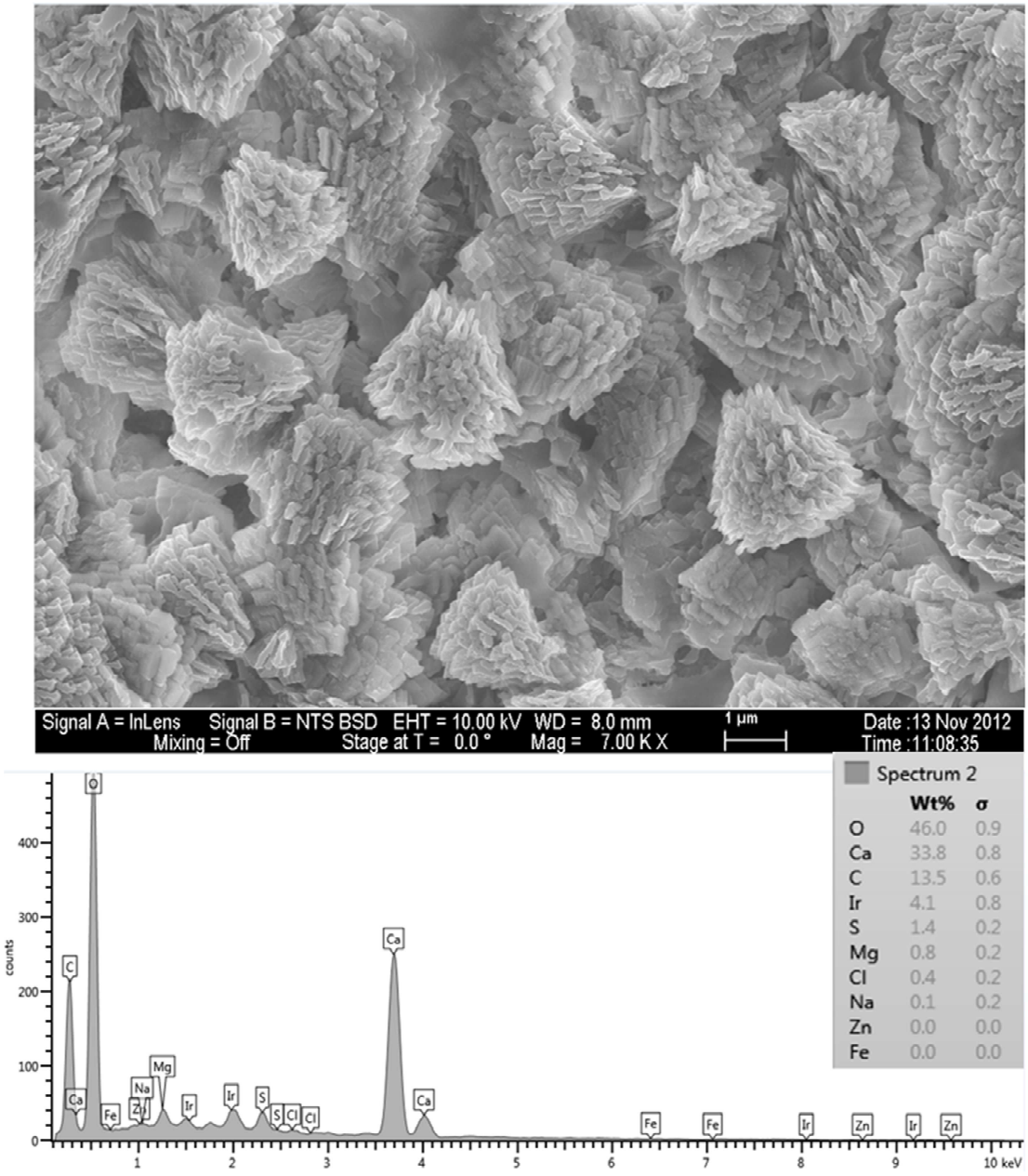

Figure C10. SEM image and EDSX spectrum of run 13.

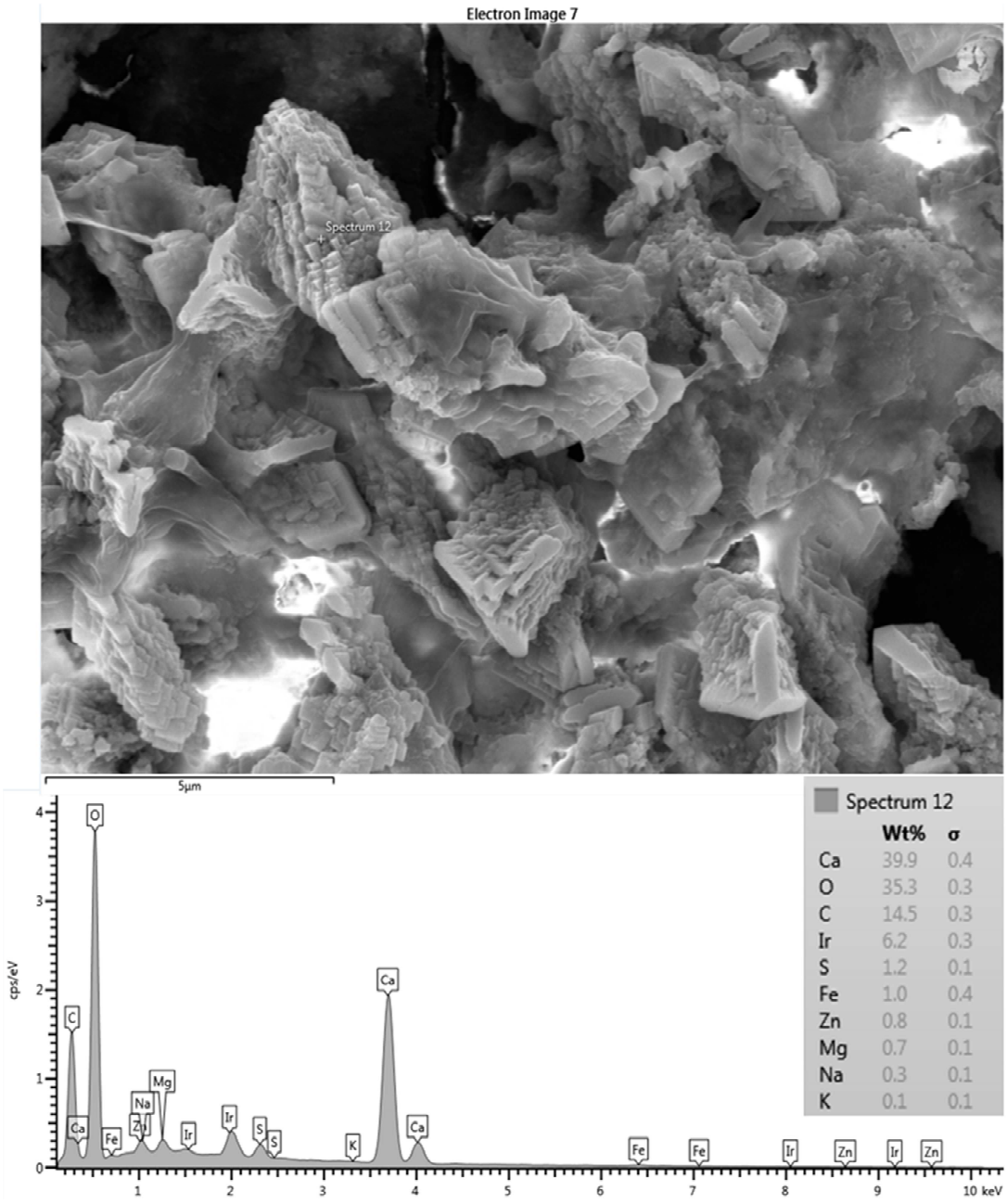

Figure C11. SEM image and EDSX spectrum of run 14.

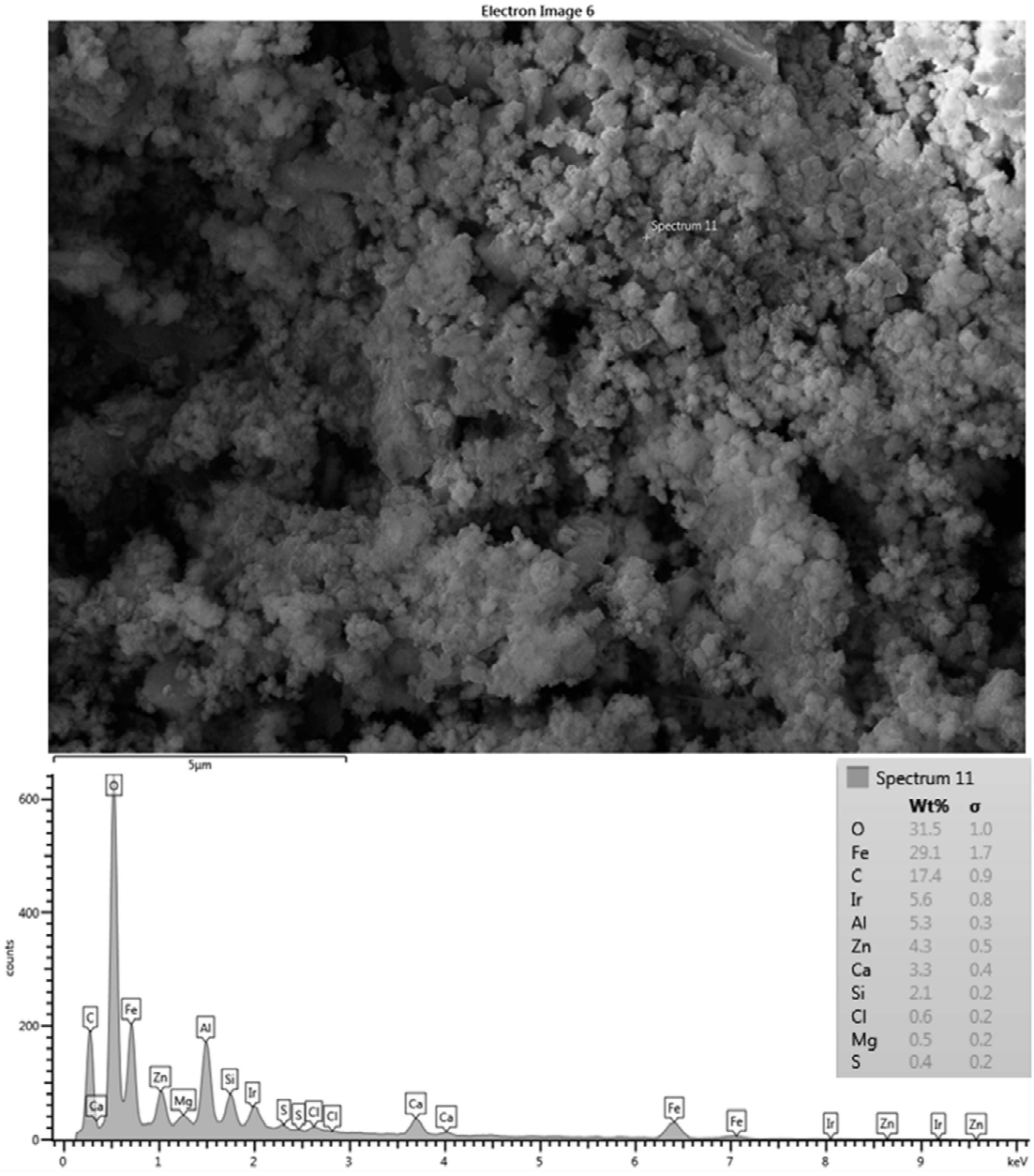

Figure C12. SEM image and EDSX spectrum of run 19.

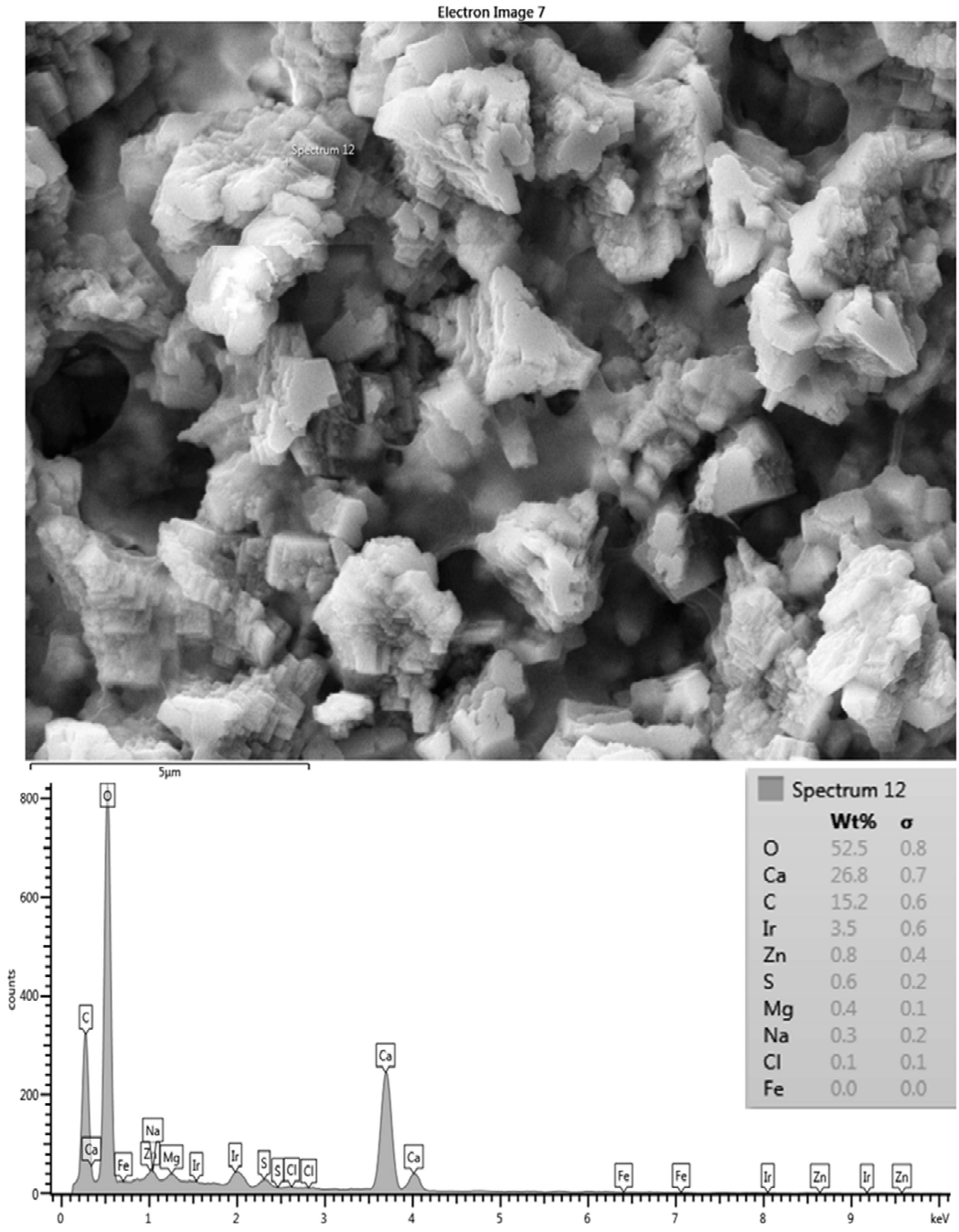

Figure C13. SEM image and EDSX spectrum of run 20.

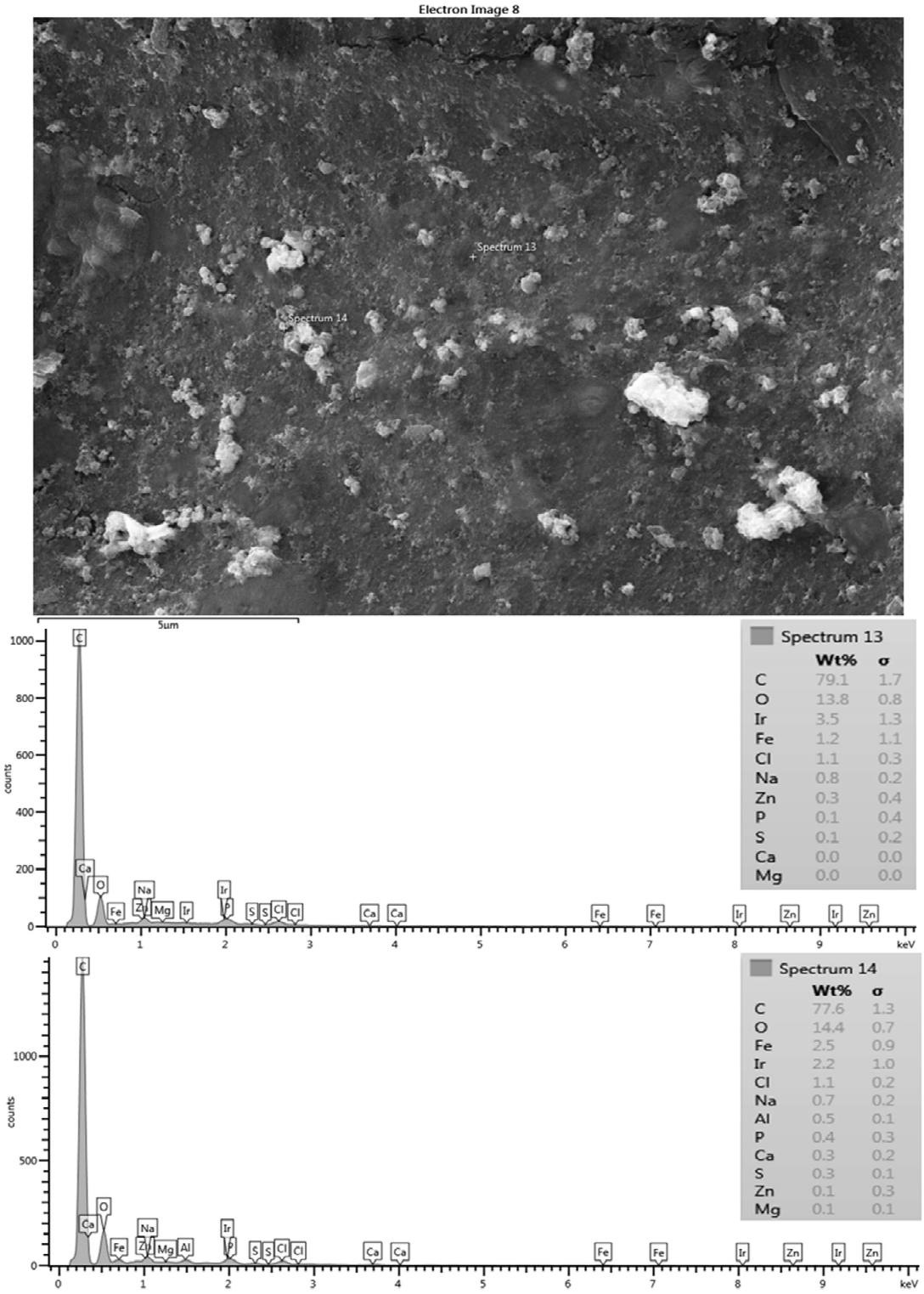

Figure C14. SEM image and EDSX spectra of run 21.

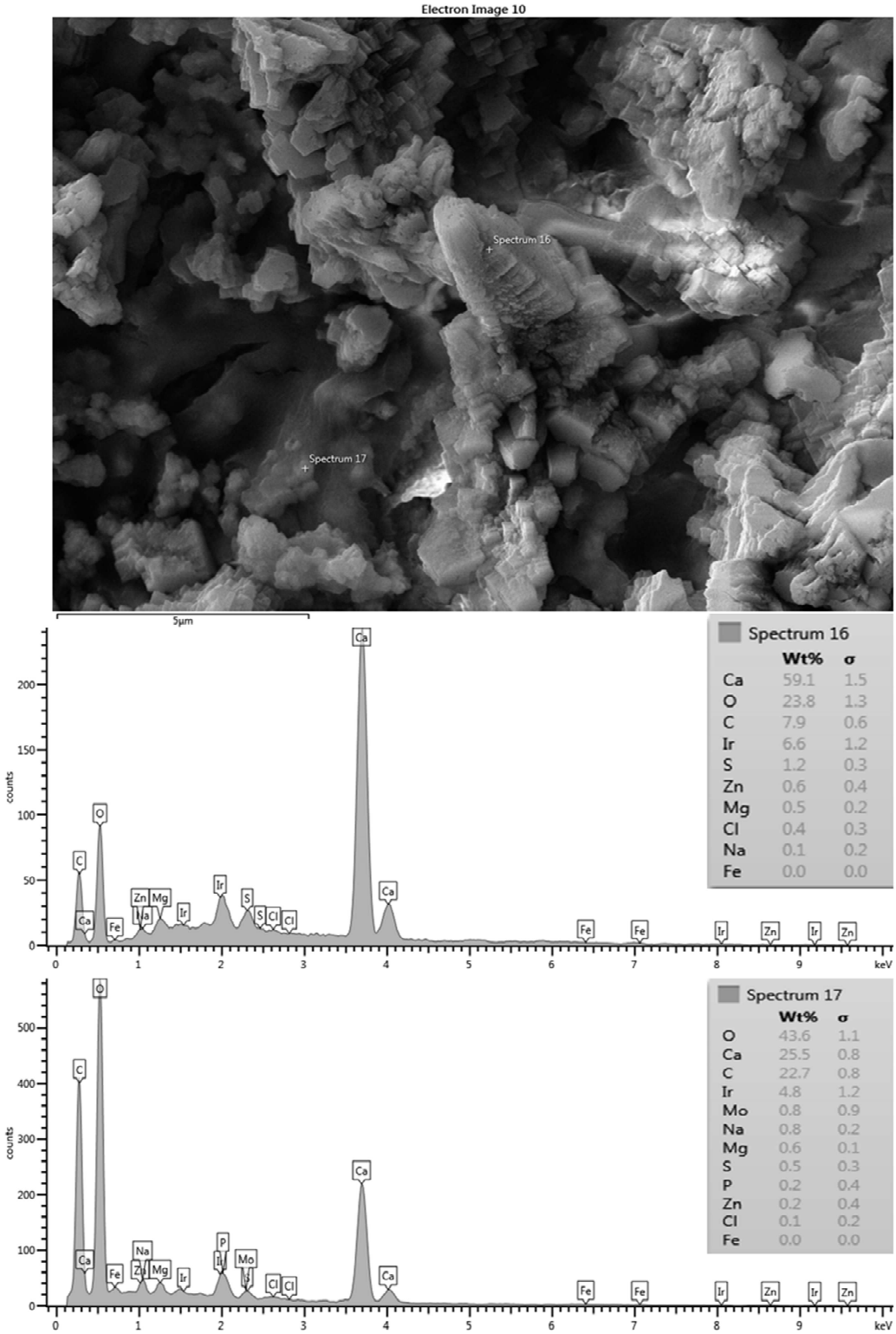

Figure C15. SEM image and EDSX spectra of run 22.

APPENDIX D: ICP ANALYSES

2/20/2013												
2013-25												
RO Water (background water)												
Ion	Na	Ca	Mg	K	SO4	B	P	Fe	Zn	Cu	Mn	Al
	ppm	ppm	ppm	ppm	ppm	ppm	ppm	ppm	ppm	ppm	ppm	ppm
Concentration	4.1	0.0	0.0	0.05	0.11	0.17	0.00	0.00	0.00	0.00	0.00	0.00

Example of salt rejection calculation:

	Time	Na^{+}	Ca^{+2}	Mg^{+2}	SO_4^{-2}	Cl^{-}
	(hrs)	ppm	ppm	ppm	ppm	ppm
R1P1	1	41.1	1.3	1.2	9.9	38.8
R1P2	36	59.9	1.4	2.1	13.5	79.5
R1P3	75.4	164.1	4.4	4.2	40.4	223.7
R1C1	1	692.1	92.1	86.2	686.8	966.9
R1C2	36	979.8	153.2	127.2	1181.1	1577.7
R1C3	75.4	2203.7	261.4	221.1	2230.2	2470.9

Concentrate (48)	661.1	78.4	66.3	669.1	741.3
Feed (48)-concentrate (48)	31.0	13.7	19.9	17.7	225.6
Permeate (48)	28.8	0.9	0.8	6.9	27.1
Fouled	2.2	12.8	19.0	10.8	198.5
Removed (%)	95.8	99.0	99.0	99.0	97.2

	Time	Na^{+}	Ca^{+2}	Mg^{+2}	SO_4^{-2}	Cl^{-}
	(hrs)	ppm	ppm	ppm	ppm	ppm
R2P1	1.8	25.2	1.6	0.7	4.4	33.0
R2P2	46.0	44.3	1.7	0.9	8.5	58.0
R2P3	92.0	91.5	3.0	1.2	11.4	125.2
R2C1	1.8	712.2	103.7	85.3	668.1	1075.1
R2C2	46.0	986.7	145.2	115.7	906.7	1581.7
R2C3	92.0	1929.7	293.2	225.7	1828.5	2788.3

R1P1 = run 1 permeate start
R1P2 = run 1 permeate middle
R1P3 = run 1 permeate end
R1C1 = run1 concentrate start
R1C2 = run1 concentrate middle
R1C1 = run1 concentrate end

	Time	Na^{+}	Ca^{+2}	Mg^{+2}	SO_4^{-2}	Cl^{-}
	(hrs)	ppm	ppm	ppm	ppm	ppm
R3P1	1.2	51.4	2.3	2.1	11.9	84.6
R3P2	39.0	75.1	4.1	2.9	14.5	110.8
R3P3	80.8	179.2	6.2	3.6	28.4	292.2
R3C1	1.2	688.3	103.1	81.8	719.6	947.8
R3C2	39.0	992.5	141.5	122.5	1000.0	1317.9
R3C3	80.8	2153.7	227.1	223.7	2313.2	2795.3

	Time	Na^{+}	Ca^{+2}	Mg^{+2}	SO_4^{-2}	Cl^{-}
	(hrs)	ppm	ppm	ppm	ppm	ppm
R4P1	0.7	44.3	3.2	1.2	7.8	65.9
R4P2	52.0	89.6	3.0	1.8	9.3	137.1
R4P3	103.0	199.2	5.0	3.5	12.3	303.6
R4C1	0.7	711.8	98.3	83.7	687.4	944.2
R4C2	52.0	937.7	135.9	125.3	996.8	1488.4
R4C3	103.0	2154.0	229.5	215.6	2026.0	2745.0

	Time	Na^{+}	Ca^{+2}	Mg^{+2}	SO_4^{-2}	Cl^{-}
	(hrs)	ppm	ppm	ppm	ppm	ppm
R6P1	4.0	11.4	1.1	0.8	6.7	13.6
R6P2	47.3	13.7	0.8	0.6	8.6	18.4
R6P3	95.9	23.9	0.9	0.8	9.6	36.1
R6C1	4.0	711.8	98.3	83.7	685.6	944.2
R6C2	47.3	1093.1	154.2	130.0	1065.4	1400.0
R6C3	95.9	2209.1	278.1	245.1	2117.1	2732.8

	Time	Na^{+}	Ca^{+2}	Mg^{+2}	SO_4^{-2}	Cl^{-}
	(hrs)	ppm	ppm	ppm	ppm	ppm
R7P1	0.5	19.6	1.0	1.0	5.6	29.3
R7P2	30.0	33.8	1.8	1.2	8.9	49.0
R7P3	63.0	75.0	3.0	1.8	13.5	113.0
R7C1	0.5	709.0	98.5	85.7	686.4	965.3
R7C2	30.0	997.0	178.0	117.0	912.8	1498.5
R7C3	63.0	2167.0	312.0	264.0	2134.0	2865.1

	Time	Na^{+}	Ca^{+2}	Mg^{+2}	SO_4^{-2}	Cl^{-}
	(hrs)	ppm	ppm	ppm	ppm	ppm
R9P1	1.4	45.7	0.9	1.3	5.3	80.1
R9P2	39.7	70.4	3.3	1.6	6.7	101.4
R9P3	76.5	170.8	5.2	4.3	20.2	269.4
R9C1	1.4	771.3	107.4	89.1	752.4	965.7
R9C2	39.7	912.0	128.6	105.4	905.5	1127.2
R9C3	76.5	2329.8	259.7	212.5	2449.2	2699.7

	Time	Na^{+}	Ca^{+2}	Mg^{+2}	SO_4^{-2}	Cl^{-}
	(hrs)	ppm	ppm	ppm	ppm	ppm
R10P1	1.8	42.6	0.8	0.9	4.1	72.1
R10P2	46.0	85.5	1.7	1.8	7.2	129.6
R10P3	92.0	298.6	7.0	4.9	11.7	474.0
R10C1	1.8	713.6	102.3	88.5	673.3	963.4
R10C2	46.0	971.0	174.4	121.1	1077.5	1289.9
R10C3	92.0	2162.5	315.7	274.1	2179.0	2754.7

	Time	Na^{+}	Ca^{+2}	Mg^{+2}	SO_4^{-2}	Cl^{-}
	(hrs)	ppm	ppm	ppm	ppm	ppm
R13P1	1.3	13.3	2.6	1.5	4.9	25.8
R13P2	31.1	23.9	2.9	1.6	6.6	30.5
R13P3	62.3	68.7	4.5	1.8	12.7	90.7
R13C1	1.3	322.0	78.0	49.5	312.0	509.0
R13C2	31.1	713.0	146.0	93.7	622.9	1045.0
R13C3	62.3	1208.0	247.0	176.2	1228.7	1913.0

	Time	Na^{+}	Ca^{+2}	Mg^{+2}	SO_4^{-2}	Cl^{-}
	(hrs)	ppm	ppm	ppm	ppm	ppm
R14P1	0.8	14.2	1.2	1.1	8.5	27.5
R14P2	44.4	18.3	2.5	1.0	7.6	29.2
R14P3	88.8	52.6	4.2	2.1	14.8	83.7
R14C1	0.8	355.0	80.4	52.7	318.0	512.0
R14C2	44.4	774.3	159.7	102.3	623.4	995.8
R14C3	88.8	1324.0	251.6	192.5	1198.7	1950.0

	Time	Na^{+}	Ca^{+2}	Mg^{+2}	SO_4^{-2}	Cl^{-}
	(hrs)	ppm	ppm	ppm	ppm	ppm
R19P1	1.0	12.8	0.4	0.2	2.8	8.9
R19P2	30.7	18.1	0.3	0.1	4.3	12.4
R19P3	63.9	36.0	2.3	1.5	9.0	46.7
R19C1	1.0	178.8	47.4	17.0	93.3	265.9
R19C2	30.7	285.9	56.7	27.2	147.0	414.0
R19C3	63.9	710.6	96.5	59.6	331.4	1108.0

	Time	Na^{+}	Ca^{+2}	Mg^{+2}	SO_4^{-2}	Cl^{-}
	(hrs)	ppm	ppm	ppm	ppm	ppm
R20P1	0.9	11.8	1.2	0.2	1.6	9.3
R20P2	37.0	21.4	1.8	0.5	2.0	28.4
R20P3	74.0	72.3	2.6	1.3	6.2	97.3
R20C1	0.9	198.9	57.4	21.6	113.6	308.6
R20C2	37.0	420.0	102.5	44.6	257.1	667.4
R20C3	74.0	889.0	156.8	88.1	541.6	1431.1

	Time	Na^{+}	Ca^{+2}	Mg^{+2}	SO_4^{-2}	Cl^{-}
	(hrs)	ppm	ppm	ppm	ppm	ppm
R21P1	0.8	23.9	1.7	0.8	1.2	34.3
R21P2	37.0	46.8	3.1	1.2	1.3	68.2
R21P3	74.0	83.6	4.5	1.7	2.7	122.8
R21C1	0.8	217.8	47.4	21.6	113.6	308.6
R21C2	37.0	383.0	87.1	39.5	215.0	526.1
R21C3	74.0	882.7	193.2	71.8	480.6	1208.0

	Time	Na^{+}	Ca^{+2}	Mg^{+2}	SO_4^{-2}	Cl^{-}
	(hrs)	ppm	ppm	ppm	ppm	ppm
R22P1	1.6	14.0	1.6	0.8	1.5	20.5
R22P2	41.0	31.9	1.8	0.6	1.9	44.9
R22P3	82.0	92.6	3.4	1.8	4.4	135.9
R22C1	1.6	201.8	56.9	18.8	107.1	279.2
R22C2	41.0	395.2	63.6	36.9	218.8	532.1
R22C3	82.0	856.5	98.7	81.6	478.8	1220.1

	Time	Na^{+}	Ca^{+2}	Mg^{+2}	SO_4^{-2}	Cl^{-}
	(hrs)	ppm	ppm	ppm	ppm	ppm
R23P1	0.5	4.1	1.3	0.2	1.0	2.4
R23P2	36.0	3.2	1.2	0.0	0.5	1.6
R23P3	71.6	3.9	0.9	0.1	0.8	3.3
R23C1	0.5	195.1	43.3	18.0	105.1	263.0
R23C2	36.0	274.7	61.1	24.6	142.9	368.3
R23C3	71.6	528.0	119.3	49.3	290.9	777.0

	Time	Na^{+}	Ca^{+2}	Mg^{+2}	SO_4^{-2}	Cl^{-}
	(hrs)	ppm	ppm	ppm	ppm	ppm
R24P1	1.0	2.5	1.1	0.1	0.8	2.1
R24P2	53.4	3.9	1.1	0.1	0.8	2.4
R24P3	107.7	9.6	0.6	0.1	1.6	10.3
R24C1	1.0	196.8	40.2	15.5	99.3	267.9
R24C2	53.4	367.2	74.8	28.9	186.4	493.5
R24C3	107.7	941.5	109.8	70.3	465.9	1302.6

APPENDIX E: TEMPERATURE EFFECT ON PERMEATE FLUX

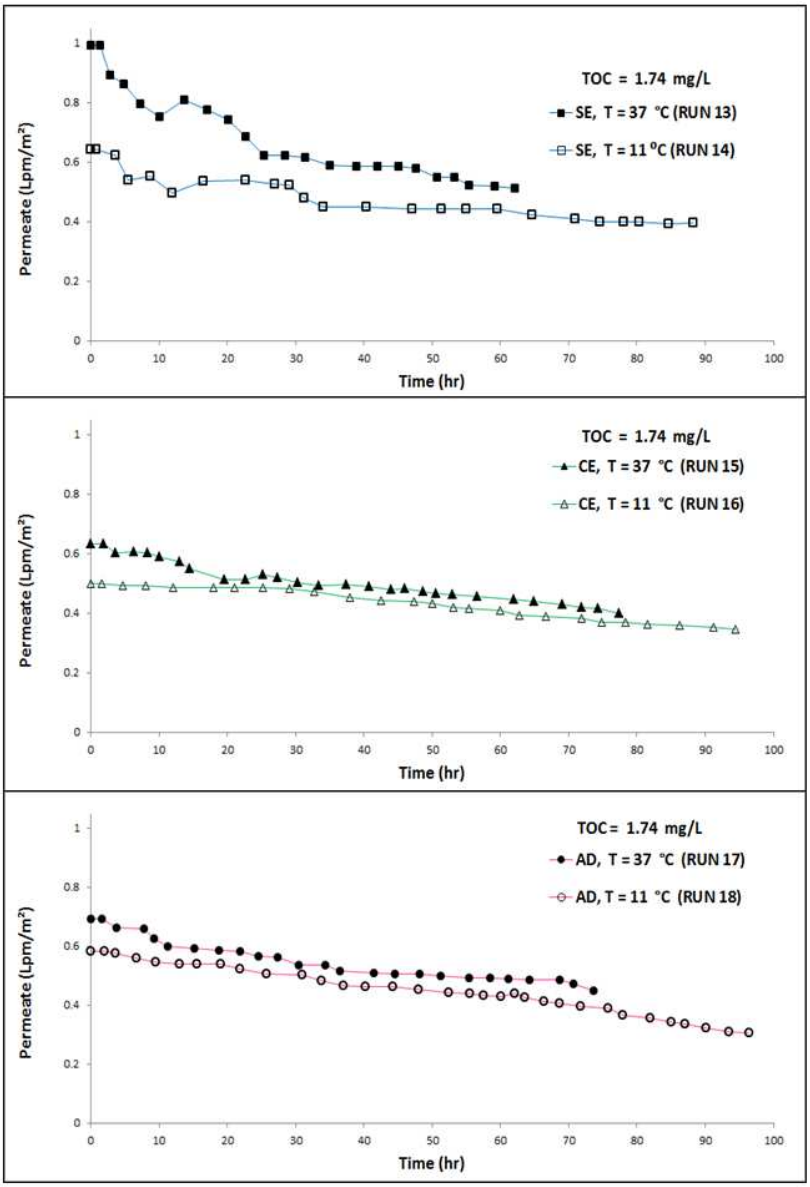

Figure E1. Temperature effect on permeate flux of runs 13 through 18 of location 1.

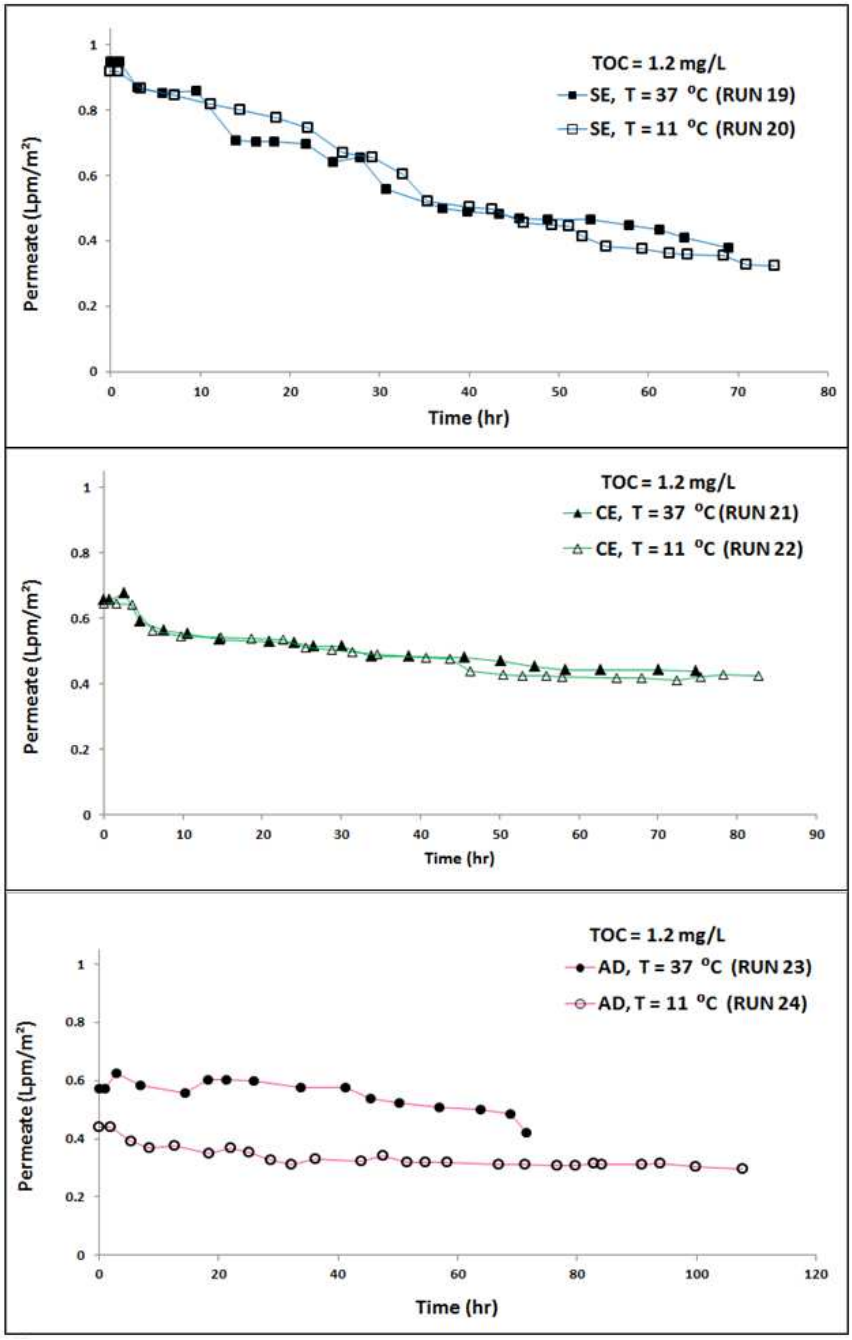

Figure E2. Temperature effect on permeate flux of runs 19 through 24 of location 5.

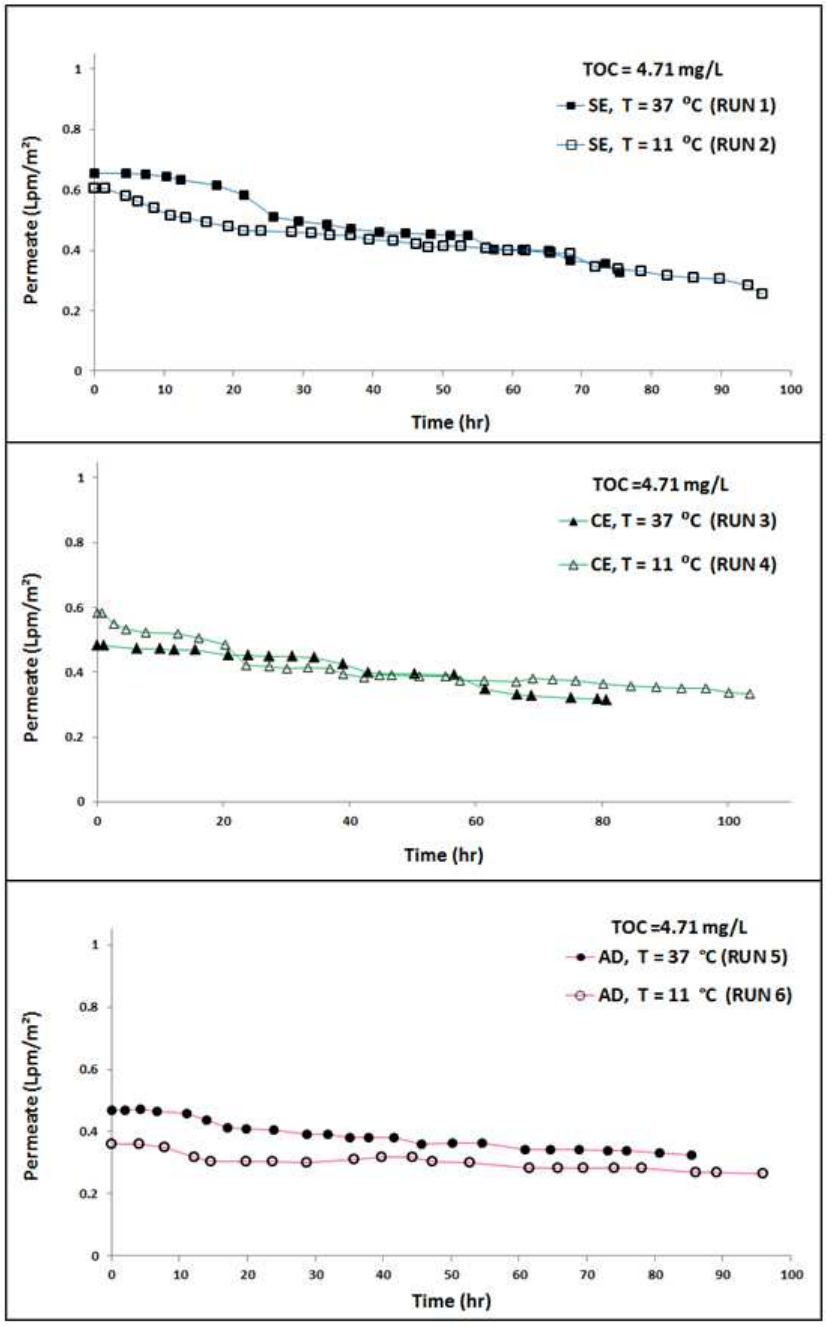

Figure E3. Temperature effect on permeate flux of runs 1 through 6 of location 6.

VITA

Dawood Eisa Sachit

Candidate for the Degree of

Doctor of Philosophy

Thesis: ANALYSIS OF REVERSE OSMOSIS MEMBRANE PERFORMANCE DURING DESALINATION OF SIMULATED BRACKISH SURFACE WATERS

Major Field: Civil and Environmental Engineering

Biographical:

Education:

Completed the requirements for the Doctor of Philosophy in Civil and Environmental Engineering at Oklahoma State University, Stillwater, Oklahoma in December, 2013.

Completed the requirements for the Master of Science in Civil Engineering at Al-Mustansiria University, Baghdad, Iraq in 2000.

Completed the requirements for the Bachelor of Science in Civil Engineering at Al-Mustansiria University, Baghdad, Iraq in 1994.

Experience:

2000-2007 Instructor for the following courses: Sanitary Engineering, Environmental Lab Analysis, and Engineering Drawing at the Department of Environmental Engineering, Al-Mustansiria University, Baghdad, Iraq.
1994-1997 Civil Engineer for several projects. Materials testing engineer with soil investigation and roads testing requirements.

Professional Memberships:

American Water Works Association (AWWA)
Phi Kappa Phi National Honor Society
Golden Key National Honor Society
The Iraqi Engineers Union